



OPEN ACCESS

Original research

# Residual homing of $\alpha 4\beta 7$ -expressing $\beta 1^+PI16^+$ regulatory T cells with potent suppressive activity correlates with exposure-efficacy of vedolizumab

Emily Becker,<sup>1</sup> Mark Dedden,<sup>1</sup> Christine Gall,<sup>2</sup> Maximilian Wiendl,<sup>1</sup> Arif Bülent Ekici,<sup>3</sup> Anja Schulz-Kuhnt,<sup>1</sup> Anna Schweda,<sup>1</sup> Caroline Voskens,<sup>4,5</sup> Ahmed Hegazy,<sup>6,7,8</sup> Francesco Vitali,<sup>1</sup> Raja Atreya,<sup>1,5</sup> Tanja Martina Müller,<sup>1,5</sup> Imke Atreya,<sup>1,5</sup> Markus F Neurath ,<sup>1,5</sup> Sebastian Zundler <sup>1,5</sup>

► Additional supplemental material is published online only. To view, please visit the journal online (<http://dx.doi.org/10.1136/gutjnl-2021-324868>).

For numbered affiliations see end of article.

## Correspondence to

Dr Sebastian Zundler, Department of Medicine 1, University Hospital Erlangen, Friedrich-Alexander-Universität Erlangen-Nürnberg, Bayern, 91054 Erlangen, Germany; [sebastian.zundler@uk-erlangen.de](mailto:sebastian.zundler@uk-erlangen.de)

Received 10 April 2021  
Accepted 8 August 2021  
Published Online First  
30 August 2021



► <http://dx.doi.org/10.1136/gutjnl-2021-325893>



© Author(s) (or their employer(s)) 2021. Re-use permitted under CC BY-NC. No commercial re-use. See rights and permissions. Published by BMJ.

**To cite:** Becker E, Dedden M, Gall C, *et al.* Gut 2022;**71**:1551–1566.

## ABSTRACT

**Objective** The anti- $\alpha 4\beta 7$  integrin antibody vedolizumab is administered at a fixed dose for the treatment of IBDs. This leads to a wide range of serum concentrations in patients and previous studies had suggested that highest exposure levels are associated with suboptimal clinical response. We aimed to determine the mechanisms underlying these non-linear exposure-efficacy characteristics of vedolizumab.

**Design** We characterised over 500 samples from more than 300 subjects. We studied the binding of vedolizumab to T cells and investigated the functional consequences for dynamic adhesion, transmigration, gut homing and free binding sites *in vivo*. Employing single-cell RNA sequencing, we characterised  $\alpha 4\beta 7$  integrin-expressing T cell populations 'resistant' to vedolizumab and validated our findings *in vitro* and in samples from vedolizumab-treated patients with IBD. We also correlated our findings with a post-hoc analysis of the Gemini II and III studies.

**Results** Regulatory T ( $T_{Reg}$ ) cells exhibited a right-shifted vedolizumab binding profile compared with effector T ( $T_{Eff}$ ) cells. Consistently, in a certain concentration range, the residual adhesion, transmigration, homing of and availability of functional  $\alpha 4\beta 7$  on  $T_{Reg}$  cells *in vivo* was higher than that of/on  $T_{Eff}$  cells. We identified a vedolizumab-'resistant'  $\alpha 4\beta 7$ -expressing  $\beta 1^+PI16^+$   $T_{Reg}$  cell subset with pronounced regulatory properties as the substrate for this effect. Our observations correlated with exposure-efficacy data from Gemini II and III trials.

**Conclusion** Completely blocking  $T_{Eff}$  cell trafficking with vedolizumab, while simultaneously permitting residual homing of powerful  $T_{Reg}$  cells in an optimal 'therapeutic window' based on target exposure levels might be a strategy to optimise treatment outcomes in patients with IBD.

## INTRODUCTION

IBDs with the main entities Crohn's disease (CD) and ulcerative colitis (UC) are characterised by chronically relapsing inflammation of the gastrointestinal tract.<sup>1</sup> The worldwide incidence and prevalence of IBDs is continuously growing,<sup>2</sup> but the exact pathogenesis is still not fully understood. However, insights into the mechanisms driving

## Significance of this study

### What is already known on this subject?

- ⇒ The anti- $\alpha 4\beta 7$  antibody vedolizumab blocks gut homing of regulatory T ( $T_{Reg}$ ) and effector T ( $T_{Eff}$ ) cells and is approved for the therapy of Crohn's disease and UC.
- ⇒  $T_{Reg}$  cells counteract active inflammation in IBDs.
- ⇒ Fixed dosing of vedolizumab in the therapy of IBD leads to a wide range of serum drug levels observed in patients.
- ⇒ Phase II trials of vedolizumab suggested a non-linear dose–response correlation at high exposure levels.

### What are the new findings?

- ⇒ Vedolizumab has a right-shifted exposure-efficacy profile regarding  $T_{Reg}$  compared with  $T_{Eff}$  cells *in vitro* and *in vivo*.
- ⇒ Single-cell RNA sequencing identifies a  $\alpha 4\beta 7^+$   $T_{Reg}$  cell subset expressing integrin  $\beta 1$  and PI16 that does not bind vedolizumab.
- ⇒  $\alpha 4\beta 7$ -expressing  $\beta 1^+PI16^+$   $T_{Reg}$  cells are 'resistant' to vedolizumab in patients with IBD.
- ⇒ Differential exposure-efficacy profiles of  $T_{Reg}$  and  $T_{Eff}$  cells correlate with outcomes in Crohn's disease phase III trials.

### How might it impact on clinical practice in foreseeable future?

- ⇒ Achieving optimal serum drug levels by personalised dosing strategies might increase the efficacy of vedolizumab therapy.

these diseases have increased and facilitated the development of new treatment strategies.<sup>3,4</sup> One of the newer therapeutic options is the anti- $\alpha 4\beta 7$  integrin antibody vedolizumab that has been approved for the treatment of IBDs in 2014. By binding to the  $\alpha 4\beta 7$  integrin heterodimer expressed on the surface of several leucocyte populations, the antibody inhibits the interaction of  $\alpha 4\beta 7$  integrin with its ligand mucosal addressin cell adhesion molecule (MAdCAM)-1 expressed on high endothelial venules of the gut.<sup>5</sup> In consequence, firm adhesion

of  $\alpha 4\beta 7$ -expressing cells to the endothelium and the subsequent steps of the extravasation process known as homing are blocked.<sup>6,7</sup> It is perceived that by interfering with gut homing, vedolizumab reduces the number of immune cells recruited to the intestine and consistently attenuates inflammation. In particular, T cells are considered an important target of vedolizumab.<sup>8,9</sup> Intriguingly, vedolizumab blocks  $\alpha 4\beta 7$ -mediated gut homing of pro-inflammatory effector T ( $T_{\text{Eff}}$ ) as well as anti-inflammatory regulatory T ( $T_{\text{Reg}}$ ) cells,<sup>10</sup> raising the question, whether the latter effect might limit the efficacy of the antibody. Yet, vedolizumab has demonstrated convincing efficacy and safety profiles in clinical trials as well as in a plethora of real world studies<sup>11–15</sup> in recent years, but due to so far unknown reasons only a part of the patients treated with vedolizumab achieves remission.

It has been proposed that serum drug levels might be one part of the explanation for non-response to vedolizumab, since the fixed-dosing regimen leads to a wide range of serum concentrations in individual patients.<sup>11,12</sup> Consistently, several drug-monitoring studies could demonstrate that achieving a certain minimum trough-level serum concentration of vedolizumab is a necessary (but not sufficient) prerequisite to enter remission<sup>16</sup> and several authors described improved outcomes with increasing vedolizumab exposure over a wide concentration range.<sup>17–21</sup> However, two independent phase II trials<sup>22,23</sup> reported worse clinical outcomes in the highest compared with medium dosage groups suggesting a non-linear exposure-efficacy correlation in the higher range of drug levels.

Therefore, the aim of this work was to investigate the dose-response characteristics of vedolizumab on cell level. We show that higher vedolizumab concentrations are necessary to block  $\alpha 4\beta 7$  integrin on  $T_{\text{Reg}}$  compared with  $T_{\text{Eff}}$  cells. This functionally translates into differential adhesion, transmigration, gut homing and  $\alpha 4\beta 7$  availability in vivo. Mechanistically, we identify a  $\beta 1^+ \text{PI16}^+ T_{\text{Reg}}$  cell subset with powerful regulatory features that is 'resistant' to vedolizumab and enriches in the gut of successfully treated patients as the putative mediator of this effect. In a post-hoc analysis of Gemini II and III trials, the impact observed coincidences with exposure-efficacy data.

## METHODS

The key methods are listed in this section. Further methods are available as online supplemental file 1.

### Human blood samples

To determine the dose-response characteristics of vedolizumab in vitro, peripheral EDTA-anticoagulated blood was collected from healthy donors and patients with UC or CD not receiving treatment with vedolizumab. For assessment of the in vivo binding of vedolizumab, EDTA-anticoagulated full blood and serum samples from patients with IBD aged 18–75 and without relevant comorbidities undergoing vedolizumab therapy were collected. These materials were obtained at the IBD Outpatient Clinic of the Department of Medicine 1 of the University Hospital Erlangen, Germany. Characteristics of study subjects with CD, UC and control donors are summarised in online supplemental table 1. For fluorescence-activated cell sorting (FACS)-based isolation of  $T_{\text{Reg}}$  and  $T_{\text{Eff}}$  cells, leucocyte cones were obtained from the Department of Transfusion Medicine and Haemostaseology of the University Hospital Erlangen. In total, 571 samples from 358 subjects were analysed (including 59 leucocytes cones).

### Flow cytometry

Flow cytometry was performed according to standard protocols using the following fluorochrome-conjugated extracellular antibodies: CD3 (VioGreen, REA613, Miltenyi Biotec), CD4 (FITC/VioBlue/VioGreen/APC-Vio770, VIT4, Miltenyi Biotec), CD45RO (BV510, UCHL1, Biolegend), CD25 (PE/Cy7, BC96, Biolegend), CD127 (APC-Vio770/VioBrightFITC, REA614, Miltenyi Biotec; APC, A019D5, Biolegend), CD49d (VioBlue/FITC, MZ18-24A9, Miltenyi Biotec; PE/Cy7, 9F10, Biolegend), integrin beta 7 (PerCP/Cy5.5/PE, FIB27, Biolegend; BV605, FIB504, BD BioSciences), integrin beta 1/CD29 (PE/PerCP/Cy5.5, TS2/16, Biolegend), PI16 (PE/VioBright FITC, REA699, Miltenyi Biotec), GTR (APC, 108–17, Biolegend), CD8 (PerCP/Cy5.5, RPA-T8, Biolegend), CD19 (VioBlue, Miltenyi Biotec), CD16 (APC/Cy7, 3G8, Biolegend), CD14 (AF488, HCD14, Biolegend), CD56 (PE-Vio770, REA196, Miltenyi Biotec), CCR3 (FITC, 5E8, Biolegend), Siglec 8 (PE-Dazzle594, 7C9, Biolegend). Where indicated, vedolizumab (Entyvio, Takeda) and MAdCAM-1 (rh Fc Chimera Protein, R&D Systems) were labelled using Alexa Fluor Antibody Labelling Kits (AF674/AF488, Life Technologies) according to the manufacturer's instructions and used for staining.

For intracellular staining, the Foxp3/Transcription Factor Staining Buffer Set (eBioscience) in combination with a specific fluorochrome-conjugated antibody targeting human Foxp3 (PE/AF700/APC, 236A/E7, Invitrogen) or interleukin 10 (IL-10) (PE, JES3-19F1, Biolegend) was used.

For the quantification of free vedolizumab binding sites, human peripheral blood mononuclear cells (PBMCs) were incubated with unlabelled vedolizumab at different concentrations (0, 2, 10, 50 and 110  $\mu\text{g/mL}$ ) for 1 hour at 37°C, then harvested and stained as described above with fluorochrome-conjugated extracellular antibodies as well as with 50  $\mu\text{g/mL}$  of fluorescently labelled vedolizumab.

Data were acquired on LSR Fortessa (BD Bioscience), MACSQuant 10 and MACSQuant 16 (Miltenyi Biotec) instruments. Data were analysed with FlowJo single-cell analysis software V.7.6.5 and V.10.06.1 (Tree Star).

### Vedolizumab ELISA

Serum from patients receiving treatment with vedolizumab was analysed for vedolizumab concentrations using the Vedolizumab Drug Level ELISA (ImmunDiagnostics) according to the manufacturer's instructions. Optical densities were determined using a NOVostar plate reader (BMG Labtech).

### Dynamic adhesion assays to MAdCAM-1

To quantify the capacity of cells to adhere to MAdCAM-1 after incubation with different concentrations of vedolizumab, FACS-isolated  $T_{\text{Reg}}$  cells were stained with CellTrace CFSE and  $T_{\text{Eff}}$  cells with CellTrace FarRed (both Invitrogen) for 15 min at 37°C. Rectangle miniature capillaries (CM Scientific) were coated with 5  $\mu\text{g/mL}$  rh MAdCAM-1 Fc Chimera (R&D Systems) in coating buffer (150 mM NaCl + 1 mM 4-(2-hydroxyethyl)-1-piperazine ethanesulfonic acid), then blocked with 5% BSA or 10% fetal bovine serum (FBS) in phosphate buffered saline (PBS). Cells were mixed in a 1:1 ratio and treated with or without 10 or 50  $\mu\text{g/mL}$  vedolizumab for 1 hour at 37°C. Next, cells were resuspended at a concentration of 1.5 Mio cells/mL in adhesion buffer (150 mM NaCl, 1 mM  $\text{CaCl}_2$ , 1 mM  $\text{MgCl}_2$ ) with 1 mM  $\text{MnCl}_2$  and then perfused through MAdCAM-1-coated capillaries for 3 min at a speed of 10  $\mu\text{L/min}$  using a peristaltic pump (Schenchen). Capillaries were rinsed for 5 min at a speed of

50  $\mu$ L/min and the adherent cells in the capillaries were imaged using a confocal microscope (Leica). Data analysis and quantification was performed using Fiji (National Institutes of Health).

### Single-cell RNA sequencing

Magnetic activated cell sorting-purified CD4<sup>+</sup> T cells were stained for dead cells with fixable viability dye (FVD) efluor780 (Invitrogen) and with the following fluorochrome-conjugated extracellular antibodies: CD4 (FITC, VIT4, Miltenyi Biotec), CD45RO (BV510, UCHL1, Biolegend), CD49d (VioBlue, MZ18-24A9, Miltenyi Biotec), integrin beta 7 (PE, FIB27, Biolegend) and 10  $\mu$ g/mL of AF647-labelled vedolizumab. Vedolizumab-negative (FVD<sup>-</sup>CD4<sup>+</sup>CD45RO<sup>+</sup>CD49d<sup>+</sup> $\beta$ 7<sup>+</sup>VDZ<sup>-</sup>) and vedolizumab-positive (FVD<sup>-</sup>CD4<sup>+</sup>CD45RO<sup>+</sup>CD49d<sup>+</sup> $\beta$ 7<sup>+</sup>VDZ<sup>+</sup>) memory CD4<sup>+</sup> T cells were sorted by FACS. Purified cells were washed, counted and viability was assessed by trypan blue staining. Cells were resuspended at a concentration of 1 Mio cells/mL in PBS+2% FBS. Single-cell RNA sequencing was performed at the Next-generation Sequencing Core facility of the University of Erlangen-Nuremberg using the Chromium Platform (10 $\times$  Genomics). Cells were subjected to 10 $\times$  Chromium Single Cell 3' Solution v3 library preparation according to the manufacturer's instructions. Library sequencing was performed on an Illumina HiSeq 2500 sequencer to a depth of 200 million reads each. Reads were converted to FASTQ format using mkfastq from Cell Ranger 3.0.1 (10 $\times$  Genomics). Reads were then aligned to the human reference genome v3.0.0 (10 $\times$  Genomics, GRCh38, Ensembl annotation release 93). Alignment was performed using the count command from Cell Ranger v3.0.1 (10 $\times$  Genomics) with standard parameters.

### Post-hoc analysis of vedolizumab phase III trials in patients with CD (Gemini II/III)

To study exposure-efficacy correlation in the Gemini II and III trials, we submitted a scientific request to Vivli. Following approval, this analysis was based on research using data from Takeda that has been made available through Vivli. Vivli has not contributed to or approved, and is not in any way responsible for the contents of this publication. To evaluate the relationship between vedolizumab trough levels and clinical remission at week 6, we determined the binary outcome 'clinical remission at week 6' considering the independent variable 'serum level at week 6' by the R-package mgcv (online supplemental file 2).<sup>24</sup> Serum level groups were defined based on our in vitro results and on data from our own patient cohort. Clinical remission was defined as a Crohn's Disease Activity Index score  $\leq$  150 points. Relative frequencies of clinical remission were calculated using Excel 2010 (Microsoft). Statistical analysis was performed with Prism 8.

## RESULTS

### Differential preferential binding of vedolizumab to T<sub>Reg</sub> and T<sub>Eff</sub> cells at different concentrations

To explore, whether non-linear exposure-efficacy correlations for vedolizumab might be due to  $\alpha$ 4 $\beta$ 7-expressing immune cells not binding vedolizumab, we analysed the frequency of  $\alpha$ 4<sup>+</sup> $\beta$ 7<sup>+</sup>VDZ<sup>-</sup> immune cells by flow cytometry using fluorescently labelled vedolizumab. We chose a concentration of 10  $\mu$ g/mL, which was in the range of trough levels associated with optimal outcomes in a phase II trial.<sup>22</sup> While the fraction of  $\alpha$ 4<sup>+</sup> $\beta$ 7<sup>+</sup> cells was highest in CD4<sup>+</sup> T cells and eosinophils, only a substantial portion of CD4<sup>+</sup> $\alpha$ 4<sup>+</sup> $\beta$ 7<sup>+</sup> T cells did not bind vedolizumab (online supplemental figure 1 and online supplemental

table 12). Thus, we decided to further focus on subsets of CD4<sup>+</sup> T cells.

To elucidate, whether vedolizumab binding to T<sub>Reg</sub> and T<sub>Eff</sub> cells differed at various concentrations, we used fluorescently labelled vedolizumab and performed flow cytometry analysis of PBMCs from patients with UC, CD and from healthy controls. We gated on CD4<sup>+</sup>CD127<sup>low</sup>CD25<sup>high</sup>Foxp3<sup>+</sup> T<sub>Reg</sub> cells and CD4<sup>+</sup>CD127<sup>high</sup>CD25<sup>low</sup> T<sub>Eff</sub> cells co-expressing integrin  $\alpha$ 4 and integrin  $\beta$ 7 and quantified the fraction of these cells that bound fluorescently labelled vedolizumab (online supplemental figure 2). Here, we used concentrations of up to 50  $\mu$ g/mL vedolizumab, a trough level that was associated with suboptimal outcomes in a phase II trial.<sup>22</sup>

The portion of  $\alpha$ 4<sup>+</sup> $\beta$ 7<sup>+</sup> cells was significantly higher in T<sub>Eff</sub> compared with T<sub>Reg</sub> cells and comparable between UC, CD and healthy controls (online supplemental figure 3A and online supplemental table 13), while the expression of  $\alpha$ 4 and  $\beta$ 7 per cell (as measured by mean fluorescence intensity (MFI)) was equal or higher on T<sub>Reg</sub> compared with T<sub>Eff</sub> cells (online supplemental figure 3B).

The portion of VDZ<sup>+</sup> cells among  $\alpha$ 4<sup>+</sup> $\beta$ 7<sup>+</sup> CD4<sup>+</sup> T cells was similar between T<sub>Reg</sub> and T<sub>Eff</sub> cells from healthy donors and higher on T<sub>Reg</sub> than on T<sub>Eff</sub> cells from patients with UC and CD after exposure with 0.4  $\mu$ g/mL vedolizumab. However, the fraction of VDZ<sup>+</sup> T<sub>Eff</sub> cells was significantly higher compared with T<sub>Reg</sub> cells in healthy donors after exposure with 2  $\mu$ g/mL vedolizumab and in all entities at 10  $\mu$ g/mL vedolizumab with some individual differences. Following exposure with 50  $\mu$ g/mL vedolizumab, virtually 100% of  $\alpha$ 4<sup>+</sup> $\beta$ 7<sup>+</sup> T<sub>Reg</sub> and T<sub>Eff</sub> cells were positive for vedolizumab (figure 1A,B). In an additional series of experiments, we sought to confirm that these differences were not due to  $\alpha$ 4 $\beta$ 7<sup>low</sup> naïve T cells in either population. However, we could reproduce our findings, when additionally gating on CD45RO to exclusively select memory T cells (online supplemental figure 3C).

Moreover, microscopic analysis of FACS-isolated T<sub>Reg</sub> and T<sub>Eff</sub> cells stained with a non-competing anti- $\beta$ 7 antibody and incubated with different concentrations of vedolizumab confirmed that less T<sub>Reg</sub> than T<sub>Eff</sub> cells bound vedolizumab at a concentration of 10  $\mu$ g/mL, which was not the case in cells exposed to 50  $\mu$ g/mL vedolizumab (figure 1C, online supplemental figure 3D).

We further explored, whether the activation status of the cells and associated differences in  $\alpha$ 4 $\beta$ 7 integrin conformation might be relevant for the differential binding pattern. However, we were also able to reproduce a right-shifted binding profile of T<sub>Reg</sub> cells following stimulation with MnCl<sub>2</sub>, phorbol-12-myristat-13-acetat/ionomycin and anti-CD3/CD28 (online supplemental figure 4, online supplemental table 14), suggesting that this is not the case.

In synopsis, our data showed that blocking  $\alpha$ 4 $\beta$ 7 integrin with vedolizumab on T<sub>Reg</sub> cells requires higher concentrations of the antibody compared with T<sub>Eff</sub> cells. This implied that clinical efficacy of vedolizumab might at least partly result from residual T<sub>Reg</sub> cell homing at concentrations already completely blocking T<sub>Eff</sub> cell homing.

### Differential vedolizumab binding to T<sub>Reg</sub> and T<sub>Eff</sub> cells leads to differential dose-dependent adhesion and transmigration profiles

To explore the functional relevance of our findings, we analysed FACS-purified CD4<sup>+</sup>CD127<sup>low</sup>CD25<sup>high</sup> T<sub>Reg</sub> and CD4<sup>+</sup>CD127<sup>high</sup>CD25<sup>low</sup> T<sub>Eff</sub> cells in functional assays in vitro.

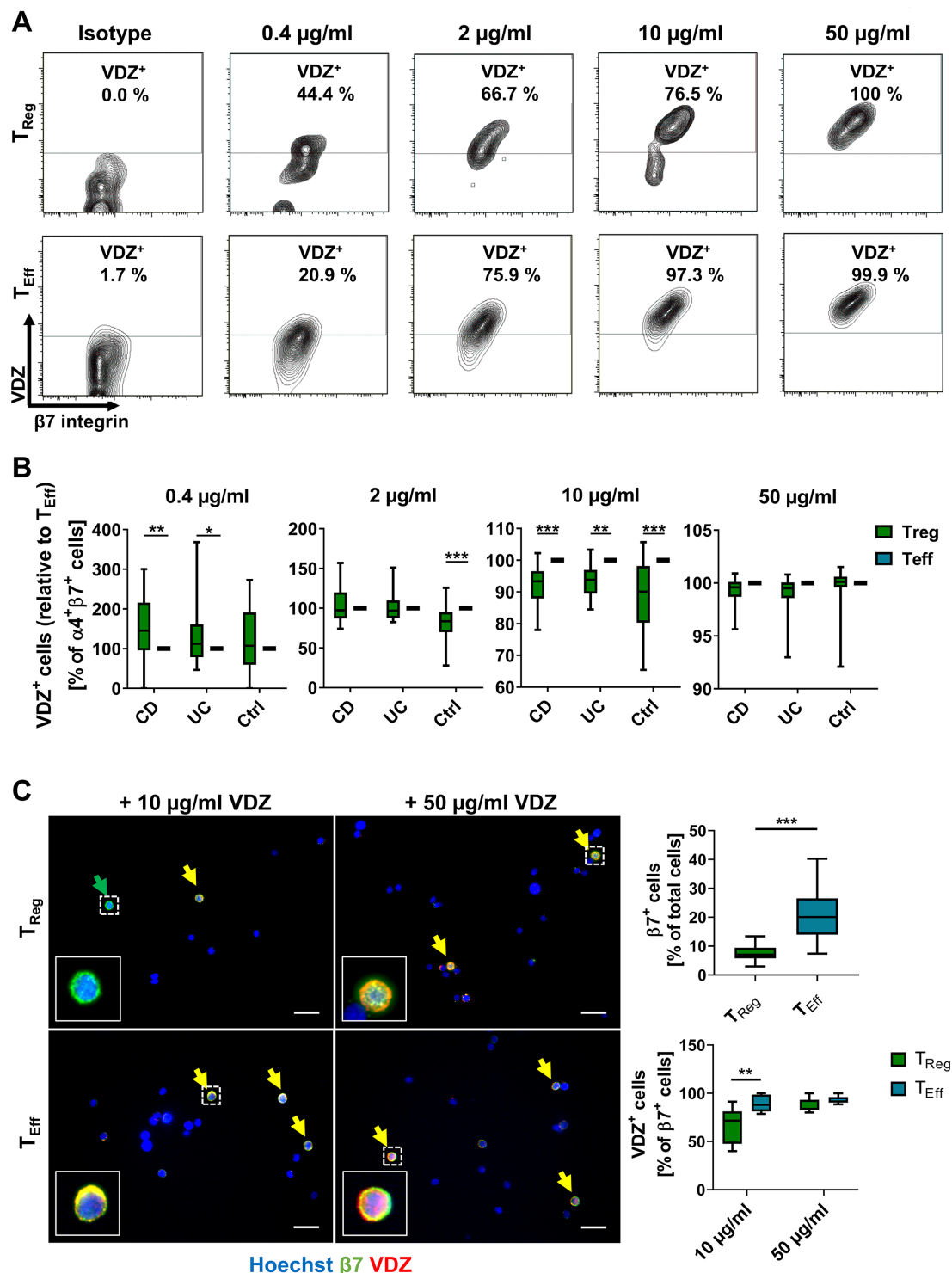


**Figure 1** Concentration-dependent binding profile of vedolizumab (VDZ) to T<sub>Reg</sub> and T<sub>Eff</sub> cells. Representative (A) and quantitative (B) flow cytometry of VDZ<sup>+</sup> cells after gating on α4β7<sup>+</sup> T<sub>Reg</sub> and T<sub>Eff</sub> cells following incubation with the indicated concentrations of fluorescently labelled VDZ. Quantitative data are expressed relative to T<sub>Reg</sub> cells. n=17–28 patients with IBD or healthy controls as indicated. (C) Representative (left) and quantitative (right) fluorescence microscopy of FACS-purified T<sub>Reg</sub> and T<sub>Eff</sub> cells stained with anti-β7 antibody (green) and different concentrations of fluorescently labelled VDZ (red) and counterstained with Hoechst (blue); scale bar 10 µm. Quantification of β7<sup>+</sup> and β7<sup>+</sup>VDZ<sup>+</sup> cells in eight high-power fields. n=5–6 (cells purified from leucocyte cones). Significant outliers were identified using Grubbs test and excluded from the analysis. Statistical comparisons were performed using two-way analysis of variance (ANOVA) with Sidak's multiple comparison test (A, B) and Student's t-test and mixed-effects analysis with Sidak's multiple comparison test (C). Sample donor characteristics are listed in online supplemental table 2. CD, Crohn's disease; FACS, fluorescence-activated cell sorting; T<sub>Eff</sub>, effector T cell; T<sub>Reg</sub>, regulatory T cell.

Sorting achieved a purity of >99% for both cell types, cells were viable and  $T_{Reg}$  cells exhibited marked suppressive abilities, when co-cultured with  $T_{Eff}$  cells (online supplemental figure 5).

We analysed the impact of in vitro treatment with vedolizumab on the dynamic adhesion of  $T_{Reg}$  and  $T_{Eff}$  cells to MAdCAM-1 (figure 2A). We focused on 10  $\mu\text{g}/\text{mL}$  and 50  $\mu\text{g}/\text{mL}$  as the most clinically relevant concentrations.<sup>25</sup> Consistent

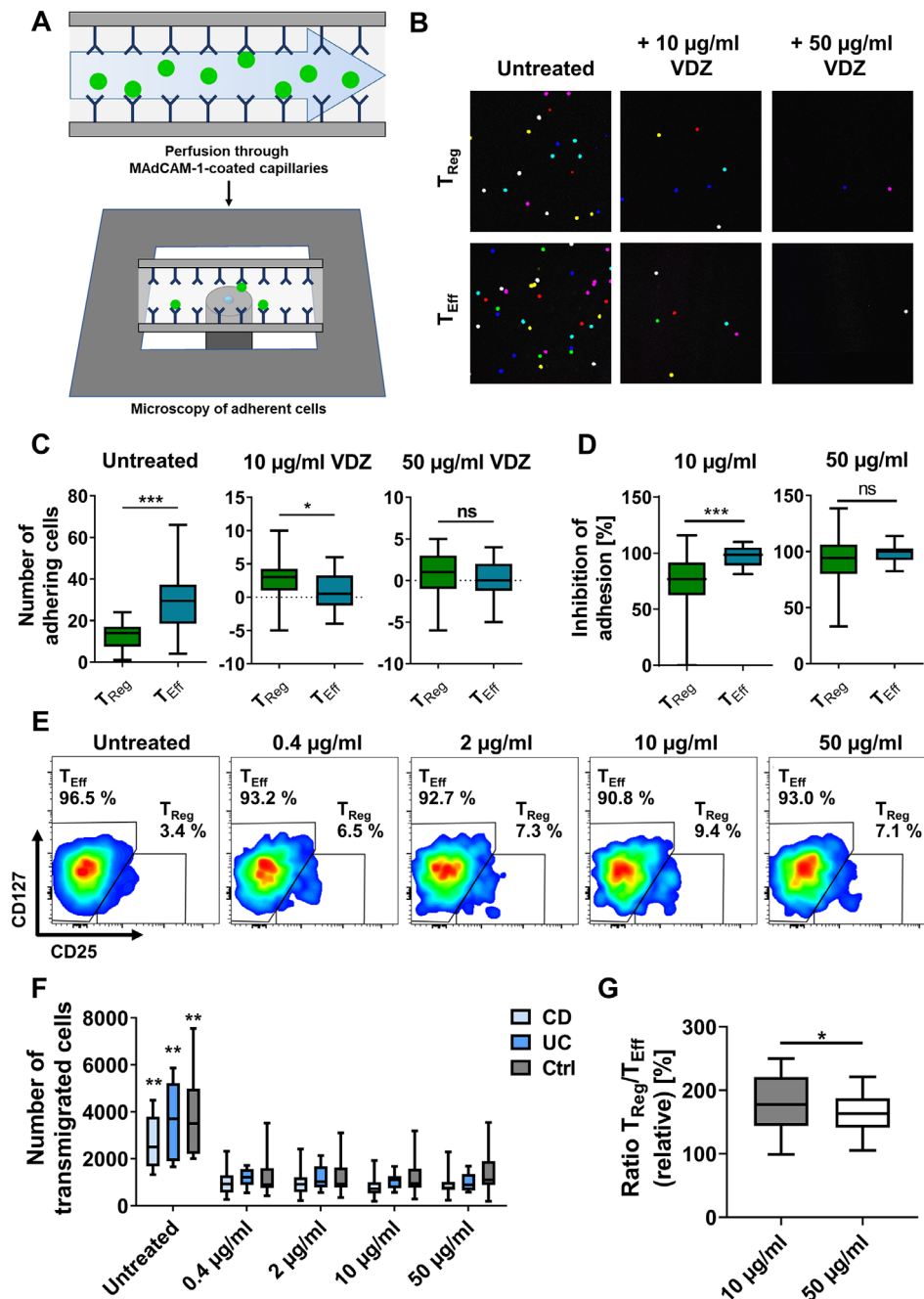


**Figure 2** Concentration-dependent adhesion and transmigration of  $T_{Reg}$  and  $T_{Eff}$  cells in functional assays in vitro. (A–D) Dynamic adhesion of  $T_{Reg}$  and  $T_{Eff}$  cells treated with different concentrations of vedolizumab to MAdCAM-1. (A) Schematic representation of the experimental setup; fluorescently labelled  $T_{Reg}$  and  $T_{Eff}$  cells were incubated with different concentrations of VDZ, perfused through MAdCAM-1-coated capillaries and adhering cells were quantified using confocal microscopy. (B) Representative microscopic images of adhered cells (overlay of counted high-power fields) and (C) quantification of the background-corrected number of  $T_{Reg}$  and  $T_{Eff}$  cells incubated with or without 10 or 50  $\mu\text{g}/\text{mL}$  VDZ adhering to MAdCAM-1. (D) Relative inhibition of adhesion of  $T_{Reg}$  and  $T_{Eff}$  cells to MAdCAM-1 after treatment with 10 or 50  $\mu\text{g}/\text{mL}$  VDZ.  $n=22$  (cells purified from leucocyte cones). (E–G) Transmigration assays with  $CD4^+$  T cells. The fraction of  $T_{Reg}$  and  $T_{Eff}$  cells in the transmigration cells was quantified by flow cytometry. Representative (E) and quantitative flow cytometry (F) of transmigration  $CD4^+$  cells after treatment with different concentrations of VDZ.  $**p<0.01$  compared with all treatment groups. (G)  $T_{Reg}/T_{Eff}$  ratio of transmigration cells after treatment with 10 versus 50  $\mu\text{g}/\text{mL}$  VDZ (G).  $n=8$ –17 patients with IBD or healthy controls as indicated. Statistical comparisons were performed using paired t-test (C, D) and mixed-effects analysis with Tukey's multiple comparisons test and paired t-test (F, G). Sample donor characteristics are listed in online supplemental table 3. CD, Crohn's disease; MAdCAM-1, mucosal addressin cell adhesion molecule-1;  $T_{Eff}$ , effector T cell;  $T_{Reg}$ , regulatory T cell; VDZ, vedolizumab.

with  $\alpha 4\beta 7$  integrin expression, adhesion was significantly higher for untreated  $T_{\text{Eff}}$  compared with untreated  $T_{\text{Reg}}$  cells (figure 2B,C). Either treatment led to a reduction of the dynamic adhesion of both cell types. However, inhibition of adhesion of  $T_{\text{Reg}}$  cells was substantially lower compared with  $T_{\text{Eff}}$  cells after treatment with 10  $\mu\text{g}/\text{mL}$  vedolizumab, while almost complete inhibition of adhesion and no difference between  $T_{\text{Reg}}$  and  $T_{\text{Eff}}$  cells could be observed after treatment with 50  $\mu\text{g}/\text{mL}$  vedolizumab (figure 2D).

In a second approach, we investigated the impact of different concentrations of vedolizumab on MAdCAM-1-dependent transmigration of  $T_{\text{Reg}}$  and  $T_{\text{Eff}}$  cells in vitro. T cells were left to transmigrate towards CCL25 over MAdCAM-1-coated transwell plates with 3  $\mu\text{m}$  pores in the presence of different vedolizumab concentrations. Treatment with all concentrations of vedolizumab led to a significant and similar reduction of transmigration of cells from patients with UC and CD as well as healthy controls. However, the ratio of transmigrated  $T_{\text{Reg}}$  to  $T_{\text{Eff}}$  cells was substantially higher after treatment with 10  $\mu\text{g}/\text{mL}$  vedolizumab compared with 50  $\mu\text{g}/\text{mL}$  (figure 2E–G).

Taken together, these data supported the notion that differential binding of vedolizumab to  $T_{\text{Reg}}$  and  $T_{\text{Eff}}$  cells has functional implications for T cell adhesion and transmigration.

### Differential vedolizumab binding to $T_{\text{Reg}}$ and $T_{\text{Eff}}$ cells leads to differential homing to the inflamed gut in vivo

We next aimed to address, whether we could detect similar effects in vivo. To this end, we made use of a previously described humanised mouse model of T cell homing to the inflamed gut (figure 3A), in which we had earlier shown a comparable or even higher reduction of  $T_{\text{Reg}}$  cell homing to the gut after treatment with high vedolizumab concentrations.<sup>10</sup> Based on our above findings, we now investigated the effect of treatment with 10  $\mu\text{g}/\text{mL}$  vedolizumab. Intravital confocal microscopy demonstrated active trafficking of the transferred cells (figure 3B). As expected, more untreated  $T_{\text{Eff}}$  cells homed to the gut compared with untreated  $T_{\text{Reg}}$  cells. Interestingly, treatment with 10  $\mu\text{g}/\text{mL}$  vedolizumab led to substantially reduced homing of  $T_{\text{Eff}}$  cells, while  $T_{\text{Reg}}$  cell homing was not significantly affected as assessed by flow cytometry and lightsheet fluorescence microscopy (figure 3C,D). These observations further supported our concept of differential responses of T cell subsets to vedolizumab.

### Differential vedolizumab binding to $T_{\text{Reg}}$ and $T_{\text{Eff}}$ cells correlates with the availability of $\alpha 4\beta 7$ integrin in vivo

We reasoned that for in vivo action of vedolizumab in patients with IBD, the remaining availability of free  $\alpha 4\beta 7$  molecules at a certain exposure is crucial. Thus, to understand, how different vedolizumab concentrations affect available  $\alpha 4\beta 7$  integrin, we exposed PBMCs to ascending doses of vedolizumab in vitro and subsequently labelled free binding sites. While we observed no significant difference in the ratio of  $T_{\text{Reg}}$  and  $T_{\text{Eff}}$  cells with free vedolizumab binding sites at a concentration of 2  $\mu\text{g}/\text{mL}$ , a significantly higher portion of  $T_{\text{Reg}}$  compared with  $T_{\text{Eff}}$  cells had free  $\alpha 4\beta 7$  molecules available on their surface after incubation with 10 and 50  $\mu\text{g}/\text{mL}$  vedolizumab. At a concentration of 110  $\mu\text{g}/\text{mL}$  vedolizumab (in the range of the highest serum levels observed in patients<sup>25</sup>), the abundance of cells with free binding sites was similar again (figure 4A,B, online supplemental figure 6A,B), further supporting the concept of a right-shifted  $T_{\text{Reg}}$  cell response to vedolizumab.

To explore, whether this holds also true in vivo, we determined the serum trough levels in patients with IBD receiving vedolizumab therapy at week 2 and 6 and simultaneously

determined free binding sites. In an exploratory analysis, we observed an optimum in the ratio of  $T_{\text{Reg}}$  and  $T_{\text{Eff}}$  cells with free  $\alpha 4\beta 7$  molecules available in the range of 40 to 55  $\mu\text{g}/\text{mL}$  vedolizumab trough level and a significantly reduced ratio at even higher serum levels (figure 4C, online supplemental figure 6C).

In conclusion, these data suggested that certain vedolizumab exposure levels go along with higher residual availability of functional  $\alpha 4\beta 7$  integrin on  $T_{\text{Reg}}$  compared with  $T_{\text{Eff}}$  cells in patients with IBD in vivo.

### Single-cell RNA sequencing identifies an $ITGB1^+PI16^+$ $T_{\text{Reg}}$ cell subset 'resistant' to vedolizumab

To further dissect the mechanisms underlying our observations, we decided to use single-cell RNA sequencing. To this end, we FACS-purified  $CD4^+CD45RO^+\alpha 4^+\beta 7^+$  cells binding fluorescently labelled vedolizumab ( $VDZ^+$ ) or not ( $VDZ^-$ ) at a concentration of 10  $\mu\text{g}/\text{mL}$ . Re-analysis of sorted cells confirmed that all selected cells expressed the integrins  $\alpha 4$  and  $\beta 7$  (online supplemental figure 7A). Moreover, we observed that the vast majority of  $\alpha 4^+\beta 7^+VDZ^-$  cells also stained positive for fluorescently labelled MAdCAM-1 (online supplemental figure 7B) and observed dynamic adhesion of  $CD4^+CD45RO^+\alpha 4^+\beta 7^+VDZ^-$  cells to MAdCAM-1, corroborating that  $\alpha 4\beta 7$  integrin expressed on cells not binding vedolizumab is functional (online supplemental figure 7C).

Following single-cell sequencing,  $VDZ^-$  and  $VDZ^+$  samples were merged for comparative analysis. Clustering analysis using unique molecular identifiers at a resolution of 1 identified 11 distinct clusters (figure 5A). Using eight different marker genes (online supplemental figure 8A,B), clusters 9 and 10 were identified as  $T_{\text{Reg}}$  cell clusters (figure 5B).

Our further analyses showed that—consistent with our previous data—the fraction of  $T_{\text{Reg}}$  cells was higher in the  $VDZ^-$  compared with the  $VDZ^+$  sample (figure 5B). Interestingly, the  $VDZ^- T_{\text{Reg}}$  cells also expressed  $T_{\text{Reg}}$  marker genes to a higher extent than  $VDZ^+ T_{\text{Reg}}$  cells (online supplemental figure 8C). When comparing  $VDZ^-$  and  $VDZ^+ T_{\text{Reg}}$  and  $T_{\text{Eff}}$  cells, we identified a specific signature of differentially expressed genes, many of which were associated with adhesion, extravasation and chemotaxis (figure 5C). As we aimed to characterise  $\alpha 4\beta 7$ -expressing  $T_{\text{Reg}}$  cells not binding vedolizumab, we further focused on  $VDZ^-$  in comparison with  $VDZ^+ T_{\text{Reg}}$  cells. Taking into account differential gene expression and the fraction of cells expressing the relevant genes, we identified a distinct  $T_{\text{Reg}}$  cell subpopulation expressing  $ITGB1$ ,  $PI16$  and  $CCR10$ , but not expressing  $CCR9$  and  $CD38$  that was predominant in the  $VDZ^-$  sample and almost completely absent in the  $VDZ^+$  sample (figure 5D, online supplemental table 16).

### $\beta 1^+PI16^+ T_{\text{Reg}}$ cells show reduced vedolizumab binding in vitro and in vivo

To validate our findings, we stained PBMCs from healthy controls with antibodies against the different molecules identified above. We confirmed that a significantly higher portion of  $T_{\text{Reg}}$  cells not binding  $VDZ$  at 10  $\mu\text{g}/\text{mL}$  expressed  $PI16$  and  $\beta 1$  integrin compared with vedolizumab-binding  $T_{\text{Reg}}$  cells (figure 6A). Vice versa, the abundance of  $VDZ^+$  cells was lower in  $\alpha 4\beta 7$ -expressing  $T_{\text{Reg}}$  cells positive for  $PI16$  or  $\beta 1$  (figure 6B). Consistently, co-expression of  $\beta 1$  integrin and  $PI16$  was observed in substantially more  $VDZ^-$  compared with  $VDZ^+$  cells and vedolizumab binding to  $\beta 1^+PI16^+$  cells was clearly lower than to  $\beta 1^-PI16^-$  cells (figure 6C).

Next, we obtained PBMCs from patients with IBD receiving clinical treatment with vedolizumab and assessed free vedolizumab binding sites (BS) on  $T_{\text{Reg}}$  cells together with the

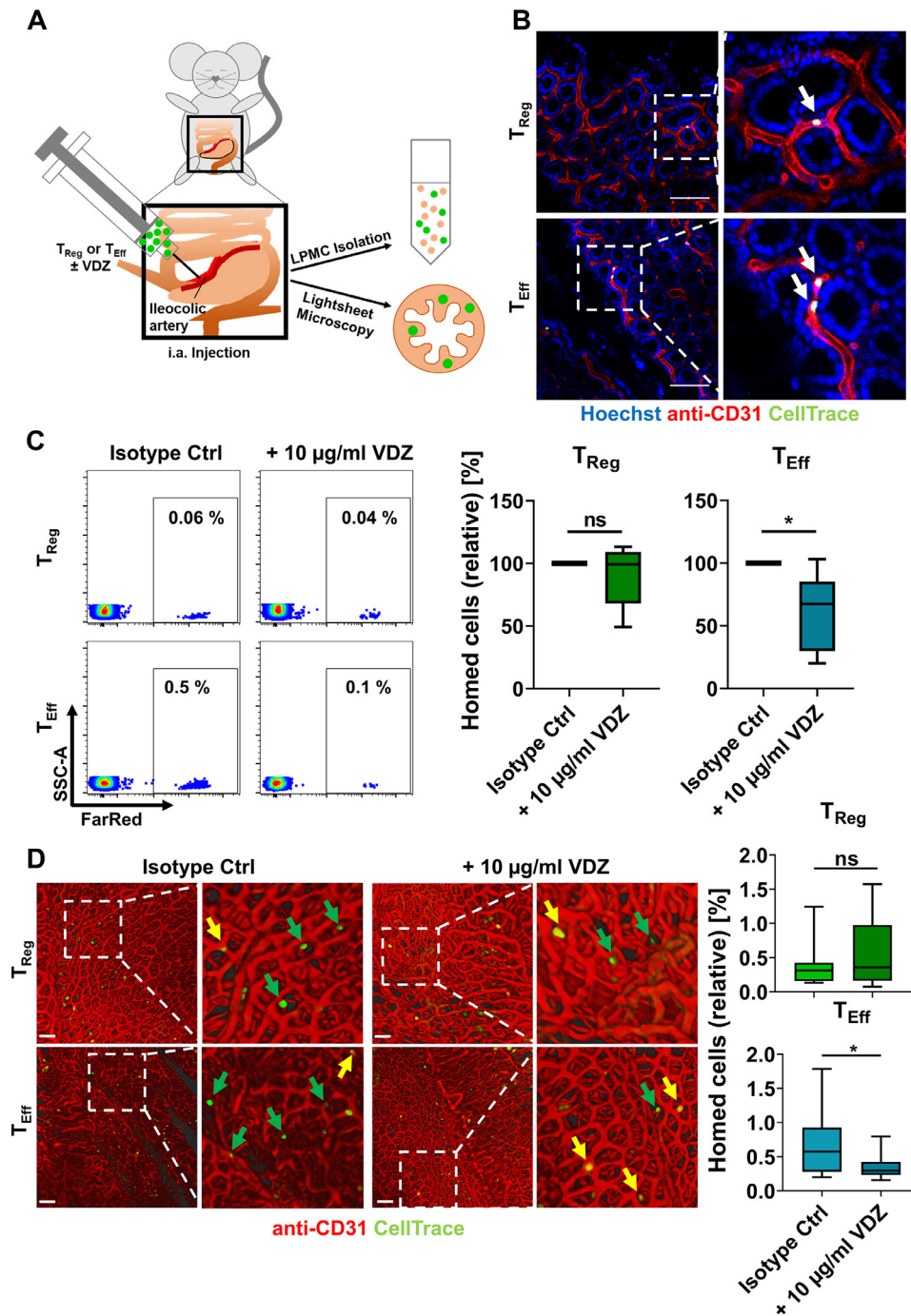


**Figure 3** In vivo homing of  $T_{Reg}$  and  $T_{Eff}$  cells in a humanised mouse model. (A) Schematic representation of in vivo homing assays. Fluorescently labelled  $T_{Reg}$  or  $T_{Eff}$  cells  $\pm 10 \mu\text{g/mL}$  VDZ were injected into the ileocolic artery of anaesthetised mice for subsequent quantification of homed cells by LPMC isolation and flow cytometry or lightsheet microscopy. (B) Visualisation of homed cells (green) using intravital confocal microscopy. Red: blood vessels stained with anti-CD31; blue: nuclear counter-stain with Hoechst. Arrows indicate adhering human cells. Scale bar  $100 \mu\text{m}$ . (C) Representative (left) and quantitative (right) flow cytometry of FarRed<sup>+</sup> human  $T_{Reg}$  and  $T_{Eff}$  cells accumulating in the lamina propria of Rag1<sup>-/-</sup> mice after treatment with either isotype control or with  $10 \mu\text{g/mL}$  VDZ.  $n=6$  per group (cells purified from leucocyte cones). (D) Representative (left) and quantitative (right) lightsheet fluorescence microscopy. Arrows indicate adherent cells still inside the vasculature (yellow) or extravasated into the tissue (green). Quantification of homed cells in 15 representative 3D cubes from three individual experiments (relative to the number of injected cells). Scale bar  $100 \mu\text{m}$ . Statistical comparisons were performed using one-sample t-test and Student's t-test. LPMC, lamina propria mononuclear cells;  $T_{Eff}$ , effector T cell;  $T_{Reg}$ , regulatory T cell; VDZ, vedolizumab.

expression of the above markers. We observed that among  $T_{Reg}$  cells expressing  $\alpha 4 \beta 7$  integrin with free binding sites for vedolizumab, cells expressing  $\beta 1$  and PI16 were significantly more abundant than among  $T_{Reg}$  cells already saturated with vedolizumab (figure 6D). Furthermore, among  $\beta 1^+ \text{PI16}^+$   $T_{Reg}$

cells, substantially more cells had free vedolizumab binding sites available than among  $\beta 1^+ \text{PI16}^-$   $T_{Reg}$  cells (figure 6E).

Together, these data corroborated our in silico findings and suggested that a  $\beta 1^+ \text{PI16}^+$   $T_{Reg}$  cell subset is the substrate of differential vedolizumab binding to  $T_{Reg}$  and  $T_{Eff}$  cells.

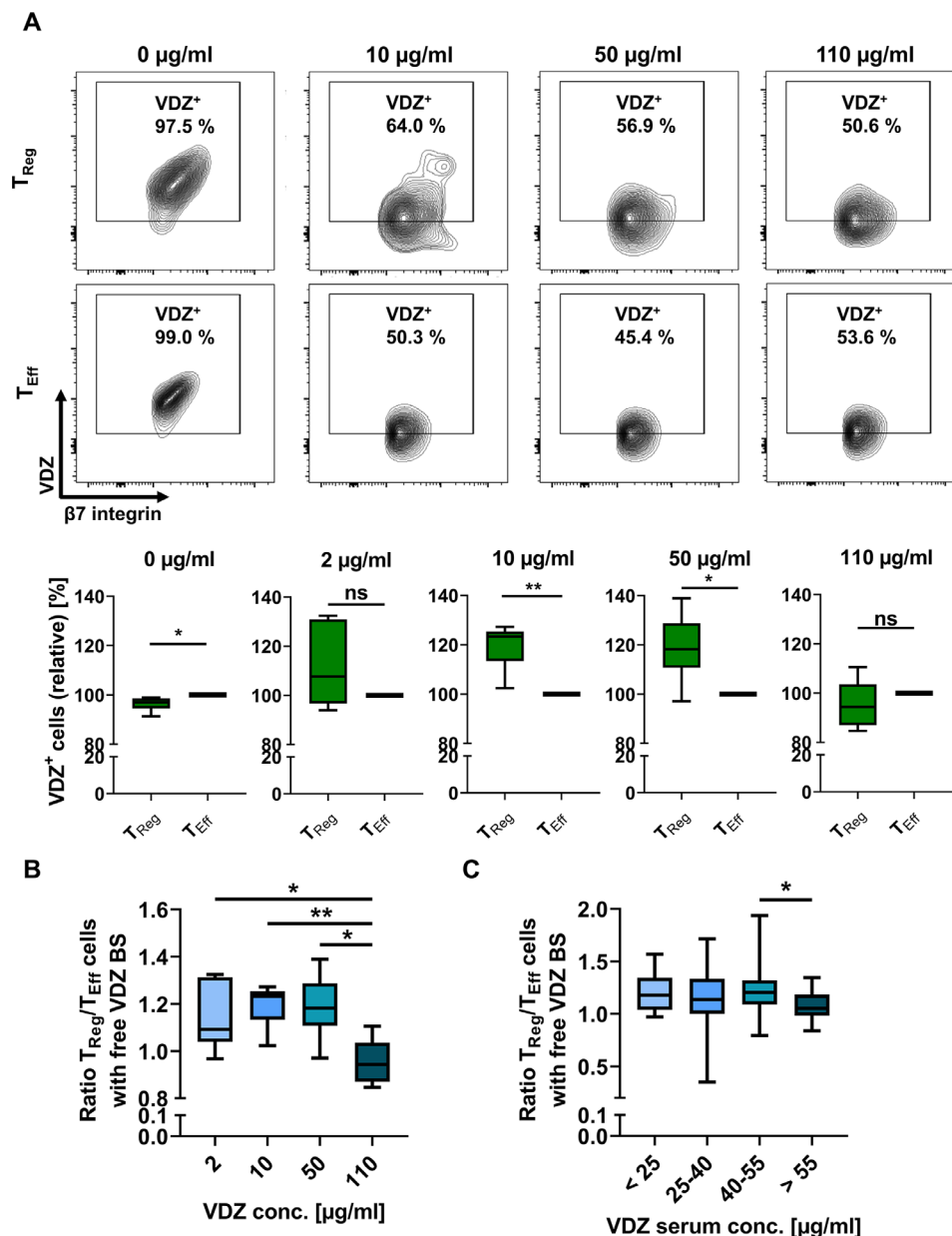


**Figure 4** Quantification of T<sub>Reg</sub> and T<sub>Eff</sub> cells with free vedolizumab binding sites in vitro and in vivo. (A) Representative and quantitative flow cytometry of free VDZ binding sites on  $\alpha 4^+ \beta 7^+$  T<sub>Reg</sub> and T<sub>Eff</sub> cells after incubation with different concentrations of unlabelled VDZ in vitro and consecutive staining with saturating concentrations of fluorescently labelled VDZ. Quantitative data are expressed relative to T<sub>Eff</sub> cells. n=5–6 patients with IBD and healthy controls. (B) T<sub>Reg</sub>/T<sub>Eff</sub> ratio of cells with free vedolizumab binding sites (free VDZ BS) after treatment with different concentrations of vedolizumab. n=5–6 patients with IBD and healthy controls. (C) T<sub>Reg</sub>/T<sub>Eff</sub> ratio of cells with free vedolizumab binding sites in patients undergoing vedolizumab therapy stratified according to VDZ trough levels. Staining was performed at week 2 and/or 6 of treatment, trough levels were determined using vedolizumab drug level ELISA. n=8–58 samples from patients with IBD per serum group, some patients provided blood at week 2 and week 6. Statistical comparisons were performed using one-sample t-test (A) and Student's t-test (B, C). Sample donor characteristics are listed in online supplemental tables 4 and 5. T<sub>Eff</sub>, effector T cell; T<sub>Reg</sub>, regulatory T cell.

### Vedolizumab-resistant' $\beta 1^+ \text{PI16}^+$ T<sub>Reg</sub> cells show a pronounced regulatory phenotype

Next, we aimed to further characterise the function of this T<sub>Reg</sub> cell subset. Transcript levels in our single-cell dataset suggested that T<sub>Reg</sub> cells not binding vedolizumab express a high level of regulatory markers and might therefore be a particularly suppressive cell population (online supplemental figure 8C).

Thus, we performed flow cytometry of CD4<sup>+</sup>CD25<sup>high</sup>C-D127<sup>low</sup> $\alpha 4^+ \beta 7^+$  T<sub>Reg</sub> cells co-expressing integrin  $\beta 1$  and PI16 or not. We observed higher expression of CD25 per cell on  $\beta 1^+ \text{PI16}^+$  than on  $\beta 1^- \text{PI16}^-$  gut-homing T<sub>Reg</sub> cells (figure 7A). In

addition, more  $\beta 1^+ \text{PI16}^+$  T<sub>Reg</sub> cells expressed Foxp3 and GTR and also to a higher extent (figure 7B,C). Functionally, after in vitro stimulation, a massively higher portion of  $\beta 1^+ \text{PI16}^+$  T<sub>Reg</sub> cells than  $\beta 1^- \text{PI16}^-$  T<sub>Reg</sub> cells produced the suppressive cytokine IL-10 (figure 7D). These observations could also be reproduced using PBMCs from patients with IBD (online supplemental figure 9, online supplemental table 15). Finally, using in vitro co-culture suppression assays, VDZ<sup>-</sup>, but not VDZ<sup>+</sup> T<sub>Reg</sub> cells clearly inhibited T<sub>Eff</sub> cell proliferation (figure 7E).

In a next step, we aimed to elucidate, whether the subset identified was also present in the gut of patients with IBD. Therefore,

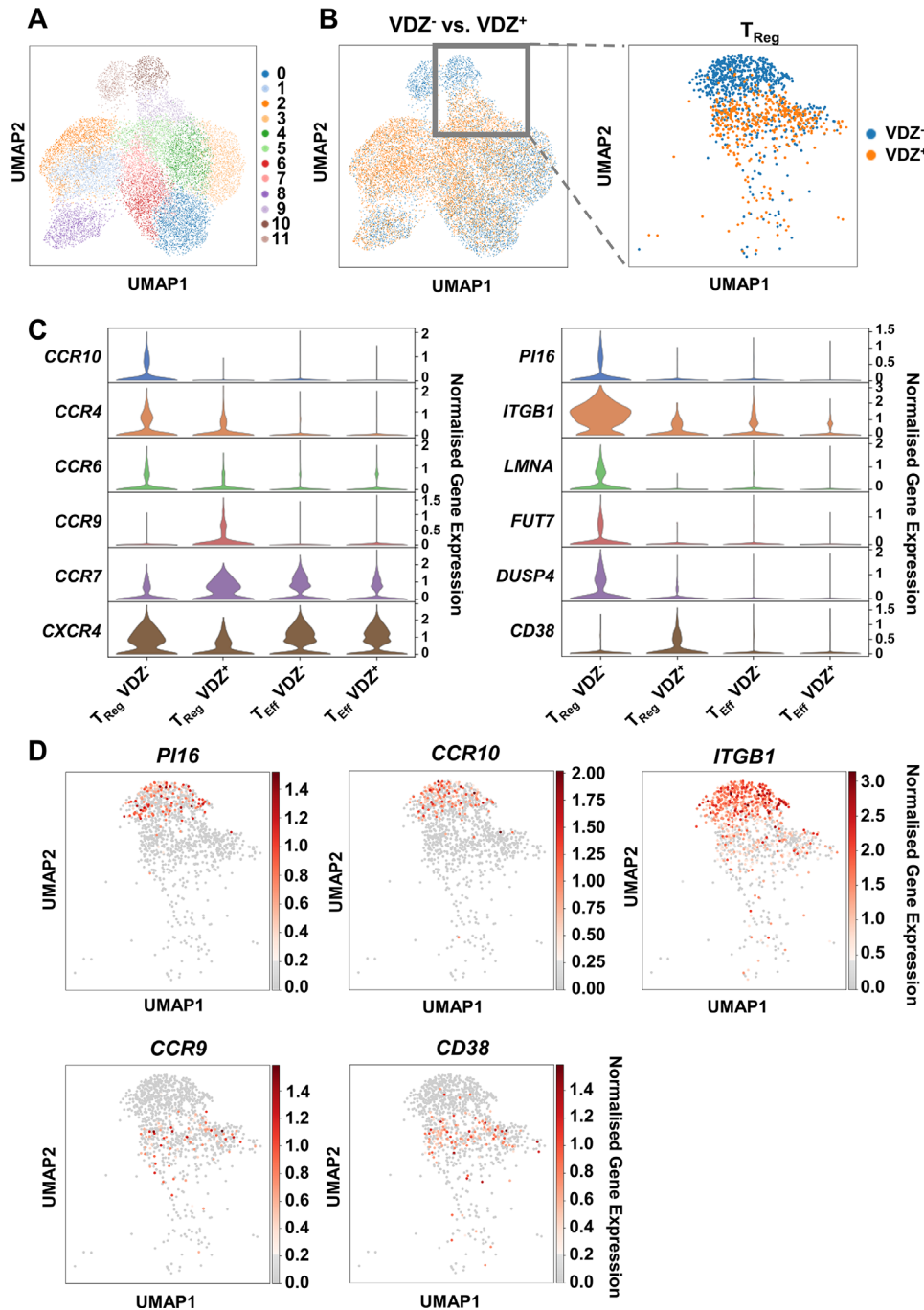


**Figure 5** Single-cell RNA-sequencing of  $CD4^+CD45RO^+\alpha4\beta7^+VDZ^+$  and  $CD4^+CD45RO^+\alpha4\beta7^+VDZ^-$  cells. (A) UMAP plot showing clustering of 14 265 cells based on Leiden algorithm at resolution 1. (B) UMAP plots showing the distribution of cells from the  $VDZ^+$  and  $VDZ^-$  sample in all cells (left panel) and in the  $T_{Reg}$  cell clusters 9 and 10 (right panel). (C) Violin plots displaying the differential gene expression of selected genes in the  $T_{Reg}$  and  $T_{Eff}$  cell clusters from the  $VDZ^+$  and  $VDZ^-$  sample. (D) UMAP plots of the  $T_{Reg}$  cell subclusters showing cells expressing *PI16*, *CCR10*, *ITGB1*, *CCR9* and *CD38*.  $T_{Eff}$  effector T cell;  $T_{Reg}$  regulatory T cell; UMAP, uniform manifold approximation and projection; VDZ, vedolizumab.

we performed in silico analyses with a publically available single-cell RNA sequencing dataset of  $CD45^+$  cells from the rectum of 11 patients with UC (GSE162335). We identified  $T_{Reg}$  cells and compared the expression of several key regulatory genes between  $\beta1^+PI16^+$  and other  $T_{Reg}$  cells. In line with our single-cell data from the peripheral blood, we observed that many of these genes were expressed by a larger fraction of  $\beta1^+PI16^+$  cells or at higher levels in these cells (figure 8A,B). To confirm these transcriptomic data, we isolated lamina propria mononuclear cells (LPMCs) from gut biopsies of patients with IBD

and analysed  $CD4^+CD25^{high}CD127^{low}Foxp3^+\beta7^+T_{Reg}$  cells co-expressing integrin  $\beta1$  and *PI16* or not using flow cytometry (online supplemental figure 10).  $\beta1^+PI16^+T_{Reg}$  cells demonstrated a clearly higher expression of *CD25* per cell (as determined by MFI) compared with  $\beta1^-PI16^-T_{Reg}$  cells (figure 8C). Moreover, in vitro stimulation of LPMCs led to a significantly higher portion of  $\beta1^+PI16^+$  than  $\beta1^-PI16^-T_{Reg}$  cells producing IL-10 (figure 8D).

Collectively, these data strongly supported the notion that vedolizumab-resistant  $\beta1^+PI16^+$  gut-homing  $T_{Reg}$  cells have a

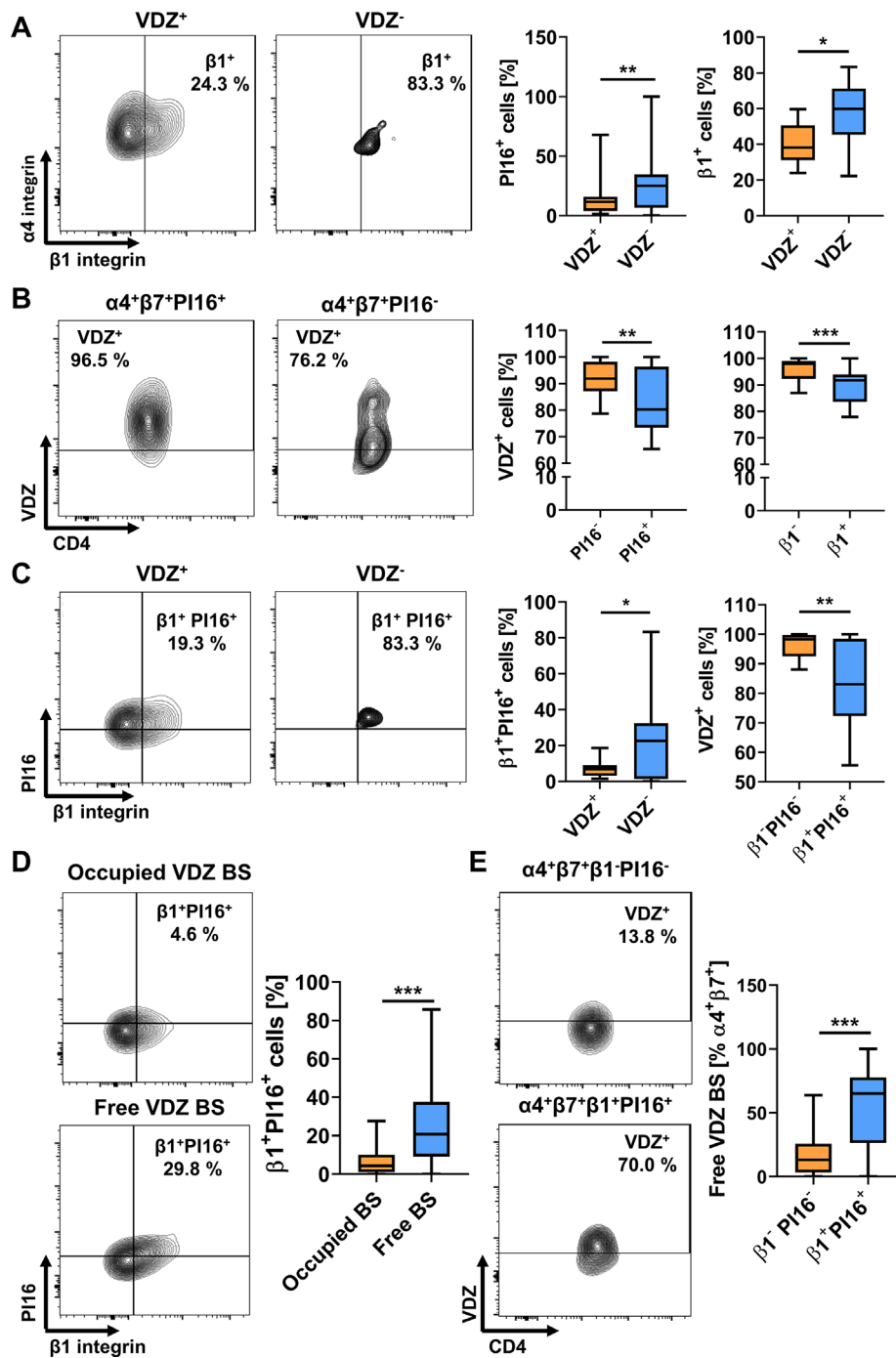


**Figure 6** Flow cytometric validation of differentially expressed marker genes between  $\text{VDZ}^{+}$  and  $\text{VDZ}^{-}$   $\text{T}_{\text{Reg}}$  cells in vitro and in vivo. (A) Representative (left) and quantitative (right) flow cytometry showing the fraction of  $\alpha 4 \beta 7^{+} \text{T}_{\text{Reg}}$  cells binding ( $\text{VDZ}^{+}$ ) or not binding ( $\text{VDZ}^{-}$ ) vedolizumab at a concentration of 10  $\mu\text{g/mL}$  and expressing PI16 or integrin  $\beta 1$ .  $n=14$  healthy donors. (B) Representative (left) and quantitative (right) flow cytometry showing vedolizumab binding to  $\alpha 4 \beta 7^{+} \text{T}_{\text{Reg}}$  cells expressing PI16 or integrin  $\beta 1$ .  $n=16$  healthy donors. (C) Representative (left) and quantitative (right) flow cytometry showing the fraction of  $\alpha 4 \beta 7^{+} \text{T}_{\text{Reg}}$  cells binding ( $\text{VDZ}^{+}$ ) or not binding ( $\text{VDZ}^{-}$ ) vedolizumab at a concentration of 10  $\mu\text{g/mL}$  and co-expressing PI16 and integrin  $\beta 1$  or showing vedolizumab binding to  $\alpha 4 \beta 7^{+} \text{T}_{\text{Reg}}$  cells co-expressing PI16 and integrin  $\beta 1$ .  $n=16$  healthy donors. (D) Representative (left) and quantitative (right) flow cytometry showing the fraction of  $\alpha 4 \beta 7^{+} \text{T}_{\text{Reg}}$  cells with occupied or with free vedolizumab binding sites (VDZ BS) expressing integrin  $\beta 1$  and PI16 in patients treated with vedolizumab.  $n=57$  samples from patients with IBD, some patients provided blood at week 2 and week 6. (E) Representative (left) and quantitative (right) flow cytometry showing free vedolizumab binding sites on  $\beta 1^{+} \text{PI16}^{+} \alpha 4 \beta 7^{+} \text{T}_{\text{Reg}}$  cells.  $n=57$  samples from patients with IBD, some patients provided blood at week 2 and week 6. Statistical comparisons were performed using paired t-test. Sample donor characteristics are listed in online supplemental tables 6 and 7.  $\text{T}_{\text{Eff}}$  effector T cell;  $\text{T}_{\text{Reg}}$  regulatory T cell.

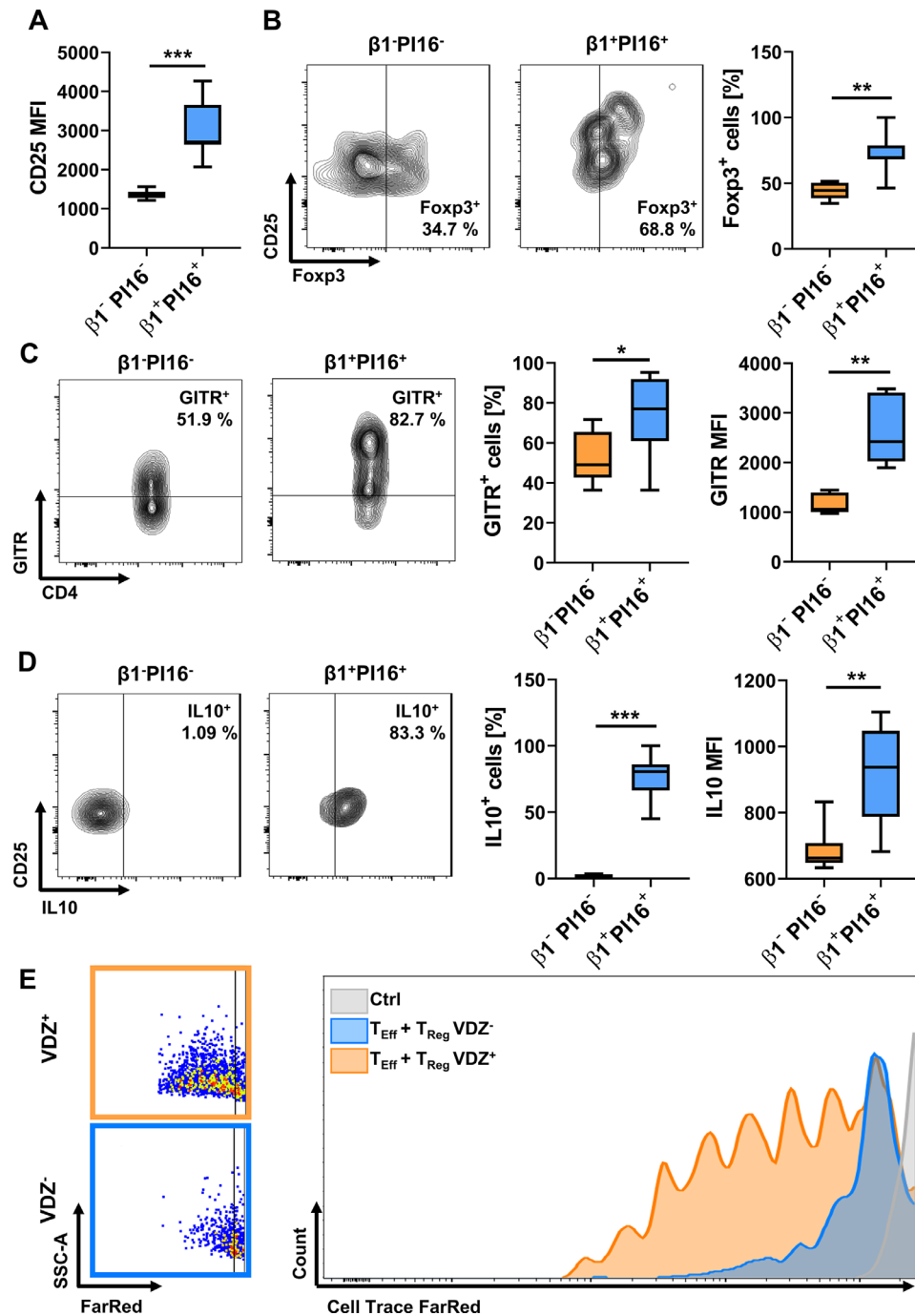


**Figure 7** Characterisation of vedolizumab-resistant  $\beta 1^+PI16^+ \alpha 4^+ \beta 7^+ T_{Reg}$  cells in the peripheral blood. (A) Quantitative flow cytometry showing mean fluorescence intensity (MFI) of CD25 on  $\beta 1^+PI16^+ \alpha 4^+ \beta 7^+ T_{Reg}$  compared with  $\beta 1^+PI16^- \alpha 4^+ \beta 7^+ T_{Reg}$  cells.  $n=8$  healthy donors. (B) Representative (left) and quantitative (right) flow cytometry showing the frequency of Foxp3-expressing  $\beta 1^+PI16^+ \alpha 4^+ \beta 7^+ T_{Reg}$  compared with  $\beta 1^+PI16^- \alpha 4^+ \beta 7^+ T_{Reg}$  cells.  $n=8$  healthy donors. (C) Representative (left) and quantitative (right) flow cytometry showing the frequency and mean fluorescence intensity (MFI) of GITR on  $\beta 1^+PI16^+ \alpha 4^+ \beta 7^+ T_{Reg}$  compared with  $\beta 1^+PI16^- \alpha 4^+ \beta 7^+ T_{Reg}$  cells.  $n=6$  healthy donors. (D) Representative (left) and quantitative (right) flow cytometry showing the frequency and the mean fluorescence intensity (MFI) of IL-10 on  $\beta 1^+PI16^+ \alpha 4^+ \beta 7^+ T_{Reg}$  compared with  $\beta 1^+PI16^- \alpha 4^+ \beta 7^+ T_{Reg}$  cells after incubation with PMA, ionomycin and brefeldin A for 4 hours.  $n=8$  healthy donors. (E) Representative flow cytometry of  $T_{Eff}$  cell proliferation as determined by dilution of CellTrace FarRed. Representative images from one out of five independent experiment (cells purified from leucocyte cones). Statistical significance was calculated using paired t-test. Sample donor characteristics are listed in online supplemental table 8. PMA, phorbol-12-myristat-13-acetat;  $T_{Eff}$  effector T cell;  $T_{Reg}$  regulatory T cell; VDZ, vedolizumab.

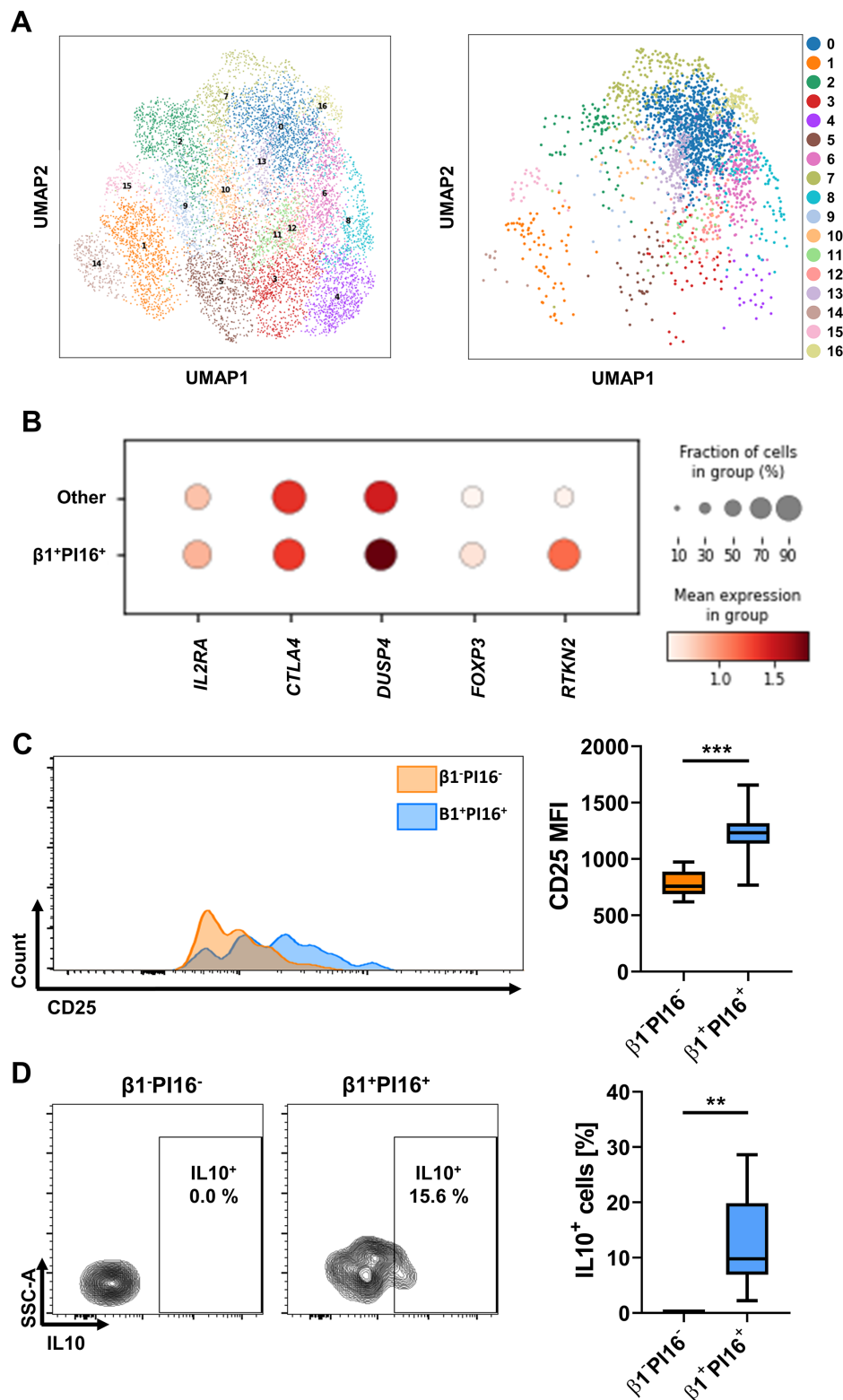


**Figure 8** Characterisation of  $\beta 1^{+}PI16^{+}\gamma 7^{+}T_{Reg}$  cells in the lamina propria of patients with IBD. (A) UMAP plot showing clustering of T cells from a publicly available single-cell RNA sequencing dataset (GSE162335) of CD45<sup>+</sup> LPMCs from the rectum of 11 patients with UC (left panel) and UMAP plots showing the distribution of  $T_{Reg}$  cells (right panel). (B) Heat map showing differential gene expression and the portion of cells expressing five prominent regulatory genes in  $\beta 1^{+}PI16^{+}$  compared to all other  $T_{Reg}$  cells from the dataset shown in (A). (C) Representative (left) and quantitative (right) flow cytometry showing mean fluorescence intensity (MFI) of CD25 on CD4<sup>+</sup>CD25<sup>high</sup>CD127<sup>low</sup>Foxp3<sup>+</sup> $\gamma 7^{+}\beta 1^{+}PI16^{+}T_{Reg}$  compared with CD4<sup>+</sup>CD25<sup>high</sup>CD127<sup>low</sup>Foxp3<sup>+</sup> $\gamma 7^{+}\beta 1^{+}PI16^{-}T_{Reg}$  cells. n=8 patients with IBD. (D) Representative (left) and quantitative (right) flow cytometry showing the frequency of IL-10 on CD4<sup>+</sup>Foxp3<sup>+</sup> $\gamma 7^{+}\beta 1^{+}PI16^{+}T_{Reg}$  compared with CD4<sup>+</sup>Foxp3<sup>+</sup> $\gamma 7^{+}\beta 1^{+}PI16^{-}T_{Reg}$  cells after incubation with PMA, ionomycin and brefeldin A for 4 hours. n=8 patients with IBD. Statistical significance was calculated using Student's t-test. Sample donor characteristics are listed in online supplemental table 9. LPMC, lamina propria mononuclear cells; PMA, phorbol-12-myristat-13-acetate;  $T_{Reg}$ , regulatory T cell; UMAP, uniform manifold approximation and projection.

powerful regulatory function in the peripheral blood as well as in the intestine and might counteract inflammation in the gut.

### $\beta 1^+PI16^+T_{Reg}$ cells are 'resistant' to vedolizumab in vivo and enrich in the gut of patients with IBD responding to vedolizumab therapy

In a next step, we aimed to study, whether vedolizumab 'resistance' of  $\alpha 4\beta 7$ -expressing  $\beta 1^+PI16^+T_{Reg}$  cells can also be observed in vivo. To this end, we quantified serum trough levels in patients with IBD receiving vedolizumab therapy and determined the availability of free vedolizumab binding sites on these cells. As expected, the portion of  $T_{Eff}$  cells with untargeted  $\alpha 4\beta 7$  integrin on their surface decreased in a dose-dependent fashion. However, this was not the case for  $\alpha 4\beta 7$ -expressing  $\beta 1^+PI16^+T_{Reg}$  cells, while  $\alpha 4\beta 7$ -expressing  $\beta 1^-PI16^-T_{Reg}$  cells exhibited a dose-dependent decrease similar to  $T_{Eff}$  cells (figure 9A).

Since these data further suggested that residual  $T_{Reg}$  cell homing might crucially contribute to clinical efficacy of vedolizumab, we stained colon biopsies from responders to vedolizumab therapy obtained before the initiation of and under vedolizumab treatment for CD4 and Foxp3. While there was no quantitative difference in overall CD4<sup>+</sup> T cells before and under therapy, the portion of Foxp3<sup>+</sup>CD4<sup>+</sup> cells was significantly increased in patients with active therapy compared with before therapy (figure 9B). Interestingly, further stainings showed that more Foxp3<sup>+</sup> cells present in the colon of patients treated with vedolizumab co-stained for  $\beta 1$  than before treatment (figure 9C). Again and on tissue level, this was consistent with the idea of residual gut homing of  $\beta 1^+T_{Reg}$  cells under vedolizumab therapy.

Finally, we performed a post-hoc analysis of phase III data from the Gemini II and III trials of vedolizumab in patients with CD to correlate our observations to clinical outcomes. We determined the primary efficacy endpoint (remission rate at week 6) depending on the corresponding vedolizumab trough levels. Intriguingly, when stratifying for serum concentrations as in our cohort, remission rates in the range from 40 to 55  $\mu\text{g/mL}$  vedolizumab were clearly higher than below and above. In a pooled analysis, the difference between the 40 to 55  $\mu\text{g/mL}$  and the above 55  $\mu\text{g/mL}$  group was significant (figure 9D,E). In conclusion, these observations were well reconcilable with non-linear dose-response characteristics due to residual homing of  $\beta 1^+PI16^+T_{Reg}$  cells.

## DISCUSSION

Vedolizumab is successfully used for the treatment of IBD and is applied as a fixed dose.<sup>26 27</sup> Both in clinical trials and in real-world cohorts a broad range of resulting serum drug levels has been observed,<sup>11 12 19</sup> indicating that individual pharmacokinetics substantially differ. At the same time, vedolizumab is only efficient in a portion of patients and optimising drug levels has been proposed as one strategy to improve results, but yet to be further investigated and developed.<sup>16 28</sup> Here, we show that  $\alpha 4\beta 7$ -expressing  $T_{Reg}$  cells exhibit a right-shifted response to vedolizumab compared with  $T_{Eff}$  cells and identify a  $\beta 1^+PI16^+T_{Reg}$  cell subset as the substrate of this effect. From a clinical perspective, our data argue for a concept of optimally exploiting residual  $T_{Reg}$  cell homing by aiming at high, but avoiding too high serum concentrations. This would mean that vedolizumab exposure would have to be increased in the vast majority, but limited in a small part of the patients, which could be achieved

by therapeutic drug monitoring and applying individual doses of the antibody.

Multiple pieces of evidence show that reaching a certain vedolizumab drug level is a prerequisite or at least increasing the odds for therapeutic benefit. Earlier post-hoc analyses of phase III trials had shown that the median trough levels in patients with clinical remission were higher than in patients without. Moreover, below a trough level of 17  $\mu\text{g/mL}$  in UC and 16  $\mu\text{g/mL}$  in CD, remission rates were not significantly different from placebo.<sup>17</sup> Another recent analyses of the GEMINI I data for UC identified target trough levels of >37.1  $\mu\text{g/mL}$ , >18.4  $\mu\text{g/mL}$  and 12.7  $\mu\text{g/mL}$  for weeks 6, 14 and maintenance to achieve clinical remission.<sup>29</sup> Similar observations have been made in real-world cohorts with regard to different end-points: Dreesen *et al* identified a trough level of >24  $\mu\text{g/mL}$  and >14  $\mu\text{g/mL}$  in week 6 and 14, respectively, to be associated with effectiveness at weeks 14 and 22.<sup>28</sup> In a cohort described by Yacoub *et al*, trough levels at week 6 were clearly higher in those patients achieving mucosal healing within 1 year.<sup>30</sup> Another prospective study identified serum trough levels at week 2 (median 24.8  $\mu\text{g/mL}$  vs 20  $\mu\text{g/mL}$ ) and 6 (median 25  $\mu\text{g/mL}$  vs 17.3  $\mu\text{g/mL}$ ) to be associated with long-term endoscopic remission at week 52.<sup>31</sup> A French retrospective cohort study was able to link higher vedolizumab serum levels with higher rates of histological healing.<sup>32</sup> And in the cohort of Ungaro *et al*, patients with trough levels of >11.5  $\mu\text{g/mL}$  were more than twice as likely as patients below this threshold to enter steroid-free endoscopic remission after 1 year.<sup>33</sup> While all those data point into the same direction, the cohorts described, the endpoints assessed and the time points of trough level determination were heterogeneous. Consistently, therapeutic management based on trough level monitoring has not entered clinical practice so far.

On first view, these real-world studies seem to contradict the postulation of a non-linear exposure-efficacy correlation of vedolizumab at high concentrations. However, one has to acknowledge that only very few patients actually reach drug levels at which we observed inhibition of residual  $T_{Reg}$  cell homing and decreased efficacy in Gemini II and III. As a consequence, such patients are likely to 'vanish' in the patient population with optimal drug exposure, particularly since many of the studies mentioned are based on quartiles of trough levels.<sup>17 32</sup> Moreover, two independent dose-ranging phase II trials reported non-linear correlations in the high exposure range<sup>22 23</sup> and a phase II trial of the anti- $\beta 7$  integrin antibody etrolizumab revealed a similar correlation.<sup>34</sup>

Thus, our data are not only significant for providing a mechanistic explanation for the efficacy of vedolizumab in the optimal drug level range through residual gut homing of  $T_{Reg}$  cells, but also underscore that a 'therapeutic window' might exist for this effect that is lost at very high concentrations. Obviously, the ranges observed for this window slightly differed depending on the experimental technique used (eg, binding analyses vs analyses of free binding sites). However, this is not unsurprising regarding the different approaches employed and the overlap is still substantial and consistent with read-outs of the same effect. Our data are different from earlier data reporting an  $EC_{50}$  for binding of vedolizumab to T cells of 0.042  $\mu\text{g/mL}$ .<sup>35</sup> Yet, this might also be explained by different methodology; importantly the flow cytometric read-out was based on MFI and not as in our case on the fraction of cells with positive staining.

In particular, we show that an  $\alpha 4\beta 7$ -expressing  $\beta 1^+PI16^+T_{Reg}$  cell subset is 'resistant' to vedolizumab. A question yet to answer in future studies is, what drives resistance of these cells. The specific expression profile of chemokine receptors in this

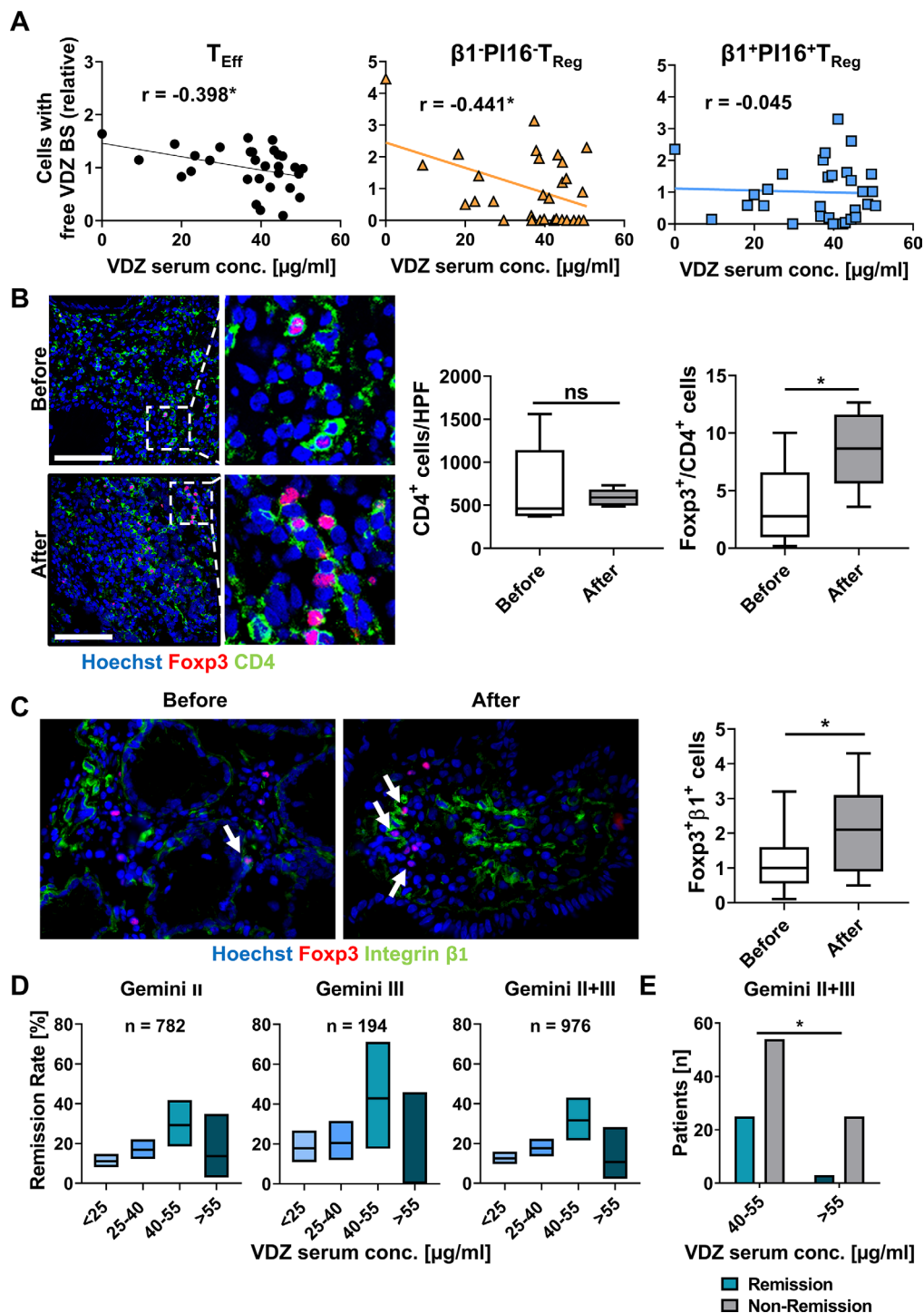


**Figure 9** Resistance of  $\beta 1^+ \text{PI16}^+ \alpha 4^+ \beta 7^+ T_{\text{Reg}}$  cells to vedolizumab in patients with IBD in vivo and correlation with Gemini II and III trials. (A) Correlation of  $T_{\text{Eff}}$  cells (left),  $\beta 1^+ \text{PI16}^+ \alpha 4^+ \beta 7^+ T_{\text{Reg}}$  cells (middle) and  $\beta 1^+ \text{PI16}^- \alpha 4^+ \beta 7^+ T_{\text{Reg}}$  cells with free vedolizumab binding sites (VDZ BS) as determined by flow cytometry with serum trough levels of vedolizumab as determined by ELISA in a cohort of patients with IBD treated with vedolizumab. Line showing simple linear regression.  $n=30$  patients with IBD. (B, C) Representative (left) and quantitative (right) immunohistochemistry of human colon biopsies obtained from patients before or under treatment with VDZ. (B) CD4 (green), Foxp3 (red) and nuclei counterstain with Hoechst (blue), (C) Integrin  $\beta 1$  (green), Foxp3 (red) and nuclei counterstain with Hoechst (blue). Scale bar 100  $\mu\text{m}$  (B), 50  $\mu\text{m}$  (C). Quantification of eight high-power fields (HPF) per sample.  $n=6$  (B),  $n=12-16$  (C) patients with IBD. (D) Percentage of patients with CD from Gemini II and/or III trials achieving clinical remission at week 6 stratified according to VDZ trough levels at week 6. 28–463 patients with CD per group. Boxes indicate remission rates with 95% Clopper-Pearson CI. (E) Comparison of the number of patients with or without clinical remission at week 6 in Gemini II and III with a trough level between 40–55  $\mu\text{g/mL}$  and >55  $\mu\text{g/mL}$ . Statistical comparisons were performed using Student's t-test (B, C) and Fisher's exact test (E). Sample donor characteristics are listed in online supplemental tables 10 and 11.  $T_{\text{Eff}}$ , effector T cell;  $T_{\text{Reg}}$ , regulatory T cell; VDZ, vedolizumab.

population raises the questions, whether chemokine signalling<sup>36,37</sup> might induce particular conformations of the  $\alpha 4\beta 7$  integrin that might be better or worse accessible for vedolizumab. Similarly, differential post-translational modifications of  $\alpha 4\beta 7$  integrin might regulate accessibility. And as in mice,<sup>38</sup> high expression of  $\beta 1$  integrin has been reported to interfere with the functionality of  $\alpha 4\beta 7$  integrin.

More importantly, also in a broader context, the  $\beta 1^+PI16^+$   $T_{Reg}$  cell subset we identified seems to be a functionally clearly distinct cell population and we show that these cells have a pronounced regulatory phenotype predesignating them as powerful anti-inflammatory cells capable of counteracting intestinal inflammation. PI16 expression by  $T_{Reg}$  cells had first been described in 2010.<sup>39</sup> Fully consistent with our characterisation of the subset, a later study yielded first hints at particular migratory features of  $PI16^+ T_{Reg}$  cells by identifying enhanced migration to CCL17 and CCL20.<sup>40</sup> Moreover, a recent study characterising  $PI16^+$  vs  $PI16^- T_{Reg}$  cells, provided a first glimpse at the phenotype of our subset by describing increased expression of ITBG1 by and suggesting enhanced functional fitness of  $PI16^+ T_{Reg}$  cells.<sup>41</sup>

Importantly, our data do not provide a formal proof that  $T_{Reg}$  cells such as the  $\beta 1^+PI16^+$  subset we identified are causally related with clinical efficacy of vedolizumab and we cannot definitely exclude that similar features apply to other small cell subsets. However, apart from the fact that such a proof would be almost impossible to provide and although effects of vedolizumab on innate immune cells have recently been proposed<sup>42</sup> and interference with  $\alpha 4\beta 7$ -dependent homing of non-classical monocytes has been shown,<sup>43</sup>  $T$  cells are still considered to be the main target of vedolizumab therapy.<sup>8,9,44</sup>

Yet, when envisioning translation of our findings into clinical practice, our data provide a clear rationale to perform prospective studies, which should (1) characterise  $T_{Reg}$  cell populations over the course of vedolizumab therapy, (2) define the optimal target trough levels at pre-specified time points and (3) time points for and (4) the kind of intervention to correct deviations from these exposure targets.

In conclusion, we show that a  $\beta 1^+PI16^+ T_{Reg}$  cell subset that displays 'resistance' to vedolizumab with a right-shifted binding curve might explain efficacy of vedolizumab and define an optimal 'therapeutic window' that is consistent with the data from randomised clinical trials. Our data support further efforts to optimise vedolizumab therapy by tailoring drug exposure in vivo in a personalised approach.

#### Author affiliations

<sup>1</sup>Department of Medicine 1, University Hospital Erlangen, Friedrich-Alexander-Universität Erlangen-Nürnberg, Erlangen, Bayern, Germany

<sup>2</sup>Institute for Medical Informatics, Biometry and Epidemiology, Friedrich-Alexander-Universität Erlangen-Nürnberg, Erlangen, Bayern, Germany

<sup>3</sup>Institute of Human Genetics, University Hospital Erlangen, Friedrich-Alexander-Universität Erlangen-Nürnberg, Erlangen, Bayern, Germany

<sup>4</sup>Department of Dermatology, University Hospital Erlangen, Friedrich-Alexander-Universität Erlangen-Nürnberg, Erlangen, Bayern, Germany

<sup>5</sup>Deutsches Zentrum Immuntherapie (DZI), University Hospital Erlangen, Erlangen, Bayern, Germany

<sup>6</sup>Department of Gastroenterology, Infectiology and Rheumatology, Charité Universitätsmedizin Berlin, Campus Benjamin Franklin, Berlin, Berlin, Germany

<sup>7</sup>Berlin Institute of Health (BIH), Berlin, Germany

<sup>8</sup>Deutsches Rheumaforschungszentrum Berlin (DRFZ), an Institute of the Leibniz Association, Berlin, Germany

**Correction notice** This article has been corrected since it published Online First. The funding statement has been added.

**Acknowledgements** The research of SZ, RA, IA and MFN was supported by the Interdisciplinary Center for Clinical Research (IZKF) and the ELAN programme of the

University Erlangen-Nuremberg, the Fritz-Bender-Stiftung, the Ernst Jung-Stiftung, the Else Kröner-Fresenius-Stiftung, the Thyssen-Stiftung, the German Crohn's and Colitis Foundation (DCCV), the DFG topic programme on Microbiota, the Emerging Field Initiative, the DFG Collaborative Research Centers 643, 796, 1181 and TRR241, the Rainin Foundation and the Litwin IBD Pioneers programme of the Crohn's and Colitis Foundation of America (CCFA). ANH is supported by a Lichtenberg fellowship by Volkswagen Foundation, a Berlin Institute of Health Clinician Scientist grant and German Research Foundation (DFG-TRR241-A05). The authors thank J. Derdau, D. Dziony, J. Marcks, J. Schuster and M. Slawik for their invaluable technical assistance. Furthermore, we thank the Core Unit for cell sorting and immune monitoring and the Core Unit Next generation Sequencing from the Friedrich-Alexander University Erlangen-Nuremberg for their excellent technical support. Parts of this publication are based on research using data from Takeda that has been made available through Vivli. Vivli has not contributed to or approved, and is not in any way responsible for, the contents of this publication.

**Contributors** EB and AS performed experiments. EB and SZ designed the study. EB, MW, AS-K, RA, IA, TMM, CV, ANH, FV, MFN and SZ provided clinical samples, protocols or reagents; ABE and MD performed and analysed RNA sequencing; CG, EB and SZ performed statistical analysis of the phase III data; EB, MD, MW, MFN and SZ analysed and interpreted the data. EB and SZ drafted the manuscript with the help of MFN; all authors critically revised the manuscript for important intellectual content.

**Funding** Else Kröner-Fresenius Stiftung (2016\_A182), European Crohn's and Colitis Organization (ECCO), German Research Foundation (ZU 377/4-1).

**Competing interests** MFN has served as an advisor for Pentax, Giuliani, MSD, Abbvie, Janssen, Takeda and Boehringer. SZ received honoraria from Takeda, Roche and Janssen. MFN and SZ received research support from Takeda, Shire (a part of Takeda) and Roche. The other authors declare no conflicts of interest.

**Patient consent for publication** Not required.

**Ethics approval** All samples were collected following informed written consent from the participants and all procedures were approved by the Ethics Committee of the Friedrich-Alexander-University Erlangen-Nuremberg, Germany (40\_16B, 249\_13B, 135\_20B).

**Provenance and peer review** Not commissioned; externally peer reviewed.

The scRNA-seq data generated for this study are available at the Gene Expression Omnibus under the following accession number: GSE162624. The Python pipeline of the scRNA-seq analysis is available on Github as a Jupyter notebook file at [https://github.com/MarkDedden/Vedolizumab\\_scRNA\\_Treg](https://github.com/MarkDedden/Vedolizumab_scRNA_Treg). Other data are available upon reasonable request.

**Supplemental material** This content has been supplied by the author(s). It has not been vetted by BMJ Publishing Group Limited (BMJ) and may not have been peer-reviewed. Any opinions or recommendations discussed are solely those of the author(s) and are not endorsed by BMJ. BMJ disclaims all liability and responsibility arising from any reliance placed on the content. Where the content includes any translated material, BMJ does not warrant the accuracy and reliability of the translations (including but not limited to local regulations, clinical guidelines, terminology, drug names and drug dosages), and is not responsible for any error and/or omissions arising from translation and adaptation or otherwise.

**Open access** This is an open access article distributed in accordance with the Creative Commons Attribution Non Commercial (CC BY-NC 4.0) license, which permits others to distribute, remix, adapt, build upon this work non-commercially, and license their derivative works on different terms, provided the original work is properly cited, appropriate credit is given, any changes made indicated, and the use is non-commercial. See: <http://creativecommons.org/licenses/by-nc/4.0/>.

#### ORCID iDs

Markus F Neurath <http://orcid.org/0000-0003-4344-1474>

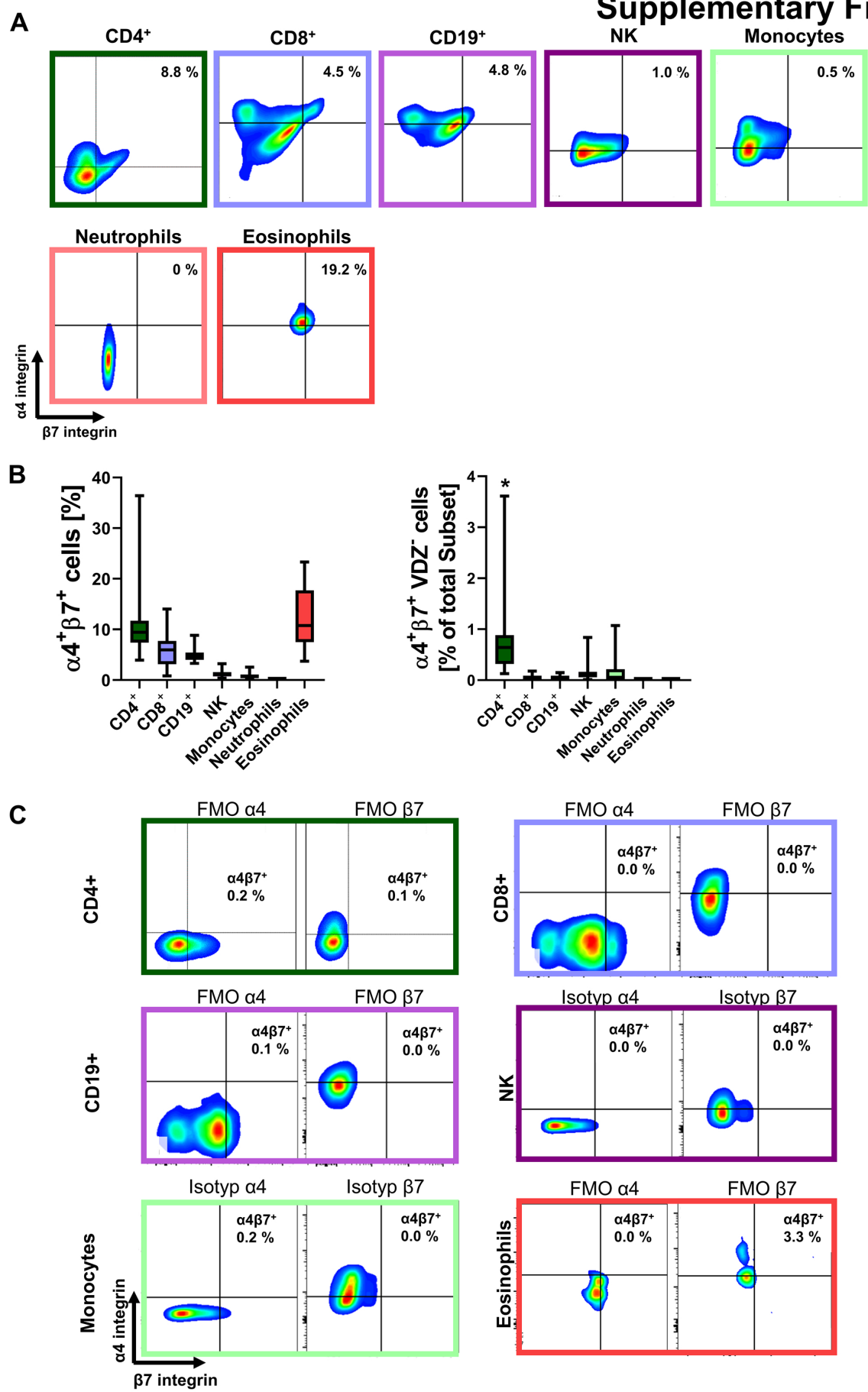
Sebastian Zundler <http://orcid.org/0000-0003-0888-2784>

#### REFERENCES

- Kaser A, Zeissig S, Blumberg RS. Inflammatory bowel disease. *Annu Rev Immunol* 2010;28:573–621.
- Molodecky NA, Soon IS, Rabi DM, et al. Increasing incidence and prevalence of the inflammatory bowel diseases with time, based on systematic review. *Gastroenterology* 2012;142:e42:46–54.
- Monteleone G, Caruso R, Pallone F. Targets for new immunomodulation strategies in inflammatory bowel disease. *Autoimmun Rev* 2014;13:11–14.
- Neurath MF. Current and emerging therapeutic targets for IBD. *Nat Rev Gastroenterol Hepatol* 2017;14:269–78.
- Zundler S, Becker E, Schulze LL, et al. Immune cell trafficking and retention in inflammatory bowel disease: mechanistic insights and therapeutic advances. *Gut* 2019;68:1688–700.

- 6 Ley K, Laudanna C, Cybulsky MI, *et al.* Getting to the site of inflammation: the leukocyte adhesion cascade updated. *Nat Rev Immunol* 2007;7:678–89.
- 7 Neurath MF. Targeting immune cell circuits and trafficking in inflammatory bowel disease. *Nat Immunol* 2019;20:970–9.
- 8 Uzzan M, Tokuyama M, Rosenstein AK, *et al.* Anti- $\alpha 4\beta 7$  therapy targets lymphoid aggregates in the gastrointestinal tract of HIV-1-infected individuals. *Sci Transl Med* 2018;10. doi:10.1126/scitranslmed.aau4711. [Epub ahead of print: 03 10 2018].
- 9 Veny M, Garrido-Trigo A, Corraliza AM, *et al.* Dissecting common and unique effects of anti- $\alpha 4\beta 7$  and anti-tumor necrosis factor treatment in ulcerative colitis. *J Crohns Colitis* 2021;15:441–52.
- 10 Fischer A, Zundler S, Atreya R, *et al.* Differential effects of  $\alpha 4\beta 7$  and GPR15 on homing of effector and regulatory T cells from patients with UC to the inflamed gut in vivo. *Gut* 2016;65:1642–64.
- 11 Feagan BG, Rutgeerts P, Sands BE, *et al.* Vedolizumab as induction and maintenance therapy for ulcerative colitis. *N Engl J Med* 2013;369:699–710.
- 12 Sandborn WJ, Feagan BG, Rutgeerts P, *et al.* Vedolizumab as induction and maintenance therapy for Crohn's disease. *N Engl J Med* 2013;369:711–21.
- 13 Kopylov U, Ron Y, Avni-Biron I, *et al.* Efficacy and safety of Vedolizumab for induction of remission in inflammatory bowel disease—the Israeli real-world experience. *Inflamm Bowel Dis* 2017;23:404–8.
- 14 Amiot A, Serrero M, Peyrin-Biroulet L, *et al.* One-year effectiveness and safety of vedolizumab therapy for inflammatory bowel disease: a prospective multicentre cohort study. *Aliment Pharmacol Ther* 2017;46:310–21.
- 15 Vermeire S, Loftus EV, Colombel J-F, *et al.* Long-term efficacy of vedolizumab for crohn's disease. *J Crohns Colitis* 2017;11:412–24.
- 16 Pouillon L, Vermeire S, Bossuyt P. Vedolizumab trough level monitoring in inflammatory bowel disease: a state-of-the-art overview. *BMC Med* 2019;17:89.
- 17 Rosario M, French JL, Dirks NL, *et al.* Exposure-efficacy relationships for vedolizumab induction therapy in patients with ulcerative colitis or crohn's disease. *J Crohns Colitis* 2017;11:921–9.
- 18 Schulze H, Esters P, Hartmann F, *et al.* A prospective cohort study to assess the relevance of vedolizumab drug level monitoring in IBD patients. *Scand J Gastroenterol* 2018;53:670–6.
- 19 Al-Bawardy B, Ramos GP, Willrich MAV, *et al.* Vedolizumab drug level correlation with clinical remission, biomarker normalization, and mucosal healing in inflammatory bowel disease. *Inflamm Bowel Dis* 2019;25:580–6.
- 20 Ungar B, Kopylov U, Yavzori M, *et al.* Association of vedolizumab level, anti-drug antibodies, and  $\alpha 4\beta 7$  occupancy with response in patients with inflammatory bowel diseases. *Clin Gastroenterol Hepatol* 2018;16:697–705.
- 21 Ward MG, Sparrow MP, Roblin X. Therapeutic drug monitoring of vedolizumab in inflammatory bowel disease: current data and future directions. *Therap Adv Gastroenterol* 2018;11:175628481877278.
- 22 Feagan BG, Greenberg GR, Wild G, *et al.* Treatment of ulcerative colitis with a humanized antibody to the  $\alpha 4\beta 7$  integrin. *N Engl J Med* 2005;352:2499–507.
- 23 Parikh A, Leach T, Wyant T, *et al.* Vedolizumab for the treatment of active ulcerative colitis: a randomized controlled phase 2 dose-ranging study. *Inflamm Bowel Dis* 2012;18:1470–9.
- 24 Wood SN. Fast stable restricted maximum likelihood and marginal likelihood estimation of semiparametric generalized linear models. *J R Stat Soc Ser B Stat Methodol* 2011;73:3–36.
- 25 Rosario M, Dirks NL, Milch C, *et al.* A review of the clinical pharmacokinetics, pharmacodynamics, and immunogenicity of Vedolizumab. *Clin Pharmacokinet* 2017;56:1287–301.
- 26 Rosario M, Dirks NL, Gastonguay MR, *et al.* Population pharmacokinetics-pharmacodynamics of vedolizumab in patients with ulcerative colitis and crohn's disease. *Aliment Pharmacol Ther* 2015;42:188–202.
- 27 Sandborn WJ, Baert F, Danese S, *et al.* Efficacy and safety of Vedolizumab subcutaneous formulation in a randomized trial of patients with ulcerative colitis. *Gastroenterology* 2020;158:e12:562–72.
- 28 Dreesen E, Verstockt B, Bian S, *et al.* Evidence to support monitoring of vedolizumab trough concentrations in patients with inflammatory bowel diseases. *Clin Gastroenterol Hepatol* 2018;16:1937–46.
- 29 Osterman MT, Rosario M, Lasch K, *et al.* Vedolizumab exposure levels and clinical outcomes in ulcerative colitis: determining the potential for dose optimisation. *Aliment Pharmacol Ther* 2019;49:408–18.
- 30 Yacoub W, Williet N, Pouillon L, *et al.* Early vedolizumab trough levels predict mucosal healing in inflammatory bowel disease: a multicentre prospective observational study. *Aliment Pharmacol Ther* 2018;47:906–12.
- 31 Yarur AJ, Bruss A, Naik S, *et al.* Vedolizumab concentrations are associated with long-term endoscopic remission in patients with inflammatory bowel diseases. *Dig Dis Sci* 2019;64:1651–9.
- 32 Pouillon L, Rousseau H, Busby-Venner H, *et al.* Vedolizumab trough levels and histological healing during maintenance therapy in ulcerative colitis. *J Crohns Colitis* 2019;13:970–5.
- 33 Ungaro RC, Yarur A, Jossen J, *et al.* Higher trough vedolizumab concentrations during maintenance therapy are associated with corticosteroid-free remission in inflammatory bowel disease. *J Crohns Colitis* 2019;13:963–9.
- 34 Vermeire S, O'Byrne S, Keir M, *et al.* Etrolizumab as induction therapy for ulcerative colitis: a randomised, controlled, phase 2 trial. *Lancet* 2014;384:309–18.
- 35 Wyant T, Yang L, Fedyk E. In vitro assessment of the effects of vedolizumab binding on peripheral blood lymphocytes. *MAbs* 2013;5:842–50.
- 36 Wang S, Wu C, Zhang Y, *et al.* Integrin  $\alpha 4\beta 7$  switches its ligand specificity via distinct conformer-specific activation. *J Cell Biol* 2018;217:2799–812.
- 37 Sun H, Liu J, Zheng Y, *et al.* Distinct chemokine signaling regulates integrin ligand specificity to dictate tissue-specific lymphocyte homing. *Dev Cell* 2014;30:61–70.
- 38 DeNucci CC, Pagán AJ, Mitchell JS, *et al.* Control of  $\alpha 4\beta 7$  integrin expression and CD4 T cell homing by the  $\beta 1$  integrin subunit. *J Immunol* 2010;184:2458–67.
- 39 Sadlon TJ, Wilkinson BG, Pederson S, *et al.* Genome-wide identification of human FOXP3 target genes in natural regulatory T cells. *J Immunol* 2010;185:1071–81.
- 40 Nicholson IC, Mavragelos C, Bird DRG, *et al.* PI16 is expressed by a subset of human memory treg with enhanced migration to CCL17 and CCL20. *Cell Immunol* 2012;275:12–18.
- 41 Hope CM, Welch J, Mohandas A, *et al.* Peptidase inhibitor 16 identifies a human regulatory T-cell subset with reduced FOXP3 expression over the first year of recent onset type 1 diabetes. *Eur J Immunol* 2019;49:1235–50.
- 42 Zeissig S, Rosati E, Dowds CM, *et al.* Vedolizumab is associated with changes in innate rather than adaptive immunity in patients with inflammatory bowel disease. *Gut* 2019;68:25–39.
- 43 Schleier L, Wiendl M, Heidbreder K, *et al.* Non-classical monocyte homing to the gut via  $\alpha 4\beta 7$  integrin mediates macrophage-dependent intestinal wound healing. *Gut* 2020;69:252–63.
- 44 Wyant T, Fedyk E, Abhyankar B. An overview of the mechanism of action of the monoclonal antibody vedolizumab. *J Crohns Colitis* 2016;10:1437–44.

Supplementary Figure 1



**Supplementary Figure 1:  $\alpha 4\beta 7$ -expression on and vedolizumab binding to different leukocyte subsets**

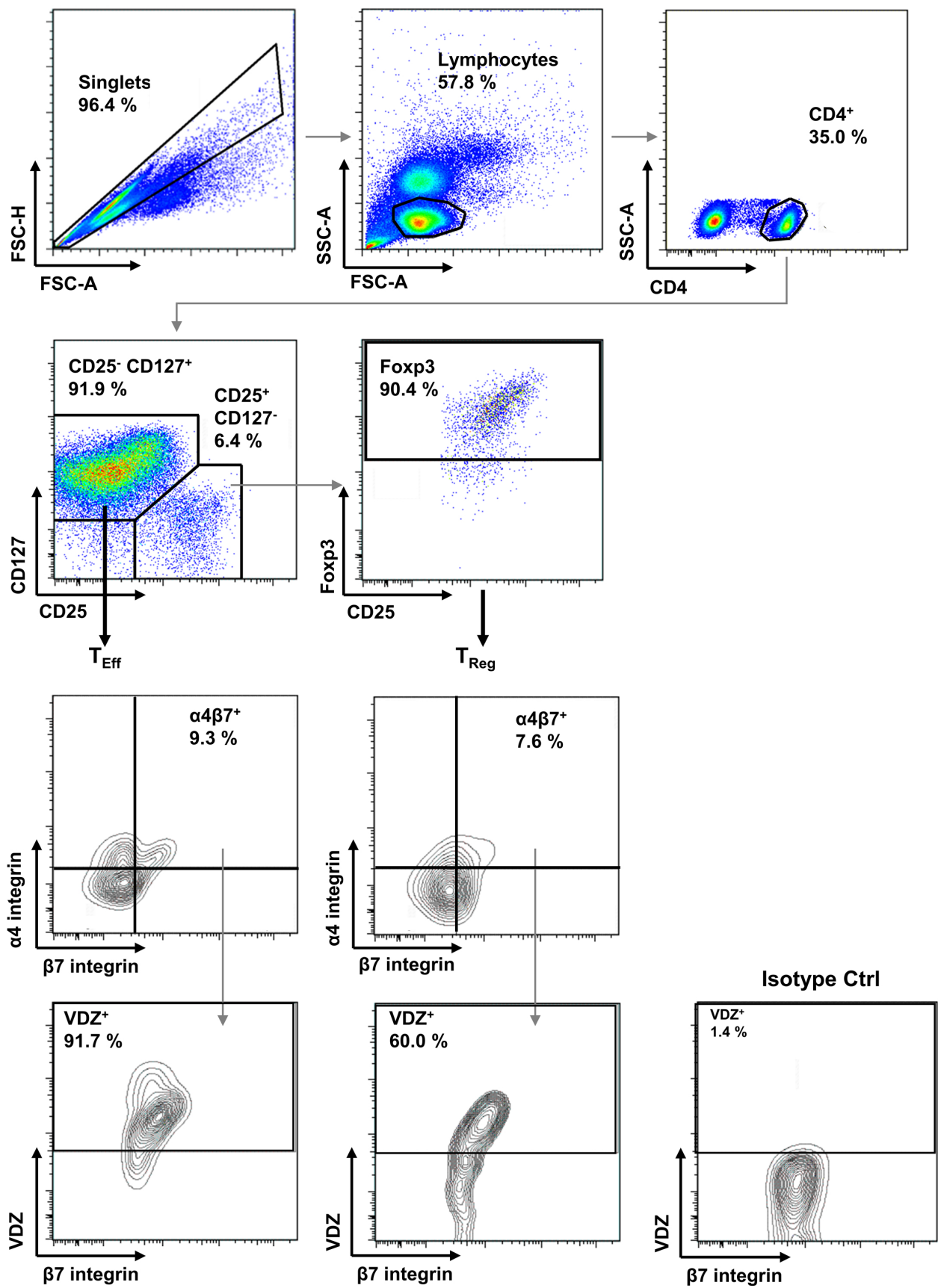
**(A,B)** Representative (A) and quantitative (B) flow cytometry of  $\alpha 4\beta 7^+$  cells within  $CD4^+$ ,  $CD3^+CD8^+$ ,  $CD3^+CD19^+$ ,  $CD3^+CD56^+CD16^+$  NK cells,  $CD3^+CD16^+CD14^+$  monocytes,  $CD16^+$  neutrophils and  $CD16^-CCR3^+Siglec8^+$  eosinophils (left panel) and quantification of  $\alpha 4\beta 7^+VDZ^-$  cells after incubation with 10  $\mu g/ml$  VDZ.  $n = 6-53$  IBD patients or healthy controls per group as indicated.

Statistical comparisons were performed using One-Way-Anova with Tukey's multiple comparisons post-hoc test

**(C)** Representative flow cytometry of controls for  $\alpha 4^+$  and  $\beta 7^+$  cells in the different leukocyte subsets shown in A and B.

Sample donor characteristics are listed in *Supplementary Table S12*.

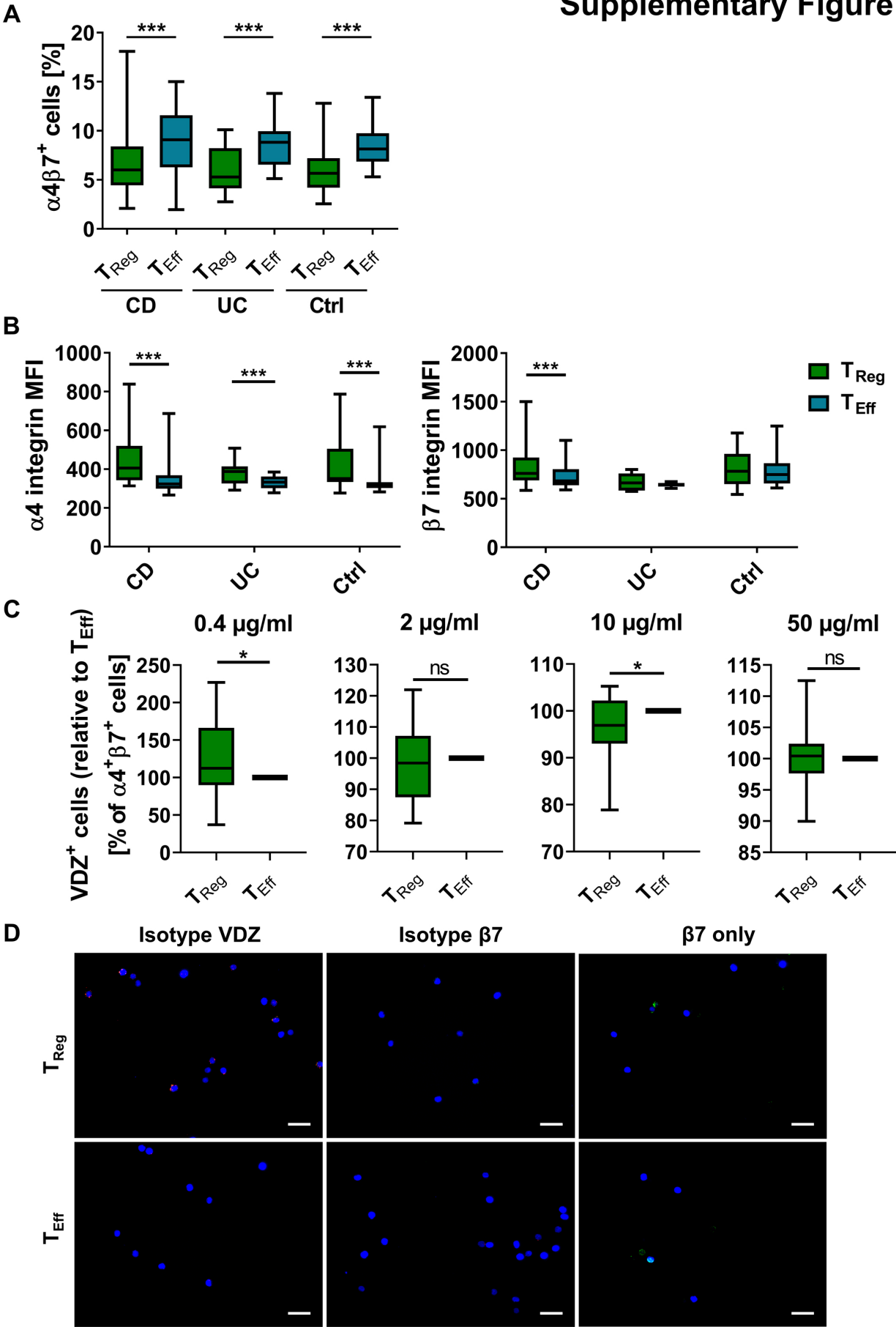
Supplementary Figure 2



**Supplementary Figure 2: Representative gating of CD4<sup>+</sup>α4β7<sup>+</sup>VDZ<sup>+</sup> T<sub>Reg</sub> and T<sub>Eff</sub> cells.**

Following doublet exclusion and gating on vital lymphocytes based on forward and sideward scatter, we selected CD4<sup>+</sup> T cells and defined T<sub>Reg</sub> cells as CD25<sup>+</sup>CD127<sup>low</sup>Foxp3<sup>+</sup> and T<sub>Eff</sub> cells as CD25<sup>-</sup>CD127<sup>high</sup>. Next we gated on α4β7<sup>+</sup> cells and determined VDZ<sup>+</sup> cells in this subset.

Supplementary Figure 3



**Supplementary Figure 3:  $\alpha 4$  and  $\beta 7$  integrin expression on T<sub>Reg</sub> and T<sub>Eff</sub> cells, vedolizumab binding to memory CD4<sup>+</sup> T cells and controls for VDZ binding.**

**(A)** Quantitative flow cytometry of  $\alpha 4\beta 7^+$  T<sub>Reg</sub> and T<sub>Eff</sub> cells in patients with UC and CD compared with healthy controls. n = 17-28 IBD patients or healthy controls as indicated.

**(B)** Mean fluorescence intensity (MFI) of  $\alpha 4$  and  $\beta 7$  integrin on T<sub>Reg</sub> and T<sub>Eff</sub> cells in patients with UC and CD and in healthy controls. n = 17-28 IBD patients or healthy controls as indicated.

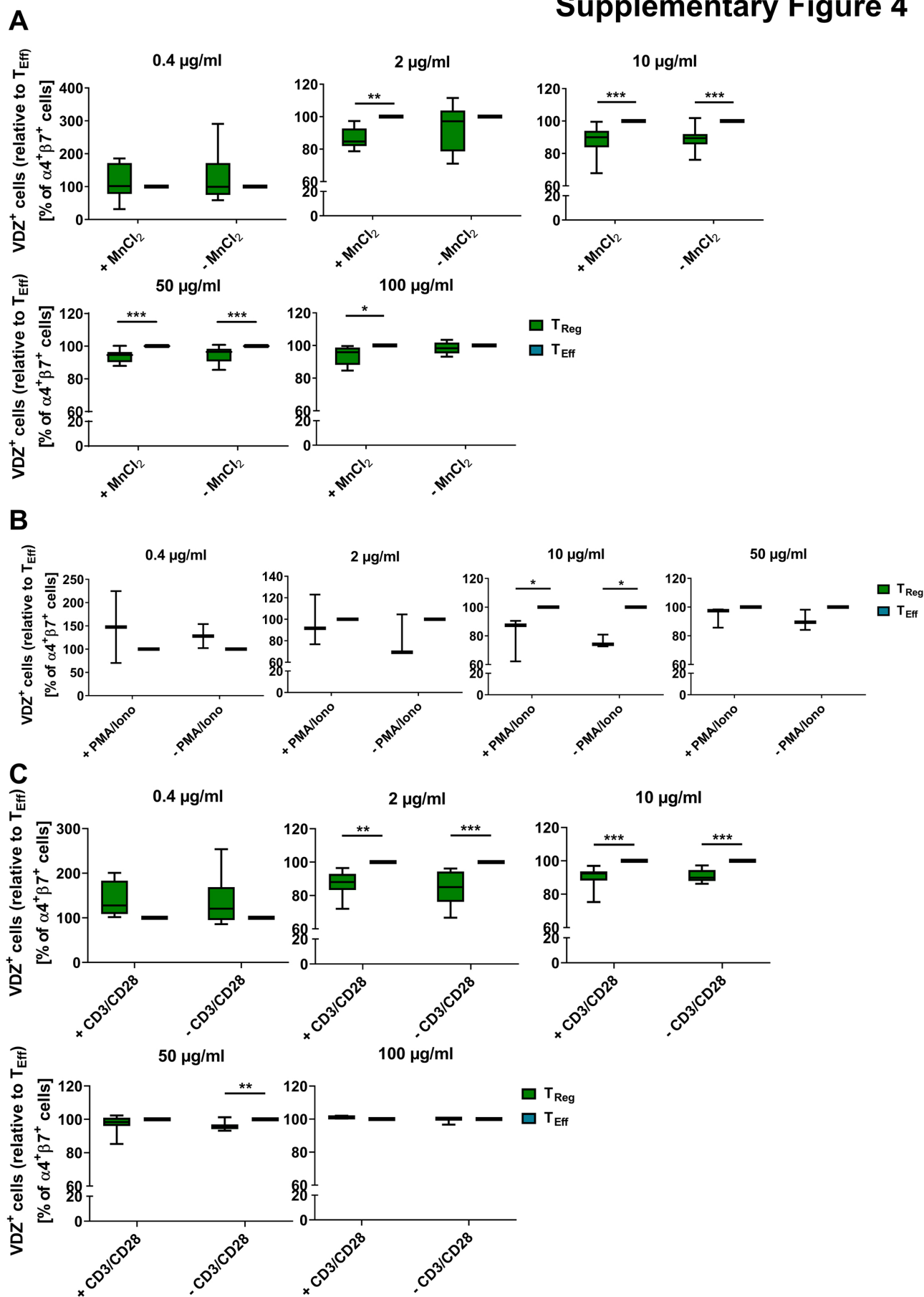
**(C)** Quantitative flow cytometry of VDZ<sup>+</sup> cells after gating on  $\alpha 4\beta 7^+$  CD45RO<sup>+</sup> T<sub>Reg</sub> and T<sub>Eff</sub> cells following incubation with the indicated concentrations of fluorescently labelled vedolizumab. Quantitative data are expressed relative to T<sub>Eff</sub> cells. n = 25 IBD patients and healthy controls.

**(D)** Representative fluorescence microscopy of FACS-purified T<sub>Reg</sub> and T<sub>Eff</sub> cells stained with isotype controls for  $\beta 7$  antibody (green) and VDZ (red) and counterstained with Hoechst (blue); Scale bar 10  $\mu$ m. Representative images from 1 out of 6 independent experiments (cells purified from leukocyte cones).

Statistical comparisons were performed using paired t-test (A, C), 2way ANOVA with Sidak's multiple comparison test (B)

Sample donor characteristics are listed in *Supplementary Table S13*.

## Supplementary Figure 4

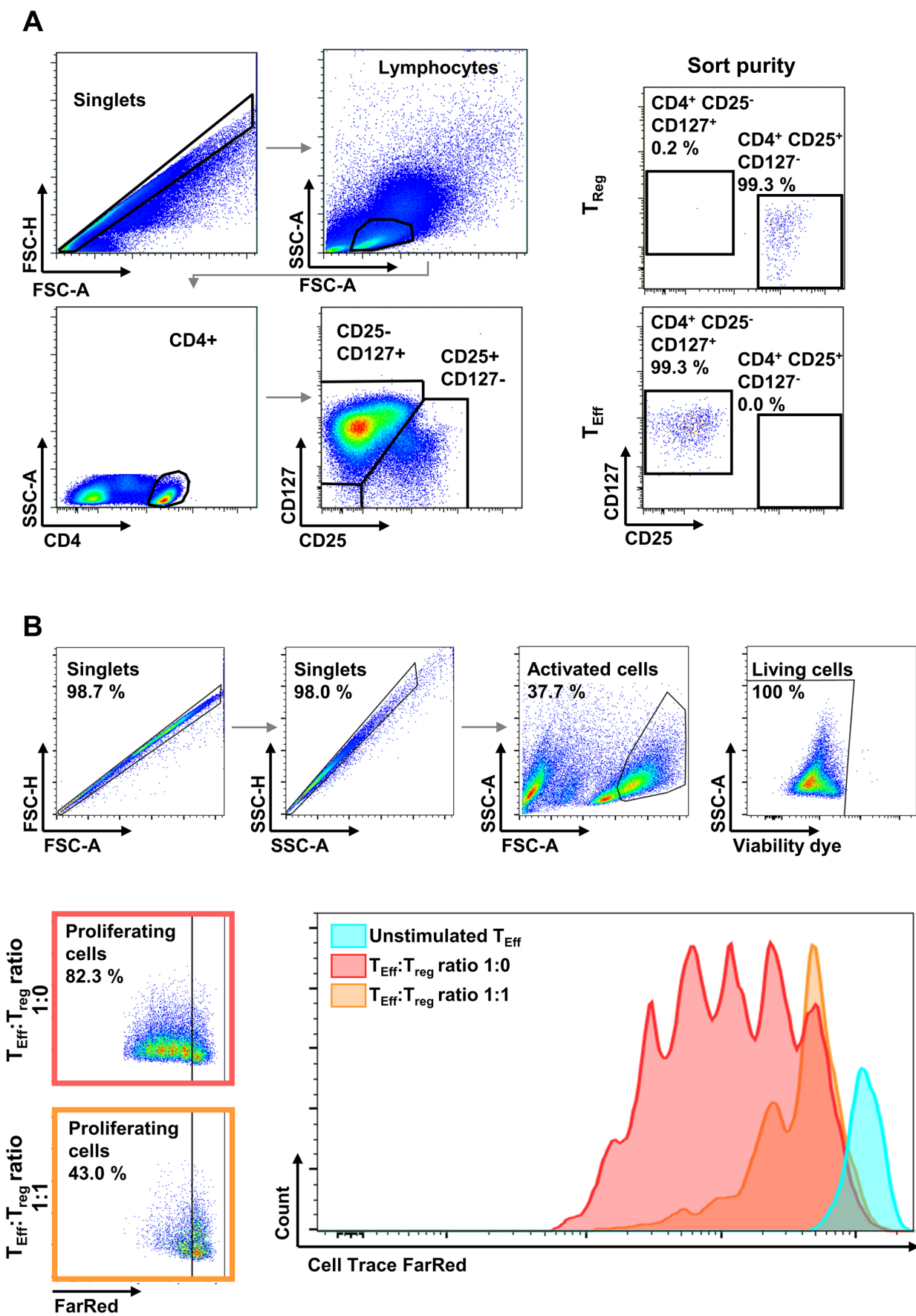


**Supplementary Figure 4: Concentration-dependent binding profile of vedolizumab to T<sub>Reg</sub> and T<sub>Eff</sub> cells under different culture conditions.**

**(A), (B), (C)** Quantitative flow cytometry of VDZ<sup>+</sup> cells among  $\alpha 4\beta 7^+$  T<sub>Reg</sub> and T<sub>Eff</sub> cells after incubation or stimulation with MnCl<sub>2</sub> (A), PMA/ionomycin (B) or anti-CD3/CD28 (C) and subsequent staining with the indicated concentrations of fluorescently labelled VDZ. Data are expressed relative to T<sub>Eff</sub> cells. Statistical significance was calculated using Student's t-test and mixed-effects analysis with Sidak's multiple comparison test. n = 2-14 healthy controls per group.

Sample donor characteristics are listed in *Supplementary Table S14*.

Supplementary Figure 5

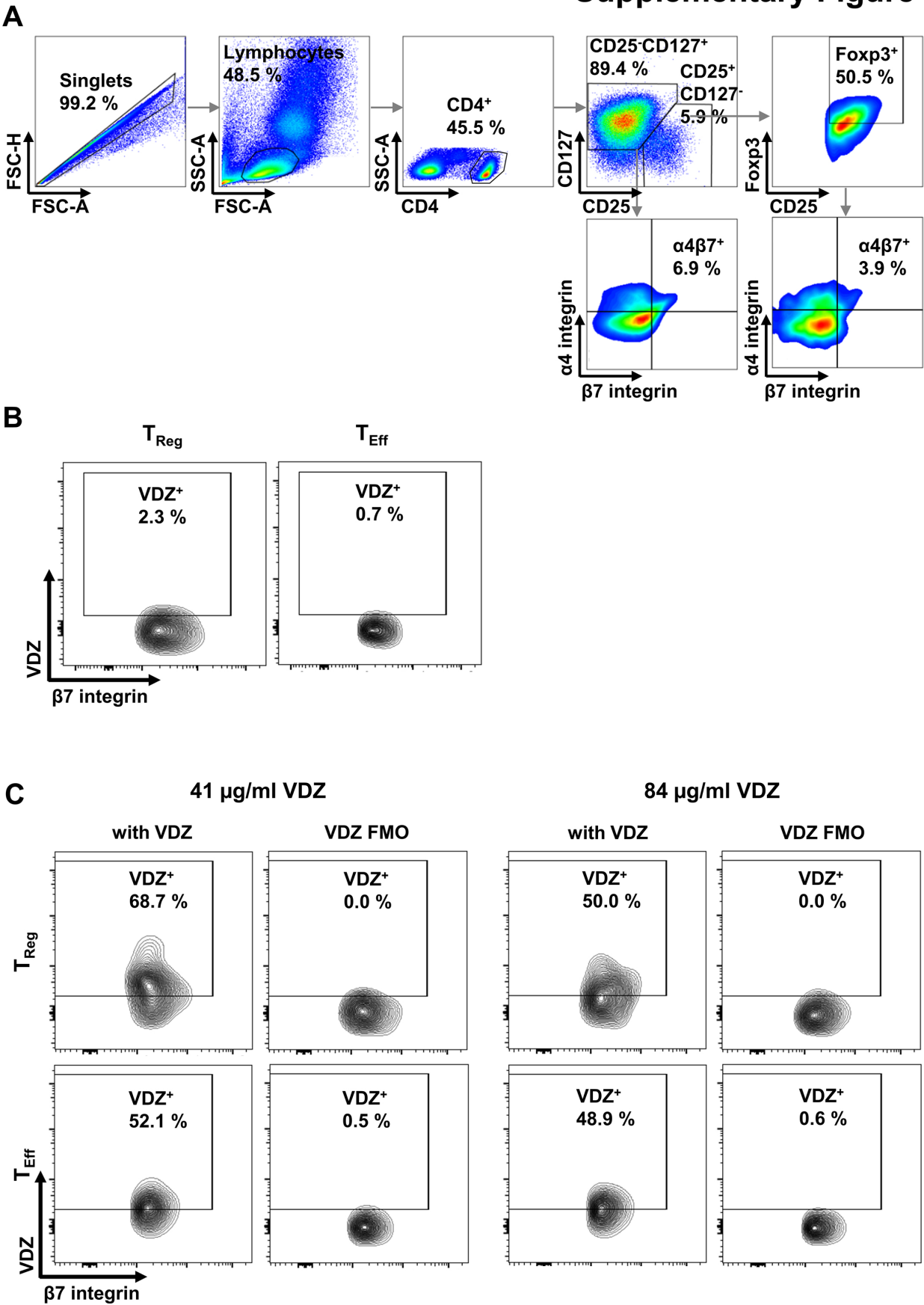


**Supplementary Figure 5: Purity and suppressive function of FACS-isolated T<sub>Reg</sub> and T<sub>Eff</sub> cells.**

**(A)** Left panels: Representative gating strategy for FACS-based isolation of T<sub>Reg</sub> and T<sub>Eff</sub> cells. Right panels: Re-analysis of isolated cells. T<sub>Eff</sub> cells were characterised as CD4<sup>+</sup>CD127<sup>+</sup>CD25<sup>-</sup>, T<sub>Reg</sub> cells as CD4<sup>+</sup>CD127<sup>-</sup>CD25<sup>+</sup>.

**(B)** Representative flow cytometry of T<sub>Eff</sub> cell proliferation as determined by dilution of Cell Trace FarRed. Representative images from 1 out of 3 independent experiments (cells purified from leukocyte cones).

Supplementary Figure 6



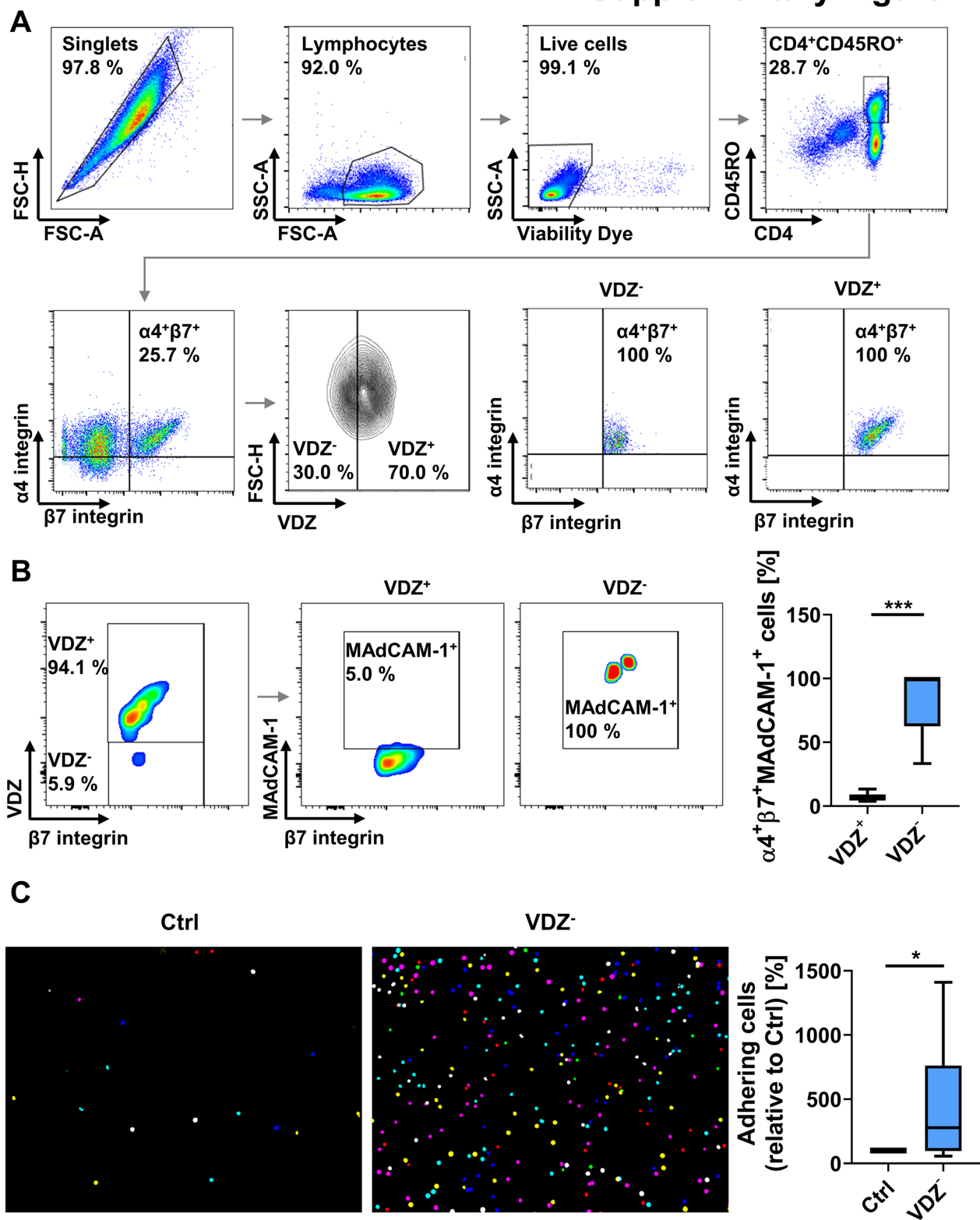
**Supplementary Figure 6: VDZ binding to T<sub>Reg</sub> and T<sub>Eff</sub> cells *in vitro* and *in vivo***

**(A)** Representative gating strategy. T<sub>Eff</sub> cells were characterised as CD4<sup>+</sup>CD127<sup>+</sup>CD25<sup>-</sup> cells, T<sub>Reg</sub> cells as CD4<sup>+</sup>CD127<sup>-</sup>CD25<sup>+</sup>Foxp3<sup>+</sup> cells. The expression of  $\alpha 4\beta 7$  integrin was determined prior to further analysis for free vedolizumab binding sites.

**(B)** Representative flow cytometry of T<sub>Reg</sub> and T<sub>Eff</sub> cells without fluorescently labelled vedolizumab as gating control for detection of free VDZ binding sites.

**(C)** Representative flow cytometry of T<sub>Reg</sub> and T<sub>Eff</sub> cells with free VDZ binding sites from a patient treated with vedolizumab. Stainings from week 2 and week 6 with respective VDZ trough levels indicated.

Supplementary Figure 7



**Supplementary Figure 7: Quality control of FACS-isolated CD4<sup>+</sup>CD45RO<sup>+</sup>α4<sup>+</sup>β7<sup>+</sup> VDZ<sup>+</sup> and VDZ<sup>-</sup> cells.**

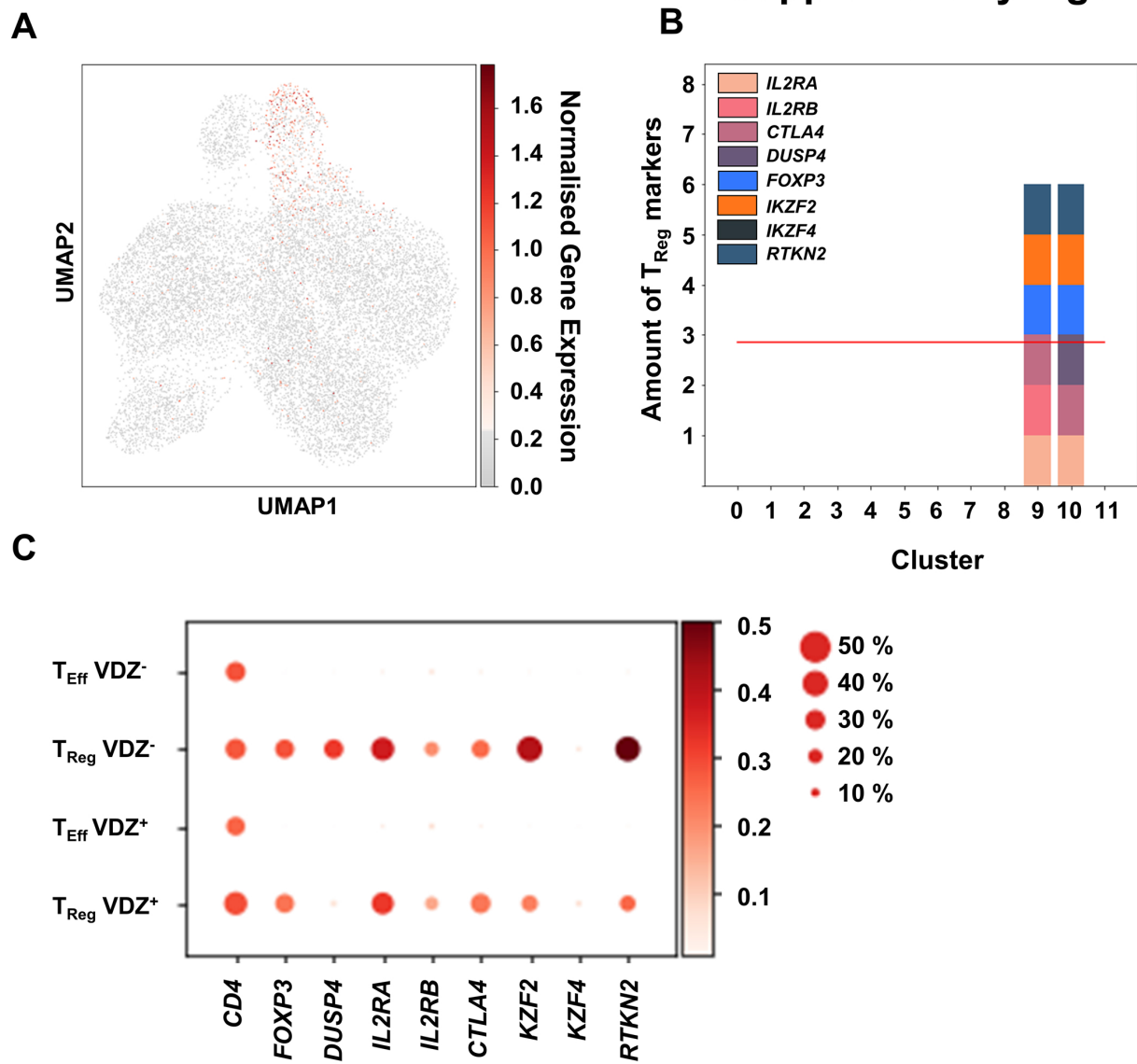
**(A)** Representative gating strategy and subsequent re-analysis. Cells were defined as CD4<sup>+</sup>CD45RO<sup>+</sup>α4<sup>+</sup>β7<sup>+</sup>VDZ<sup>+</sup> and CD4<sup>+</sup>CD45RO<sup>+</sup>α4<sup>+</sup>β7<sup>+</sup>VDZ<sup>-</sup> cells.

**(B)** Representative (left) and quantitative (right) flow cytometry of α4<sup>+</sup>β7<sup>+</sup>VDZ<sup>+</sup>MAdCAM<sup>+</sup> and α4<sup>+</sup>β7<sup>+</sup>VDZ<sup>-</sup>MAdCAM<sup>+</sup> T<sub>Reg</sub> cells incubated with different concentrations of fluorescently labelled VDZ and subsequently with fluorescently labelled MAdCAM-1. n = 8 healthy donors.

**(C)** Dynamic cell adhesion assays with VDZ<sup>-</sup> cells. Left panels: Representative microscopic images of adhering cells (overlay of 8 counted high-power fields). Right panels: Quantification of adhering cells relative to Ctrl. n = 9 (cells purified from leukocyte cones).

Statistical comparisons were performed using paired t-test (B) and Student's t-test (C).

Supplementary Figure 8



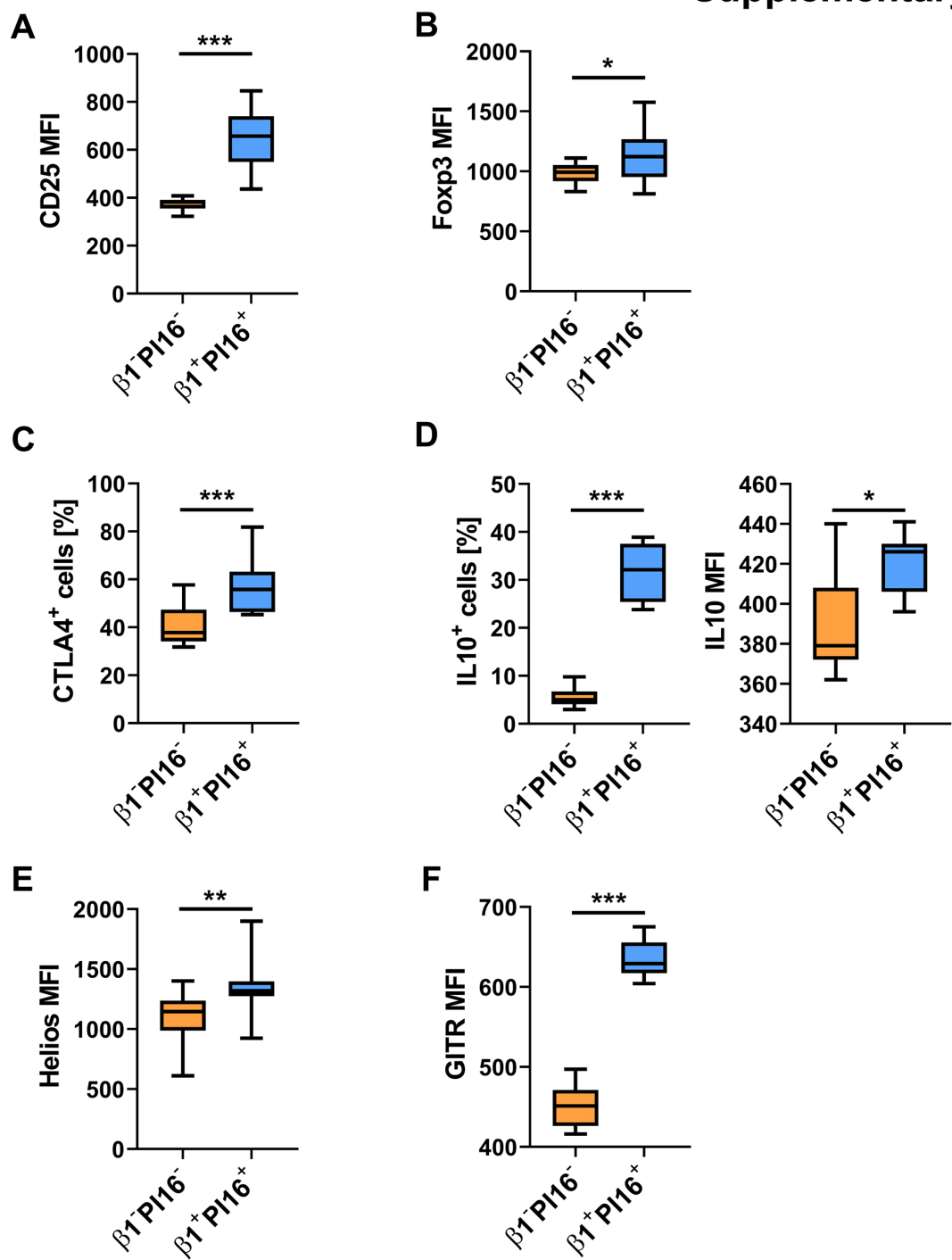
**Supplementary Figure 8: Characterisation of T<sub>Reg</sub> cell subclusters in single cell RNA sequencing analysis.**

**(A)** UMAP plot showing cells expressing *FOXP3*.

**(B)** Identification of subcluster 9 and 10 as T<sub>Reg</sub> cell clusters based on the expression of 8 different marker genes for T<sub>Reg</sub> cells.

**(C)** Heat map showing differential gene expression and portion of cells expressing eight prominent T<sub>Reg</sub> cell marker genes in VDZ<sup>-</sup> and VDZ<sup>+</sup> T<sub>Reg</sub> and T<sub>Eff</sub> cells.

Supplementary Figure 9



**Supplementary Figure 9: Characterisation of vedolizumab-“resistant”  
 $\beta 1^{+}PI16^{+}\alpha 4^{+}\beta 7^{+} T_{Reg}$  cells in the peripheral blood of IBD patients**

**(A,B)** Quantitative flow cytometry showing mean fluorescence intensity (MFI) of CD25 (A) and Foxp3 (B) on  $\beta 1^{+}PI16^{+}\alpha 4^{+}\beta 7^{+} T_{Reg}$  compared with  $\beta 1^{-}PI16^{-}\alpha 4^{+}\beta 7^{+} T_{Reg}$  cells. n = 11 IBD patients.

**(C)** Quantitative flow cytometry showing the frequency of CTLA4-expressing  $\beta 1^{+}PI16^{+}\alpha 4^{+}\beta 7^{+} T_{Reg}$  compared with  $\beta 1^{-}PI16^{-}\alpha 4^{+}\beta 7^{+} T_{Reg}$  cells. n = 11 IBD patients.

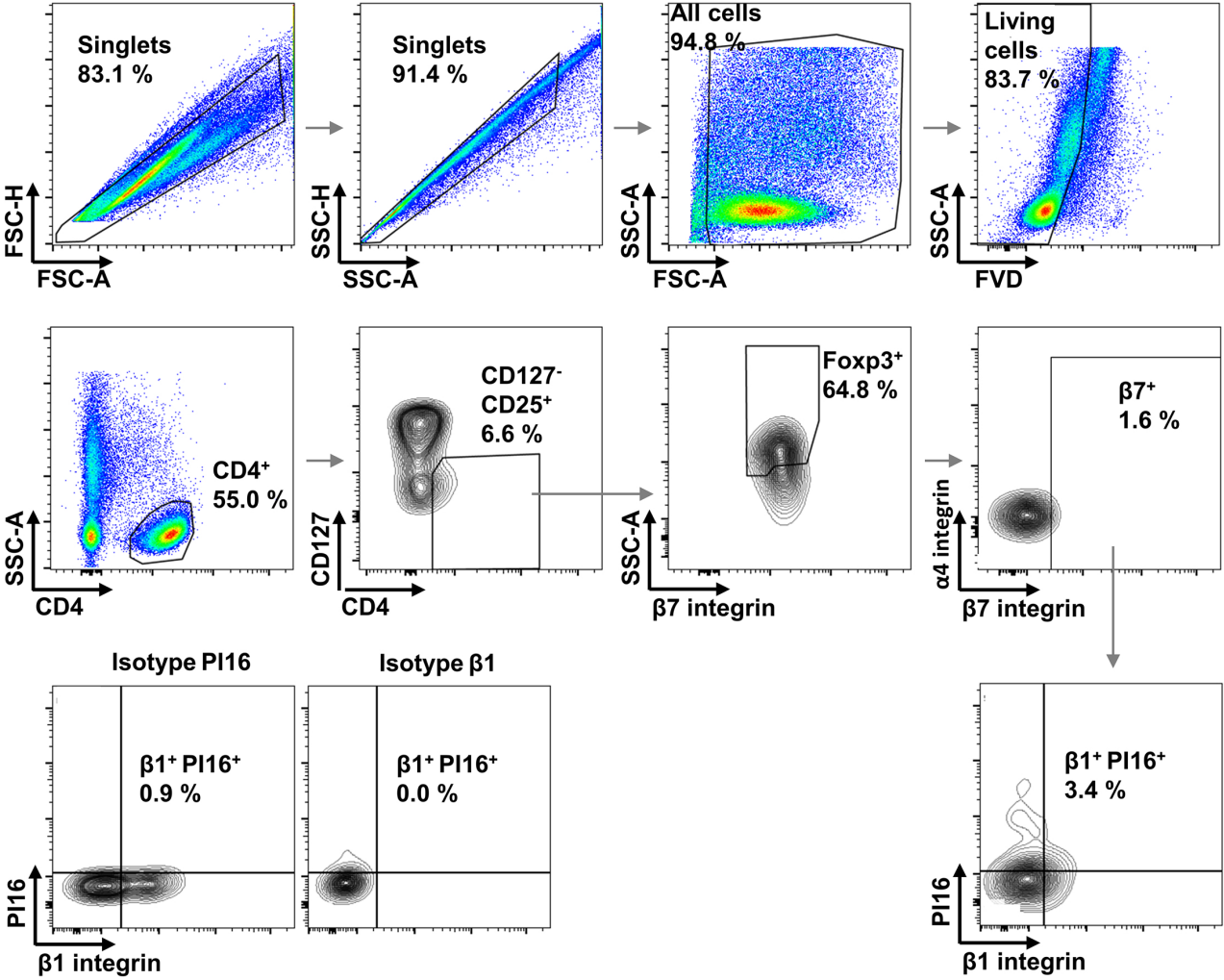
**(D)** Quantitative flow cytometry showing the frequency and mean fluorescence intensity (MFI) of IL10 on  $\beta 1^{+}PI16^{+}\alpha 4^{+}\beta 7^{+} T_{Reg}$  compared with  $\beta 1^{-}PI16^{-}\alpha 4^{+}\beta 7^{+} T_{Reg}$  cells after incubation with PMA, ionomycin and brefeldin A for 4 h. n = 11 IBD patients.

**(E,F)** Quantitative flow cytometry showing mean fluorescence intensity (MFI) of Helios (E) and GITR (F) on  $\beta 1^{+}PI16^{+}\alpha 4^{+}\beta 7^{+} T_{Reg}$  compared with  $\beta 1^{-}PI16^{-}\alpha 4^{+}\beta 7^{+} T_{Reg}$  cells. n = 11 IBD patients.

Statistical comparisons were performed using paired t-test.

Sample donor characteristics are listed in *Supplementary Table S15*.

Supplementary Figure 10



**Supplementary Figure 10: Representative gating on CD4<sup>+</sup>CD25<sup>+</sup>CD127<sup>-</sup>Foxp3<sup>+</sup>β7<sup>+</sup> β1<sup>+</sup>PI16<sup>+</sup> T<sub>Reg</sub> cells in the lamina propria.**

Following doublet exclusion and gating on vital cells based on forward and sideward scatter and Fixable viability Dye (FVD), we selected CD4<sup>+</sup> T cells and defined T<sub>Reg</sub> cells as CD25<sup>+</sup>CD127<sup>low</sup>Foxp3<sup>+</sup>. Next we gated on β7<sup>+</sup> cells and determined β1<sup>+</sup>PI16<sup>+</sup> and β1<sup>-</sup>PI16<sup>-</sup> cells in this subset (controls shown).

Supplementary Table 1: Summary of patient characteristics in total

		CON	CD	UC
<b>Number Patients</b>		61	120	118
<b>Number Samples</b>		135	183	194
<b>Age (Ø, range)</b>		28 (18-44)	39 (18-75)	45 (18-82)
<b>Female [%]</b>		68.1	56.3	45.9
<b>HBI (Ø, range)</b>			5.0 (0-25)	
<b>Mayo c.s. (Ø, range)</b>				2.1 (0-11)
<b>Therapy [%]</b>	<i>Aminosalisylates</i>		19.6	41.3
	<i>Steroids</i>		21.2	37.6
	<i>Immunosuppressants</i>		3.2	1.6
	<i>Anti-TNF antibodies</i>		37.0	23.8
	<i>Vedolizumab</i>		48.7	68.8
	<i>Ustekinumab</i>		6.9	0.5
<b>Disease localization [%]</b>			L1: 19.2	E1: 24.3
			L2: 14.7	E2: 23.7
			L3: 45.2	E3: 52.0
			L4: 0.0	
			L4+: 20.9	

Supplementary Table 2: Patient information for Figure 1

		CON	CD	UC
<b>Number</b>		27	33	27
<b>Age (Ø, range)</b>		26 (18-37)	40 (21-75)	44 (25-74)
<b>Female [%]</b>		66.7	54.5	44.4
<b>HBI (Ø, range)</b>			3.5 (0-17)	
<b>Mayo c.s. (Ø, range)</b>				1.3 (0-6)
<b>Therapy [%]</b>	<i>Aminosalisylates</i>		3.1	20.8
	<i>Steroids</i>		12.5	16.7
	<i>Immunosuppressants</i>		0.0	8.3
	<i>Anti-TNF antibodies</i>		93.8	83.3
	<i>Vedolizumab</i>		0.0	0.0
	<i>Ustekinumab</i>		9.4	0.0
<b>Disease localization [%]</b>			L1: 25.8	E1: 30.8
			L2: 12.9	E2: 7.7
			L3: 45.2	E3: 61.5
			L4: 0.0	
			L4+: 16.1	

Supplementary Table 3: Patient information for Figure 2

		CON	CD	UC
<b>Number</b>		22	11	10
<b>Age (Ø, range)</b>		29 (22-42)	40 (24-70)	46 (27-69)
<b>Female [%]</b>		59.1	63.6	40.0
<b>HBI (Ø, range)</b>			6.3 (1-25)	
<b>Mayo c.s. (Ø, range)</b>				1.5 (0-5)
<b>Therapy [%]</b>	<i>Aminosalisylates</i>		9.1	60.0
	<i>Steroids</i>		18.2	20.0
	<i>Immunosuppressants</i>		0.0	10.0
	<i>Anti-TNF antibodies</i>		81.8	80.0
	<i>Vedolizumab</i>		0.0	0.0
	<i>Ustekinumab</i>		18.2	0.0
	<i>Tofacitinib</i>		0.0	10.0
<b>Disease localization [%]</b>			L1: 18.2	E1: 40.0
			L2: 0.0	E2: 10.0
			L3: 54.5	E3: 50.0
			L4: 0.0	
			L4+: 27.3	

Supplementary Table 4: Patient information for Figure 4 A, B

		CON	CD	UC
<b>Number</b>		2	2	3
<b>Age (Ø, range)</b>		31 (28-33))	55 (38-72)	22 (18-31)
<b>Female [%]</b>		100.0	0.0	100.0
<b>HBI (Ø, range)</b>			4 (3-5)	
<b>Mayo c.s. (Ø, range)</b>				1 (0-1)
<b>Therapy [%]</b>	<i>Aminosalisylates</i>		0.0	66.7
	<i>Steroids</i>		0.0	0.0
	<i>Immunosuppressants</i>		0.0	0.0
	<i>Anti-TNF antibodies</i>		50.0	100.0
	<i>Vedolizumab</i>		0.0	0.0
	<i>Ustekinumab</i>		50.0	0.0
<b>Disease localization [%]</b>			L1: 0.0	E1: 33.3
			L2: 0.0	E2: 33.3
			L3: 50.0	E3: 33.3
			L4: 0.0	
			L4+ <sup>1</sup> : 50.0	

<sup>1</sup> Concomitant lower and upper gastrointestinal disease

Supplementary Table 5: Patient information for Figure 4 C

		CD	UC
<b>Number Patients</b>		33	49
<b>Number Samples</b>		46	78
<b>Age (Ø, range)</b>		41 (18-71)	47 (19-82)
<b>Female [%]</b>		56.5	52.6
<b>HBI (Ø, range)</b>		5.4 (1-12)	
<b>Mayo c.s. (Ø, range)</b>			2.6 (0-7)
<b>Therapy [%]</b>	<i>Aminosalisylates</i>	24.4	36.4
	<i>Steroids</i>	35.6	54.5
	<i>Immunosuppressants</i>	6.7	0.0
	<i>Anti-TNF antibodies</i>	0.0	0.0
	<i>Vedolizumab</i>	100.0	100.0
	<i>Ustekinumab</i>	0.0	0.0
<b>Disease localization [%]</b>		L1: 18.2	E1: 23.9
		L2: 22.7	E2: 32.4
		L3: 34.1	E3: 43.7
		L4: 0.0	
		L4+: 25.0	

Supplementary Table 6: Patient information for Figure 6 A-C

	CON
Number Patients	16
Age (Ø, range)	28 (20-44)
Female [%]	76.5

Supplementary Table 7: Patient information for Figure 6 D, E

		CD	UC
<b>Number Patients</b>		17	26
<b>Number Samples</b>		25	30
<b>Age (Ø, range)</b>		39 (18-66)	42 (19-68)
<b>Female [%]</b>		52.0	36.7
<b>HBI (Ø, range)</b>		4.2 (1-10)	
<b>Mayo c.s. (Ø, range)</b>			0.9 (0-4)
<b>Therapy [%]</b>	<i>Aminosalisylates</i>	25.0	40.8
	<i>Steroids</i>	16.7	17.2
	<i>Immunosuppressants</i>	4.2	0.0
	<i>Anti-TNF antibodies</i>	0.0	0.0
	<i>Vedolizumab</i>	100.0	100.0
	<i>Ustekinumab</i>	0.0	0.0
<b>Disease localization [%]</b>		L1: 17.4	E1: 24.0
		L2: 17.4	E2: 28.0
		L3: 56.5	E3: 48.0
		L4: 0.0	
		L4+: 8.7	

**Supplementary Table 8: Patient information for Figure 7**

	CON
<b>Number Patients</b>	7
<b>Age (Ø, range)</b>	29 (22-44)
<b>Female [%]</b>	71.4

Supplementary Table 9: Patient information for Figure 8

		CD	UC
<b>Number Patients</b>		8	2
<b>Number Samples</b>		10	2
<b>Age (Ø, range)</b>		39 (17-63)	42 (26-58)
<b>Female [%]</b>		70.0	0.0
<b>HBI (Ø, range)</b>		5 (2-8)	
<b>Mayo c.s. (Ø, range)</b>			1.5 (1-2)
<b>Therapy [%]</b>	<i>Aminosalisylates</i>	37.5	50.0
	<i>Steroids</i>	0.0	0.0
	<i>Immunosuppressants</i>	0.0	0.0
	<i>Anti-TNF antibodies</i>	62.5	0.0
	<i>Vedolizumab</i>	0.0	0.0
	<i>Ustekinumab</i>	37.5	100.0
<b>Disease localization [%]</b>		L1: 30.0	E1: 0.0
		L2: 30.0	E2: 0.0
		L3: 30.0	E3: 100.0
		L4: 0.0	
		L4+: 10.0	

Supplementary Table 10: Patient information for Figure 9A

		CD	UC
<b>Number Patients</b>		9	11
<b>Number Samples</b>		14	16
<b>Age (Ø, range)</b>		34 (18-57)	48 (19-66)
<b>Female [%]</b>		50.0	37.5
<b>HBI (Ø, range)</b>		4.9 (1-9)	
<b>Mayo c.s. (Ø, range)</b>			2.8 (0-6)
<b>Therapy [%]</b>	<i>Aminosalisylates</i>	61.5	46.7
	<i>Steroids</i>	30.8	73.3
	<i>Immunosuppressants</i>	0.0	0.0
	<i>Anti-TNF antibodies</i>	0.0	0.0
	<i>Vedolizumab</i>	100.0	100.0
	<i>Ustekinumab</i>	0.0	0.0
<b>Disease localization [%]</b>		L1: 21.4	E1: 15.4
		L2: 28.6	E2: 38.5
		L3: 42.9	E3: 46.1
		L4: 0.0	
		L4+: 7.1	

Supplementary Table 11: Patient information for Figure 9 B+C

		CD	UC
<b>Number Patients</b>		15	10
<b>Number Samples</b>		20	10
<b>Age (Ø, range)</b>		36 (18-59)	41 (22-62)
<b>Female [%]</b>		60.0	30.0
<b>HBI (Ø, range)</b>		9 (2-22)	
<b>Mayo c.s. (Ø, range)</b>			5.6 (1-11)
<b>Therapy [%]</b>	<i>Aminosalisylates</i>	15.0	50.0
	<i>Steroids</i>	35.0	30.0
	<i>Immunosuppressants</i>	10.0	0.0
	<i>Anti-TNF antibodies</i>	30.0	10.0
	<i>Vedolizumab</i>	55.0	70.0
	<i>Ustekinumab</i>	0.0	0.0
<b>Disease localization [%]</b>		L1: 20.0	E1: 30.0
		L2: 0.0	E2: 0.0
		L3: 45.0	E3: 70.0
		L4: 0.0	
		L4+: 35.0	

Supplementary Table 12: Patient information for Suppl. Figure 1 A, B

		CON	CD	UC
<b>Number</b>		36	26	23
<b>Age (Ø, range)</b>		27 (18-44)	40 (22-70)	46 (25-74)
<b>Female [%]</b>		63.9	53.8	43.5
<b>HBI (Ø, range)</b>			4.2 (0-17)	
<b>Mayo c.s. (Ø, range)</b>				1.0 (0-4)
<b>Therapy [%]</b>	<i>Aminosalisylates</i>		7.7	31.8
	<i>Steroids</i>		7.7	18.2
	<i>Immunosuppressants</i>		0.0	9.1
	<i>Anti-TNF antibodies</i>		80.8	77.3
	<i>Vedolizumab</i>		0.0	0.0
	<i>Ustekinumab</i>		19.2	4.5
<b>Disease localization [%]</b>			L1: 24.0	E1: 28.6
			L2: 12.0	E2: 9.5
			L3: 40.0	E3: 61.9
			L4: 0.0	
			L4+: 24.0	

Supplementary Table 13: Patient information for Supplementary Figure 3

		CON	CD	UC
<b>Number</b>		10	11	6
<b>Age (Ø, range)</b>		28 (22-36)	40 (25-60)	46 (23-72)
<b>Female [%]</b>		50.0	63.6	50.0
<b>HBI (Ø, range)</b>			4.6 (0-10)	
<b>Mayo c.s. (Ø, range)</b>				1.4 (0-3)
<b>Therapy [%]</b>	<i>Aminosalisylates</i>		9.1	16.7
	<i>Steroids</i>		0.0	16.7
	<i>Immunosuppressants</i>		0.0	0.0
	<i>Anti-TNF antibodies</i>		90.9	83.3
	<i>Vedolizumab</i>		0.0	0.0
	<i>Ustekinumab</i>		9.1	0.0
<b>Disease localization [%]</b>			L1: 0.0	E1: 0.0
			L2: 0.0	E2: 33.3
			L3: 81.8	E3: 66.7
			L4: 0.0	
			L4+: 18.2	

**Supplementary Table 14: Patient information for Supplementary Figure 4**

	CON
<b>Number Patients</b>	23
<b>Number Samples</b>	28
<b>Age (Ø, range)</b>	32 (19-44)
<b>Female [%]</b>	85.7

Supplementary Table 15: Patient information for Supplementary Figure 9

		CD	UC
<b>Number</b>		5	6
<b>Age (Ø, range)</b>		35 (25-60)	38 (25-44)
<b>Female [%]</b>		40.0	66.7
<b>HBI (Ø, range)</b>		2.8 (0-7)	
<b>Mayo c.s. (Ø, range)</b>			1.3 (0-2)
<b>Therapy [%]</b>	<i>Aminosalisylates</i>	20.0	100.0
	<i>Steroids</i>	40.0	33.3
	<i>Immunosuppressants</i>	0.0	0.0
	<i>Anti-TNF antibodies</i>	80.0	66.7
	<i>Vedolizumab</i>	0.0	0.0
	<i>Ustekinumab</i>	20.0	33.3
<b>Disease localization [%]</b>		L1: 40.0	E1: 16.7
		L2: 0.0	E2: 0.0
		L3: 20.0	E3: 83.3
		L4: 0.0	
		L4+: 40.0	

Differential gene expression analysis T <sub>Reg</sub> VDZ <sup>+</sup> vs VDZ <sup>-</sup>				
	gene	Pr(>Chisq)	log2fc_coef	FDR
1	ITGB1	3,44419E-81	-0,883217881	5,60921E-77
7	VIM	6,78636E-37	-0,607905444	1,57889E-33
5	S100A4	1,45131E-38	-0,570339321	4,72722E-35
22	IL32	2,82908E-25	-0,544134167	2,09429E-22
6	LGALS1	4,16662E-37	-0,506959928	1,13096E-33
25	S100A6	3,43747E-24	-0,405365872	2,2393E-21
8	HLA-DPB1	1,95076E-36	-0,400331338	3,97127E-33
10	HLA-DRB1	1,21059E-35	-0,367438698	1,97156E-32
12	HLA-DPA1	6,62329E-34	-0,363506346	8,98891E-31
34	AHNAK	6,46101E-17	-0,350386769	3,06853E-14
36	CXCR4	2,24835E-16	-0,3294199	1,01713E-13
20	ALOX5AP	1,45158E-26	-0,309097995	1,18202E-23
44	CD74	6,68181E-14	-0,300902614	2,47318E-11
15	HPGD	1,73677E-31	-0,299412017	1,88567E-28
62	TSC22D3	2,01911E-10	-0,291719654	5,30374E-08
37	ANXA2	2,45007E-16	-0,289730629	1,07843E-13
19	HLA-DQB1	4,0429E-27	-0,277630084	3,4654E-24
29	PLP2	3,59786E-20	-0,268320538	2,02051E-17
3	LMNA	1,40183E-43	-0,263579888	7,61004E-40
4	CSGALNACT1	1,06631E-40	-0,263187541	4,34147E-37
17	DUSP4	2,90674E-29	-0,259179309	2,78466E-26
21	HLA-DRB5	2,10654E-26	-0,258837852	1,63367E-23
35	FAM129A	6,59452E-17	-0,258266034	3,06853E-14
78	COTL1	4,73529E-09	-0,256039016	9,88704E-07
63	FOSB	3,18156E-10	-0,252978784	8,22458E-08
45	TTC39C	2,29866E-13	-0,248614533	8,31912E-11
40	HERPUD1	8,48821E-15	-0,248417231	3,45597E-12
53	FLNA	2,53891E-11	-0,242437787	7,80163E-09
72	GSTK1	1,06633E-09	-0,241003863	2,41199E-07
71	RTKN2	1,01257E-09	-0,238594408	2,32264E-07
101	S100A10	2,16134E-07	-0,234197687	3,48511E-05
42	HLA-C	2,73093E-14	-0,22387524	1,05895E-11
23	C15orf53	1,21036E-24	-0,223191482	8,57039E-22
50	PMAIP1	7,53376E-12	-0,221752965	2,4539E-09
108	KLF6	3,56552E-07	-0,218440536	5,37667E-05
110	MTRNR2L12	4,48513E-07	-0,20761775	6,64044E-05
59	MBP	1,61859E-10	-0,206384745	4,46787E-08
9	CCR10	4,19025E-36	-0,205655832	7,5825E-33
46	LGALS3	3,91455E-13	-0,20560529	1,38592E-10
51	SORL1	1,09889E-11	-0,205457023	3,50913E-09
56	IKZF2	1,04886E-10	-0,204497948	3,05032E-08
41	HLA-DRA	1,73013E-14	-0,203994162	6,87241E-12
32	B2M	3,61107E-18	-0,201226674	1,83781E-15
83	TTN	1,67325E-08	-0,196531678	3,28319E-06
95	CRIP1	5,10312E-08	-0,194370907	8,74836E-06
124	CYBA	1,35095E-06	-0,191608283	0,000176013
105	ATP2B1	2,83614E-07	-0,189022706	4,39898E-05
81	ITGB2	1,37343E-08	-0,189018198	2,76145E-06
122	CD99	1,14138E-06	-0,188823453	0,000152365
26	FANK1	1,52229E-21	-0,186254043	9,53537E-19
73	SH3BGRL3	1,15154E-09	-0,185115489	2,56905E-07
91	EMB	3,57329E-08	-0,184165468	6,39502E-06
49	C12orf75	1,97858E-12	-0,181096184	6,57617E-10
90	CLIC1	3,47847E-08	-0,177380095	6,29449E-06
193	PPP1R15A	4,0295E-05	-0,17492336	0,003411647
153	LSP1	6,81869E-06	-0,172165071	0,000733302
13	FUT7	3,3468E-32	-0,172049584	4,19276E-29
86	ANXA5	2,45339E-08	-0,171362597	4,64604E-06
169	JUNB	1,47113E-05	-0,17042547	0,001417678
145	MALAT1	4,41845E-06	-0,168958764	0,000496268
129	PAG1	1,67874E-06	-0,168145742	0,000211937
170	ZFP36L2	1,60349E-05	-0,168064026	0,001536141
43	ANXA1	3,33538E-14	-0,167301678	1,26325E-11
147	EZR	5,71851E-06	-0,165238984	0,000633549
84	CD84	1,77447E-08	-0,162818944	3,44036E-06
65	PDE3B	4,06566E-10	-0,160699397	1,02228E-07
38	JAML	5,77142E-16	-0,160663604	2,47351E-13
74	HLA-B	1,34308E-09	-0,158845161	2,95587E-07
24	HLA-DQA1	1,75349E-24	-0,158631818	1,18989E-21
79	GLUPR1	5,37111E-09	-0,154817488	1,10726E-06
18	PI16	1,08974E-27	-0,154406056	9,85974E-25
27	HLA-DQA2	2,05671E-21	-0,154222955	1,24058E-18
164	YWHAB	1,30032E-05	-0,148053377	0,001299494
130	HLA-A	1,83444E-06	-0,145999532	0,000229813
114	MAL	7,84108E-07	-0,144936518	0,000112017
195	DOK2	4,20239E-05	-0,140729271	0,003509747
220	ACAP1	9,35763E-05	-0,140067861	0,006864793

210	LITAF	7,35415E-05	-0,13964628	0,005703322
215	IQGAP1	8,27451E-05	-0,134434267	0,006263522
199	ITK	4,74144E-05	-0,133911215	0,003880354
112	ACTN4	6,76297E-07	-0,133389704	9,82545E-05
54	PRNP	4,07698E-11	-0,127611302	1,22959E-08
218	TPM4	8,85116E-05	-0,124128159	0,006612384
165	TXN	1,3449E-05	-0,122326017	0,001327462
161	MTRNR2L8	1,11909E-05	-0,114945	0,001132015
136	ENTPD1	2,80111E-06	-0,114933652	0,000335433
88	CST7	3,134E-08	-0,11416517	5,73486E-06
174	UBL3	1,94288E-05	-0,112930796	0,001818494
167	TMX4	1,42716E-05	-0,11226061	0,001391781
120	KRTCAP2	9,92783E-07	-0,110643484	0,000134737
144	CD63	4,12162E-06	-0,109196171	0,000466144
156	LPAR6	9,40425E-06	-0,109116682	0,00098178
225	MAP4K4	9,53033E-05	-0,108831988	0,006898265
181	AKNA	2,46438E-05	-0,108105569	0,002217401
194	CCR4	4,12383E-05	-0,107968158	0,003461888
232	MYO1F	0,000113512	-0,107331943	0,007968316
163	TOB1	1,30859E-05	-0,106104923	0,001299494
39	ITM2C	3,05125E-15	-0,098588558	1,27417E-12
226	MAN1A2	9,82557E-05	-0,097160674	0,007080497
197	CTSA	4,52903E-05	-0,094602448	0,003725243
175	SH3BP5	2,04531E-05	-0,094018638	0,001903428
113	TCEAL4	6,81737E-07	-0,093568187	9,82545E-05
158	P2RY8	1,02388E-05	-0,093300671	0,001055371
47	CPNE2	8,125E-13	-0,091895304	2,8154E-10
192	ELK3	4,04303E-05	-0,09130075	0,003411647
52	A1BG	1,19348E-11	-0,090753875	3,73787E-09
203	CD82	5,30239E-05	-0,086186805	0,004253931
97	SYTL3	1,02825E-07	-0,085907347	1,72639E-05
162	PTGER4	1,30829E-05	-0,082124344	0,001299494
87	CORO2A	2,6817E-08	-0,081712714	5,02003E-06
149	ADAM8	6,2918E-06	-0,0812875	0,000687707
132	SGMS1	2,42199E-06	-0,080619131	0,000298822
208	TOX	6,59302E-05	-0,08045956	0,005172784
151	BARD1	6,88906E-06	-0,077196121	0,000733302
93	SLC25A24	4,21214E-08	-0,075445442	7,37623E-06
77	SOX4	3,96728E-09	-0,074196132	8,39105E-07
127	HLA-DMA	1,52269E-06	-0,074040856	0,000195264
168	ANTXR2	1,46079E-05	-0,07263007	0,001416093
166	BEX3	1,37779E-05	-0,069464586	0,001351731
198	SLF1	4,50638E-05	-0,069096444	0,003725243
141	GPR65	3,69636E-06	-0,068328619	0,000426943
121	JAKMIP1	1,0229E-06	-0,067553898	0,000137677
206	TIAM1	6,35753E-05	-0,066490484	0,005026153
125	FGL2	1,34701E-06	-0,060368007	0,000176013
216	TNFRSF18	8,2712E-05	-0,059171305	0,006263522
150	AC006369.1	6,5786E-06	-0,055554381	0,000714261
202	RCBTB2	5,25558E-05	-0,054165616	0,004237243
235	PKIA	0,000120332	-0,053584918	0,008339254
187	ADARB1	2,77922E-05	-0,053457404	0,002420444
106	AC100793.2	3,19192E-07	-0,05203153	4,90411E-05
182	ARHGEF12	2,50608E-05	-0,051801166	0,002242532
196	SYNE3	4,26217E-05	-0,051705592	0,003541518
160	CAPG	1,11541E-05	-0,050653475	0,001132015
94	HLA-DMB	4,58069E-08	-0,049925119	7,93628E-06
68	TNFRSF9	7,28369E-10	-0,049494189	1,74444E-07
204	RARA	5,39755E-05	-0,048985714	0,004309044
222	ZNRF1	9,33173E-05	-0,047511416	0,006864793
209	ADAM12	7,06999E-05	-0,046241333	0,005509177
224	SH3BP2	9,47493E-05	-0,044100143	0,006888783
123	TGFBR3	1,16139E-06	-0,04206033	0,000153775
135	AL365203.2	2,77584E-06	-0,041126547	0,000334869
119	ZNF365	9,26808E-07	-0,040838303	0,000127708
104	GALNT3	2,58954E-07	-0,040830153	4,05512E-05
236	SMAD7	0,000135453	-0,039827193	0,009347416
159	SEMA3G	1,09696E-05	-0,038408389	0,001123592
139	AL121748.1	3,51337E-06	-0,035000553	0,000408706
96	MLF1	8,56786E-08	-0,034198316	1,4535E-05
126	GDPD5	1,47013E-06	-0,033440848	0,00019002
233	BASP1	0,000117138	-0,030954297	0,00815258
109	SEPT10	3,88811E-07	-0,030708612	5,80933E-05
146	PPP2R2B	4,47936E-06	-0,026584683	0,000499664
200	CCR3	4,86669E-05	-0,023782401	0,003943232
179	CDC42BPB	2,16543E-05	-0,023424252	0,001970179
180	COL5A3	2,1991E-05	0,017914529	0,001989696
152	HIC1	6,85158E-06	0,022566578	0,000733302
230	CDCA7L	0,000107745	0,038105093	0,007629272
137	BACH2	2,94028E-06	0,038629684	0,000349528

99	DUSP6	1,4027E-07	0,047239301	2,30752E-05
178	GIMAP5	2,12632E-05	0,047340361	0,001945465
191	METTL7A	3,8425E-05	0,048291708	0,003276381
117	NRIP1	8,62691E-07	0,052654521	0,000120597
234	SMAD3	0,000116827	0,06142632	0,00815258
103	TMEM238	2,42872E-07	0,063413978	3,84021E-05
61	LZTFL1	1,96403E-10	0,064063135	5,24364E-08
213	LINC00402	7,8695E-05	0,065654844	0,006017027
229	PLAC8	0,000106676	0,068992821	0,007586562
116	CHRM3-AS2	8,66379E-07	0,069147426	0,000120597
237	ICA1	0,000142123	0,071741223	0,009766298
143	AC012368.1	4,0848E-06	0,082053275	0,00046521
154	LINC00891	7,95917E-06	0,082155027	0,000836732
184	NTSC3A	2,68821E-05	0,084809416	0,002379355
85	ACTN1	1,88773E-08	0,086678576	3,61688E-06
66	LINC01934	5,80221E-10	0,092753681	1,43174E-07
177	SINHCAF	2,10616E-05	0,097015465	0,001937904
212	TNFRSF1B	7,70031E-05	0,098435411	0,005915436
157	RABGAP1L	9,85066E-06	0,115079656	0,001021834
28	CD38	1,6811E-20	0,115452228	9,77801E-18
142	KLRB1	3,93527E-06	0,116473594	0,000451336
186	SESN3	2,75867E-05	0,116824406	0,002415467
115	RPLP0	8,36788E-07	0,118437825	0,000118504
190	CACYBP	3,73609E-05	0,123236745	0,003202421
231	RPL15	0,00010825	0,123315867	0,007631861
98	GBP4	1,28811E-07	0,127389284	2,14063E-05
219	STK17A	9,09265E-05	0,129922566	0,006761776
201	TLK1	4,86524E-05	0,1314036	0,003943232
207	LAPTM5	6,60653E-05	0,132146458	0,005172784
185	APBB1IP	2,71263E-05	0,132744148	0,00238799
14	CCR9	1,12661E-31	0,137220094	1,31057E-28
140	IL6ST	3,50945E-06	0,137237902	0,000408706
217	RPS5	8,579E-05	0,13978404	0,006438599
211	HINT1	7,68361E-05	0,143954741	0,005915436
173	H3F3B	1,92135E-05	0,145680757	0,001808732
227	RPS13	0,000100523	0,14818737	0,007211972
80	CD59	9,59149E-09	0,149740111	1,95259E-06
221	RPS6	9,31234E-05	0,150086036	0,006864793
189	TPR	3,37923E-05	0,154863286	0,002911858
134	TCF7	2,56098E-06	0,156383843	0,000313492
223	RPL10A	9,41293E-05	0,159355353	0,006874394
155	RPS4X	7,96349E-06	0,161944179	0,000836732
171	LBH	1,62656E-05	0,162959103	0,001549133
148	YPEL3	5,8719E-06	0,163341391	0,000646147
188	G8P2	3,3321E-05	0,167239323	0,002886518
131	RARRES3	2,34588E-06	0,167330083	0,000291642
228	CD2	0,000105867	0,167448722	0,007562096
172	RPL13	1,8491E-05	0,178152701	0,001750841
118	RGS10	9,33147E-07	0,178778245	0,000127708
70	RACK1	8,62331E-10	0,183952102	2,00628E-07
107	TRAF3IP3	3,24905E-07	0,184678722	4,94524E-05
89	NOSIP	3,1232E-08	0,185766587	5,73486E-06
100	FYB1	1,91782E-07	0,186532756	3,12336E-05
133	CD247	2,57939E-06	0,188643602	0,000313492
128	RPS2	1,55835E-06	0,191385025	0,000198276
205	LTB	5,95586E-05	0,194798024	0,00473157
111	RPLP1	5,07022E-07	0,19485919	7,43906E-05
183	RPS12	2,55741E-05	0,198907874	0,002275953
76	RPS10	3,63176E-09	0,206138781	7,78249E-07
102	UCP2	2,33165E-07	0,207870454	3,72287E-05
69	KLF3	8,57814E-10	0,217712905	2,00628E-07
64	GIMAP1	4,08008E-10	0,222896692	1,02228E-07
75	RPL3	1,61516E-09	0,229438584	3,50727E-07
58	TBC1D4	1,49957E-10	0,230038838	4,2107E-08
60	LDHB	1,90171E-10	0,23241634	5,16187E-08
67	EEF1B2	7,22161E-10	0,243401288	1,74444E-07
57	FOXP1	1,30899E-10	0,248152731	3,74004E-08
55	LIMD2	8,61452E-11	0,258485118	2,55084E-08
48	RPS8	8,77967E-13	0,283887763	2,97887E-10
16	TXK	4,63333E-31	0,287691793	4,71615E-28
31	CCR7	4,43298E-19	0,29381441	2,32889E-16
33	LIMS1	1,47577E-17	0,352768158	7,28313E-15
30	GIMAP4	1,44687E-19	0,372427133	7,8546E-17
11	GIMAP7	4,09562E-34	0,564729966	6,06376E-31
2	ITGA4	1,21443E-72	0,70828248	9,8891E-69
82	NEDD4L	1,54502E-08		3,06855E-06
92	GPR55	4,15581E-08		7,3567E-06
138	CHDH	3,18856E-06		0,000376297
176	LOXL1	2,06819E-05		0,001913781
214	CNTNAP1	8,30726E-05		0,006263522

Count of T <sub>Reg</sub> cells expressing genes VDZ <sup>+</sup> vs VDZ <sup>-</sup>							
	gene	Pr(>Chisq)	log2fc_coef	FDR	Expr_Cells_Treg	Expr_Cells_Treg_VN	Expr_Cells_Treg_VP
1	ITGB1	3,44419E-81	-0,883217881	5,60921E-77	719	576	143
7	VIM	6,78636E-37	-0,607905444	1,57889E-33	1025	669	356
5	S100A4	1,45131E-38	-0,570339321	4,72722E-35	1049	665	384
22	IL32	2,82908E-25	-0,544134167	2,09429E-22	1013	659	354
6	LGALS1	4,16662E-37	-0,506959928	1,13096E-33	482	372	110
25	S100A6	3,43747E-24	-0,405365872	2,2393E-21	1008	642	366
8	HLA-DPB1	1,95076E-36	-0,400331338	3,97127E-33	451	375	76
10	HLA-DRB1	1,21059E-35	-0,367438698	1,97156E-32	365	314	51
12	HLA-DPA1	6,62329E-34	-0,363506346	8,98891E-31	401	338	63
34	AHNAK	6,46101E-17	-0,350386769	3,06853E-14	730	515	215
36	CXCR4	2,24835E-16	-0,3294199	1,01713E-13	631	455	176
20	ALOX5AP	1,45158E-26	-0,309097995	1,18202E-23	432	338	94
44	CD74	6,68181E-14	-0,300902614	2,47318E-11	710	465	245
15	HPGD	1,73677E-31	-0,299412017	1,88567E-28	276	248	28
62	TSC22D3	2,01911E-10	-0,291719654	5,30374E-08	1005	645	360
37	ANXA2	2,45007E-16	-0,289730629	1,07843E-13	607	422	185
19	HLA-DQB1	4,0429E-27	-0,277630084	3,4654E-24	352	296	56
29	PLP2	3,59786E-20	-0,268320538	2,02051E-17	476	346	130
3	LMNA	1,40183E-43	-0,263579888	7,61004E-40	221	215	6
4	CSGALNACT1	1,06631E-40	-0,263187541	4,34147E-37	247	233	14
17	DUSP4	2,90674E-29	-0,259179309	2,78466E-26	292	246	46
21	HLA-DRB5	2,10654E-26	-0,258837852	1,63367E-23	283	245	38
35	FAM129A	6,59452E-17	-0,258266034	3,06853E-14	477	348	129
78	COTL1	4,73529E-09	-0,256039016	9,88704E-07	772	501	271
63	FOSB	3,18156E-10	-0,252978784	8,22458E-08	535	384	151
45	TTC39C	2,29866E-13	-0,248614533	8,31912E-11	570	399	171
40	HERPUD1	8,48821E-15	-0,248417231	3,45597E-12	513	368	145
53	FLNA	2,53891E-11	-0,242437787	7,80163E-09	701	465	236
72	GSTK1	1,06633E-09	-0,241003863	2,41199E-07	828	539	289
71	RTKN2	1,01257E-09	-0,238594408	2,32264E-07	435	317	118
101	S100A10	2,16134E-07	-0,234197687	3,48511E-05	976	619	357
42	HLA-C	2,73093E-14	-0,22387524	1,05895E-11	1138	719	419
23	C15orf53	1,21036E-24	-0,223191482	8,57039E-22	271	234	37
50	PMAIP1	7,53376E-12	-0,221752965	2,4539E-09	434	313	121
108	KLF6	3,56552E-07	-0,218440536	5,37667E-05	840	543	297
110	MTRNR2L12	4,48513E-07	-0,20761775	6,64044E-05	1074	682	392
59	MBP	1,61859E-10	-0,206384745	4,46787E-08	663	436	227
9	CCR10	4,19025E-36	-0,205655832	7,5825E-33	166	165	1
46	LGALS3	3,91455E-13	-0,20560529	1,38592E-10	349	264	85
51	SORL1	1,09889E-11	-0,205457023	3,50913E-09	393	293	100
56	IKZF2	1,04886E-10	-0,204497948	3,05032E-08	445	322	123
41	HLA-DRA	1,73013E-14	-0,203994162	6,87241E-12	285	227	58
32	B2M	3,61107E-18	-0,201226674	1,83781E-15	1142	721	421
83	TTN	1,67325E-08	-0,196531678	3,28319E-06	434	310	124
95	CRIP1	5,10312E-08	-0,194370907	8,74836E-06	583	388	195
124	CYBA	1,35095E-06	-0,191608283	0,000176013	958	610	348
105	ATP2B1	2,83614E-07	-0,189022706	4,39898E-05	600	406	194
81	ITGB2	1,37343E-08	-0,189018198	2,76145E-06	700	452	248
122	CD99	1,14138E-06	-0,188823453	0,000152365	776	497	279
26	FANK1	1,52229E-21	-0,186254043	9,53537E-19	242	209	33
73	SH3BGR13	1,15154E-09	-0,185115489	2,56905E-07	1003	621	382
91	EMB	3,57329E-08	-0,184165468	6,39502E-06	599	400	199
49	C12orf75	1,97858E-12	-0,181096184	6,57617E-10	383	271	112
90	CLIC1	3,47847E-08	-0,177380095	6,29449E-06	888	556	332
193	PPP1R15A	4,0295E-05	-0,17492336	0,003411647	785	514	271
153	LSP1	6,81869E-06	-0,172165071	0,000733302	780	491	289
13	FUT7	3,3468E-32	-0,172049584	4,19276E-29	171	164	7
86	ANXA5	2,45339E-08	-0,171362597	4,64604E-06	526	346	180
169	JUNB	1,47113E-05	-0,17042547	0,001417678	1039	649	390
145	MALAT1	4,41845E-06	-0,168958764	0,000496268	1143	722	421
129	PAG1	1,67874E-06	-0,168145742	0,000211937	554	378	176
170	ZFP36L2	1,60349E-05	-0,168064026	0,001536141	991	628	363

43	ANXA1	3,33538E-14	-0,167301678	1,26325E-11	215	178	37
147	EZR	5,71851E-06	-0,165238984	0,000633549	735	473	262
84	CD84	1,77447E-08	-0,162818944	3,44036E-06	418	296	122
65	PDE3B	4,06566E-10	-0,160699397	1,02228E-07	351	258	93
38	JAML	5,77142E-16	-0,160663604	2,47351E-13	242	199	43
74	HLA-B	1,34308E-09	-0,158845161	2,95587E-07	1141	722	419
24	HLA-DQA1	1,75349E-24	-0,158631818	1,18989E-21	159	150	9
79	GLIPR1	5,37111E-09	-0,154817488	1,10726E-06	404	280	124
18	PI16	1,08974E-27	-0,154406056	9,85974E-25	153	148	5
27	HLA-DQA2	2,05671E-21	-0,154222955	1,24058E-18	162	149	13
164	YWHAB	1,30032E-05	-0,148053377	0,001299494	987	619	368
130	HLA-A	1,83444E-06	-0,145999532	0,000229813	1143	722	421
114	MAL	7,84108E-07	-0,144936518	0,000112017	332	241	91
195	DOK2	4,20239E-05	-0,140729271	0,003509747	656	414	242
220	ACAP1	9,35763E-05	-0,140067861	0,006864793	836	534	302
210	LITAF	7,35415E-05	-0,13964628	0,005703322	587	382	205
215	IQGAP1	8,27451E-05	-0,134434267	0,006263522	622	405	217
199	ITK	4,74144E-05	-0,133911215	0,003880354	537	362	175
112	ACTN4	6,76297E-07	-0,133389704	9,82545E-05	419	291	128
54	PRNP	4,07698E-11	-0,127611302	1,22959E-08	217	174	43
218	TPM4	8,85116E-05	-0,124128159	0,006612384	546	344	202
165	TXN	1,3449E-05	-0,122326017	0,001327462	510	328	182
161	MTRNR2L8	1,11909E-05	-0,114945	0,001132015	381	262	119
136	ENTPD1	2,80111E-06	-0,114933652	0,000335433	289	209	80
88	CST7	3,134E-08	-0,11416517	5,73486E-06	232	174	58
174	UBL3	1,94288E-05	-0,112930796	0,001818494	445	290	155
167	TMX4	1,42716E-05	-0,11226061	0,001391781	388	263	125
120	KRTCAP2	9,92783E-07	-0,110643484	0,000134737	352	240	112
144	CD63	4,12162E-06	-0,109196171	0,000466144	328	231	97
156	LPAR6	9,40425E-06	-0,109116682	0,00098178	286	210	76
225	MAP4K4	9,53033E-05	-0,108831988	0,006898265	408	273	135
181	AKNA	2,46438E-05	-0,108105569	0,002217401	420	278	142
194	CCR4	4,12383E-05	-0,107968158	0,003461888	345	246	99
232	MYO1F	0,000113512	-0,107331943	0,007968316	504	325	179
163	TOB1	1,30859E-05	-0,106104923	0,001299494	351	239	112
157	RABGAP1L	9,85066E-06	0,115079656	0,001021834	414	220	194
28	CD38	1,6811E-20	0,115452228	9,77801E-18	159	37	122
142	KLRB1	3,93527E-06	0,116473594	0,000451336	218	95	123
186	SESN3	2,75867E-05	0,116824406	0,002415467	353	178	175
115	RPLP0	8,36788E-07	0,118437825	0,000118504	1029	646	383
190	CACYBP	3,73609E-05	0,123236745	0,003202421	466	242	224
231	RPL15	0,00010825	0,123315867	0,007631861	1101	693	408
98	GBP4	1,28811E-07	0,127389284	2,14063E-05	296	136	160
219	STK17A	9,09265E-05	0,129922566	0,006761776	489	258	231
201	TLK1	4,86524E-05	0,1314036	0,003943232	559	310	249
207	LAPTM5	6,60653E-05	0,132146458	0,005172784	923	561	362
185	APBB1IP	2,71263E-05	0,132744148	0,00238799	709	409	300
14	CCR9	1,12661E-31	0,137220094	1,31057E-28	95	4	91
140	IL6ST	3,50945E-06	0,137237902	0,000408706	351	176	175
217	RPS5	8,579E-05	0,13978404	0,006438599	1045	643	402
211	HINT1	7,68361E-05	0,143954741	0,005915436	930	561	369
173	H3F3B	1,92135E-05	0,145680757	0,001808732	1119	703	416
227	RPS13	0,000100523	0,14818737	0,007211972	1080	674	406
80	CD59	9,59149E-09	0,149740111	1,95259E-06	358	174	184
221	RPS6	9,31234E-05	0,150086036	0,006864793	1108	691	417
189	TPR	3,37923E-05	0,154863286	0,002911858	800	476	324
134	TCF7	2,56098E-06	0,156383843	0,000313492	453	235	218
223	RPL10A	9,41293E-05	0,159355353	0,006874394	1079	674	405
155	RPS4X	7,96349E-06	0,161944179	0,000836732	1124	708	416
171	LBH	1,62656E-05	0,162959103	0,001549133	646	362	284
148	YPEL3	5,8719E-06	0,163341391	0,000646147	641	357	284
188	GBP2	3,3321E-05	0,167239323	0,002886518	726	418	308
131	RARRES3	2,34588E-06	0,167330083	0,000291642	579	316	263
228	CD2	0,000105867	0,167448722	0,007562096	951	575	376

172	RPL13	1,8491E-05	0,178152701	0,001750841	1133	713	420
118	RGS10	9,33147E-07	0,178778245	0,000127708	597	322	275
70	RACK1	8,62331E-10	0,183952102	2,00628E-07	1092	680	412
107	TRAF3IP3	3,24905E-07	0,184678722	4,94524E-05	932	559	373
89	NOSIP	3,1232E-08	0,185766587	5,73486E-06	515	273	242
100	FYB1	1,91782E-07	0,186532756	3,12336E-05	1033	637	396
133	CD247	2,57939E-06	0,188643602	0,000313492	831	481	350
128	RPS2	1,55835E-06	0,191385025	0,000198276	1134	714	420
205	LTB	5,95586E-05	0,194798024	0,00473157	1040	650	390
111	RPLP1	5,07022E-07	0,19485919	7,43906E-05	1132	712	420
183	RPS12	2,55741E-05	0,198907874	0,002275953	1127	708	419
76	RPS10	3,63176E-09	0,206138781	7,78249E-07	950	572	378
102	UCP2	2,33165E-07	0,207870454	3,72287E-05	863	514	349
69	KLF3	8,57814E-10	0,217712905	2,00628E-07	544	280	264
64	GIMAP1	4,08008E-10	0,222896692	1,02228E-07	604	321	283
75	RPL3	1,61516E-09	0,229438584	3,50727E-07	1126	708	418
58	TBC1D4	1,49957E-10	0,230038838	4,2107E-08	578	307	271
60	LDHB	1,90171E-10	0,23241634	5,16187E-08	973	587	386
67	EEF1B2	7,22161E-10	0,243401288	1,74444E-07	997	609	388
57	FOXP1	1,30899E-10	0,248152731	3,74004E-08	778	454	324
55	UIMD2	8,61452E-11	0,258485118	2,55084E-08	932	548	384
48	RPS8	8,77967E-13	0,283887763	2,97887E-10	1097	683	414
16	TXK	4,63333E-31	0,287691793	4,71615E-28	299	96	203
31	CCR7	4,43298E-19	0,29381441	2,32889E-16	447	199	248
33	LIMS1	1,47577E-17	0,352768158	7,28313E-15	657	343	314
30	GIMAP4	1,44687E-19	0,372427133	7,8546E-17	643	326	317
11	GIMAP7	4,09562E-34	0,564729966	6,06376E-31	803	424	379
2	ITGA4	1,21443E-72	0,70828248	9,8891E-69	483	155	328

## Online Supplementary Methods

### Isolation of human peripheral blood mononuclear cells (PBMCs), PBMC subsets and granulocytes

PBMCs were isolated using density gradient centrifugation with Pancoll (PAN-Biotech). MACS isolation of CD4<sup>+</sup> T cells (CD4 MicroBeads, human/ CD4<sup>+</sup> T Cell Isolation Kit, human, Miltenyi Biotec) was performed according to the manufacturer's instructions.

Granulocytes were isolated from the cell pellet obtained after density gradient centrifugation. After removing PBMCs as well as remaining plasma and Pancoll reagent, cells were resuspended in 1 % Dextran 500 (Roth) in PBS and erythrocytes left to sediment for 30 min at room temperature. Supernatants containing granulocytes were transferred into fresh tubes and the remaining erythrocytes were lysed with hypotonic lysis (1 min 0.2 M NaCl, 1 min 1.6 M NaCl).

### Fluorescence-activated cell sorting (FACS)

FACS was used to isolate CD4<sup>+</sup>CD127<sup>low</sup>CD25<sup>high</sup> T<sub>Reg</sub> cells and CD4<sup>+</sup>CD127<sup>high</sup>CD25<sup>low</sup> T<sub>Eff</sub> cells. To this end, PBMCs isolated from leukocyte cones were stained with following fluorochrome-conjugated extracellular antibodies: CD3 (VioGreen, REA613/REAL104, Miltenyi Biotec), CD4 (VioBlue, VIT4/REAL103 Miltenyi Biotec), CD25 (PE/Cy7/FITC, BC96, Biolegend; PE-Vio770, REAL128, Miltenyi Biotec) and CD127 (APC, A019D5, Biolegend; APC/Vio770, REA614 or APC, REAL102, Miltenyi Biotec). Isolation of T cells binding or not binding vedolizumab was performed using fluorescently labelled vedolizumab at a concentration of 10 µg/ml and following

fluorochrome-conjugated extracellular antibodies: CD4 (FITC/VioGreen, VIT4, Miltenyi Biotec), CD45RO (BV510, clone, Biolegend), CD25 (PE/Cy7, BC96, Biolegend), CD127 (VioBright FITC, REA614, Miltenyi Biotec), CD49d (VioBlue, MZ18-24A9, Miltenyi Biotec), integrin beta 7 (PE, FIB27, Biolegend). Living cells were gated as negative for fixable viability dye efluor780 (eBioscience).

FACS was performed on MoFlo Astrios EQ1, MoFlo Astrios EQ2 (Beckman Coulter) and FACS Aria II SORP (BD Bioscience) instruments. Detachment of REAlease antibodies after isolation was performed using REAlease support kit (Miltenyi Biotec) according to the manufacturer's instructions.

### **Lamina propria mononuclear cell (LPMC) isolation from human biopsies**

Human intestinal biopsies from IBD patients were obtained during colonoscopy following informed written consent according to the approval of the Ethics Committee of the Friedrich Alexander University Erlangen-Nürnberg (249\_13 B). LPMC isolation was performed using the Lamina propria dissociation kit (Miltenyi Biotec) according to manufacturer's instructions followed by density gradient centrifugation with Percoll (GE Healthcare). After isolation, cells were either incubated with 50 ng/ml PMA, 1  $\mu$ M ionomycin and 1  $\mu$ g/ml brefeldin A for 4 h at 37°C or directly stained for flow cytometry.

### **Cell culture and *in vitro* stimulation**

For stimulation with  $\text{MnCl}_2$ , PBMCs were resuspended at a concentration of 10 Mio cells/ml in adhesion buffer (150 mM NaCl + 1 % HEPES)  $\pm$  1 mM  $\text{MnCl}_2$  for 1 minute at room temperature. For stimulation with anti-CD3/CD28, PBMCs were cultured in 48-

well-plates (Sarstedt) at a concentration of 1 Mio cells/ml over night at 37°C. Stimulation with PMA (1 µg/ml) and ionomycin (1 µM) was performed with 1 Mio cells/ml in 48-well-plates for 4 h at 37°C. For *in vitro* treatment with vedolizumab, cells were cultured in 48-well plates at a concentration of 1 Mio cells/ml with the indicated vedolizumab concentrations for 1 h at 37°C. For the detection of interleukin expression, cells were stimulated with 50 ng/ml PMA, 1 µM ionomycin and Golgi export blocked using 1 µg/ml brefeldin A for 4 h at 37°C.

### **Fluorescence microscopy of vedolizumab binding to T<sub>Reg</sub> and T<sub>Eff</sub> cells**

For imaging of vedolizumab binding to T<sub>Reg</sub> and T<sub>Eff</sub> cells, FACS-isolated cells were incubated with fluorescently labelled vedolizumab and integrin beta 7 antibody (PE, FIB27, Biolegend) or adequate isotype controls for 30 min at 4°C after removal of REAlease antibodies, then fixed using 4 % PFA. Nuclei were stained using Hoechst 33342 (ThermoFisher Scientific). Cells were embedded in Mowiol (Sigma Aldrich) and subsequently imaged using a fluorescence microscope (DM600B, Leica).

### **T<sub>Reg</sub> cell suppression assay**

To analyse the suppressive function of FACS-isolated T<sub>Reg</sub> cells, sorted T<sub>Reg</sub> and T<sub>Eff</sub> cells were stained with CellTrace FarRed (Invitrogen) according to the manufacturer's instructions. FarRed<sup>+</sup> T<sub>Eff</sub> cells were incubated with T<sub>Reg</sub> Suppression Inspector (Miltenyi Biotec) in RPMI 1640 (+ 10 % FBS, + 1 % Pen/Strep, Gibco) for 6 days at 37°C with or without unstained T<sub>Reg</sub> cells according to the manufacturer's instructions. FarRed<sup>+</sup> T<sub>Reg</sub> cells were incubated without T<sub>Eff</sub> cells as a control. After incubation, cells were harvested and stained with Fixable Viability Dye efluor 506 (Invitrogen). The

portion of proliferating cells was determined by analysis of CellTrace FarRed dilution by flow cytometry.

### Transmigration assays

For the analysis of the impact of vedolizumab on MAdCAM-dependent transmigration of T<sub>Reg</sub> and T<sub>Eff</sub> cells, MACS-isolated CD4<sup>+</sup> T cells were stained with fluorochrome-conjugated extracellular antibodies against CD4 (VioBlue, VIT4, Miltenyi Biotec), CD25 (PE/Cy7, BC96, Biolegend) and CD127 (APC/Vio770, REA614, Miltenyi Biotec) and resuspended in X-Vivo15 medium (Lonza) with 1 mM MnCl<sub>2</sub> and different concentrations of vedolizumab (0, 0.4, 2, 10 and 50 µg/ml) at a concentration of 2 Mio cells/ml. 160,000 cells were seeded in duplicates into inserts of a 3 µm transwell plate (Corning) that were previously coated with 5 µg/ml rhMAdCAM-1 for 1 h. Inserts were placed into wells filled with X-Vivo15 medium + 100 nM rhCCL25 (ImmunoTools) and the plate was incubated for 4 h at 37°C. Subsequently, inserts were discarded and the number of transmigrated T<sub>Reg</sub> and T<sub>Eff</sub> cells was quantified by flow cytometry.

### Immunohistochemistry

Cryosections of colon biopsies from IBD patients before and under treatment with vedolizumab were fixed with 4 % PFA, permeabilised with 0.1 % Triton-X in PBS and subsequently blocked with Avidin-Biotin Block (Vector Laboratories) and Roti-ImmunoBlock (Carl Roth) with 5 % BSA and 20 % goat serum. Primary antibodies targeting CD4 (1:200, 13B8.2, Novus Biological), Foxp3 (1:100, 236A/E7, eBioscience) and 1:100, FJK-16s, eBioscience) and integrin β1 (1:1000, JB1B, abcam) were incubated over night at 4°C or for 2 h at room temperature. Goat anti-rabbit AF488

(1:200, Invitrogen), goat anti-mouse Cy3 (1:200, Biolegend) and goat anti-rat AF647 (1:200, Biolegend) were used as secondary antibodies, respectively, and incubated for 1 h at room temperature. Sections treated with the secondary antibodies alone served as control. Nuclei were counter-stained using Hoechst 33342 (ThermoFisher Scientific). Slides were embedded with Vectashield Mounting Medium (Vector Laboratories) and imaged using the fluorescence microscope DM600B (Leica) and the confocal microscope SP8 (Leica). Data analysis and quantification were performed with Fiji (v1.51n, National Institutes of Health).

### **Mice**

B6.129S7-Rag1<sup>tm1Mom</sup> (Rag1<sup>-/-</sup>) mice were housed in individually ventilated cages with a regular day-night cycle. For the induction of colitis, age- and sex-matched mice were given 1.5-2.5 % DSS in drinking water for 7 days. All experiments involving animals were approved by the Government of Lower Franconia, Germany.

### **Humanised *in vivo* model of T cell homing to the inflamed gut**

Quantification of cell homing *in vivo* was performed using a humanised mouse model previously established in our lab [1]. FACS-purified T<sub>Reg</sub> and T<sub>Eff</sub> cells were stained with CellTrace FarRed (Invitrogen) at 37°C for 15 min and adjusted to a concentration of 1-2 Mio cells/100 µl in PBS. Cells were treated with 10 µg/ml vedolizumab or with human IgG Isotype control (Invitrogen). B6.129S7-Rag1<sup>tm1Mom</sup> mice were anaesthetised by intraperitoneal injection of ketamine/xylazine. Fluorescently labelled cells were injected into the ileocolic artery of the mice and left to circulate for 1 h. Thereafter, mice were sacrificed and lamina propria mononuclear cells (LPMCs) were isolated from the colon

using the Lamina Propria Dissociation Kit (Miltenyi Biotec) according to the manufacturer's instructions followed by density gradient centrifugation with Percoll (GE Healthcare). Fluorescent human cells homed to the murine colon were quantified by flow cytometry.

For intravital microscopy, cells were stained with CellTrace Yellow (Invitrogen) for 15 min at 37°C, treated with vedolizumab or isotype control and injected into the ileocolic artery together with Hoechst 33342 (ThermoFisher Scientific) and 10 µg of anti-mouse CD31 antibody (AF647, MEC13.3, Biolegend). After an incubation period of 15 minutes, the 2 cm of the proximal part of the colon were opened longitudinally, cleaned from faeces and placed onto a coverslip. Cell migration was monitored over 45 min using a confocal microscope (SP8, Leica). Finally, mice were perfused with 15 ml 5 mM PBS/EDTA followed by 4 % PFA and a colon piece was post-fixed overnight and then further processed for lightsheet microscopy.

### **Lightsheet microscopy**

Preparation of samples for lightsheet microscopy was performed as described elsewhere [2]. In short, fixed colon tissue was washed with PBS and then dehydrated using an ascending ethanol series of 50, 70 and 2x 100 % ethanol for 2 h each at 4°C. Thereafter, tissue was cleared using ethyl cinnamate (Sigma) for at least 24 h at room temperature and imaged using an UltraMicroscope II (LaVision, BioTec.). 3D reconstruction of colon tissue and quantification of accumulated human cells was performed with Imaris Image Analysis software 9.0.2 (Bitplane).

### **Bioinformatic analysis of single cell RNA sequencing data**

Single cell analysis was performed in Python v3.6.13 using Scanpy v1.7 [4]. All cells with a mitochondrial content higher than 20 % were filtered out. Normalisation was achieved through size factor correction using Scrn v1.14.6 in R [5]. In order to cluster the data, Uniform Manifold Approximation and Projection (UMAP) [6] was applied to the data for dimension reduction and consecutively the Leiden algorithm was applied for community detection [7].

To define T<sub>Reg</sub> cell clusters, we subclustered all clusters and subsequently performed a ranking of gene expression in each respective subcluster, as defined in the Scanpy documentation. We manually selected the T<sub>Reg</sub> cell clusters, by calculating an overlap score using the following 8 prominent T<sub>Reg</sub> cell marker genes in humans, using a cutoff of at least 3 of these markers to define the T<sub>Reg</sub> cell subcluster: *FOXP3*, *DUSP4*, *IL2RA*, *IL2RB*, *CTLA4*, *IKZF2*, *IKZF4*, *RTKN2*. All T<sub>Reg</sub> cell subclusters were pooled into one comprehensive T<sub>Reg</sub> cell subcluster, divided by the samples VDZ<sup>+</sup> and VDZ<sup>-</sup>. Differential expression analysis was conducted using the R package MAST v1.12. Additionally, a python script was written to count the amount of cells present per gene for a certain cluster or specified group based on a previously published example [8].

The entire analysis workflow is available on Github as a Jupyter notebook file (see accession codes).

For the analysis of the publicly available single cell RNA sequencing dataset GSE162335, the same pipeline was used as described above. After selecting the T cell cluster we defined T<sub>Reg</sub> cells in this LPMC-dataset as cells expressing at least 3 out of 8 key regulatory genes (*FOXP3*, *DUSP4*, *IL2RA*, *IL2RB*, *CTLA4*, *IKZF2*, *IKZF4*, *RTKN2*).

## Statistics

Statistical analyses were performed using Prism 8 software (GraphPad). The following statistical test were used and are specified in the figure legends: When comparing two groups, two-tailed Student's t-test, paired Student's t-test with or without Welch correction, or Mann-Whitney test were used as applicable. When comparing more groups, One-Way ANOVA, Mixed effects analysis, Kruskal-Wallis test or Two-Way ANOVA were used as applicable. For relative data, One sample t test or Wilcoxon test were used as applicable. If indicated, single outliers were detected by the Grubbs' test or ROUT ( $\alpha = 0.05$ ). For contingency analysis, Chi-Square and Fisher's exact test were performed. Results are displayed as box plots indicating median and interquartile range with whiskers indicating minimum and maximum. Correlations were calculated by the Spearman or Pearson test as indicated.  $P < 0.05$  was considered statistical significant in all tests with asterisks indicating the following levels of significance: \* $p < 0.05$ , \*\* $p < 0.01$ , \*\*\* $p < 0.001$ .

- 1 Fischer A, Zundler S, Atreya R, *et al.* Differential effects of  $\alpha 4\beta 7$  and GPR15 on homing of effector and regulatory T cells from patients with UC to the inflamed gut in vivo. *Gut* 2016;**65**:1642–64. doi:10.1136/gutjnl-2015-310022
- 2 Zundler S, Klingberg A, Schillinger D, *et al.* Three-Dimensional Cross-Sectional Light-Sheet Microscopy Imaging of the Inflamed Mouse Gut. *Gastroenterology* 2017;**153**:898–900. doi:10.1053/j.gastro.2017.07.022
- 3 Three-Dimensional Cross-Sectional Light-Sheet Microscopy Imaging of the Inflamed Mouse Gut - PubMed. <https://pubmed.ncbi.nlm.nih.gov/28870528/> (accessed 8 Oct 2020).
- 4 Wolf FA, Angerer P, Theis FJ. SCANPY: large-scale single-cell gene expression data analysis. *Genome Biol* 2018;**19**:15. doi:10.1186/s13059-017-1382-0
- 5 Lun ATL, McCarthy DJ, Marioni JC. A step-by-step workflow for low-level analysis of single-cell RNA-seq data with Bioconductor. *F1000Research* 2016;**5**:2122. doi:10.12688/f1000research.9501.2
- 6 McInnes L, Healy J, Melville J. UMAP: Uniform Manifold Approximation and Projection for Dimension Reduction. *ArXiv180203426 Cs Stat* Published Online First: 17 September 2020.<http://arxiv.org/abs/1802.03426> (accessed 5 Oct 2020).
- 7 Traag VA, Waltman L, van Eck NJ. From Louvain to Leiden: guaranteeing well-connected communities. *Sci Rep* 2019;**9**:5233. doi:10.1038/s41598-019-41695-z
- 8 Luecken MD, Theis FJ. Current best practices in single-cell RNA-seq analysis: a tutorial. *Mol Syst Biol* 2019;**15**:e8746. doi:10.15252/msb.20188746

**R Script**

```
> library(haven)

> #Load CDAI datasets and filter for data at week 6 in patients treated with vedolizumab

> adcdai_171 <- read_sas(„E:/Source Data/NCT01224171/adcdai.sas7bdat”, NULL)
> adcdai_171 <- subset(adcdai_171, VISITNUM==6 & OARM_!="Placebo")
> adcdai_692 <- read_sas(“E:/Source Data/NCT00783692/adcdai.sas7bdat”, NULL)
> adcdai_692 <- subset(adcdai_692, VISITNUM==6 & OARM_!="Placebo")

> #Filter data for CDAI

> CDAI_Score_171 <- subset(adcdai_171, CFOB==“TOTAL SCORE” & CFCAT==“CDAI”,
  select = c(“USUBJID”, “OARM_”, “CFBLCHG”, “CFBLPCHG”, “CFSTRESN”))
> names(CDAI_Score_171) [names(CDAI_Score_171)==“CFSTRESN”] <- “score”
> names(CDAI_Score_171) [names(CDAI_Score_171)==“CFBLCHG”] <- “diff_score”
> names(CDAI_Score_171) [names(CDAI_Score_171)==“CFBLPCHG”] <- “diff_score_perc”
> CDAI_Score_692 <- subset(adcdai_692, CFOB==“TOTAL SCORE” & CFCAT==“CDAI”,
  select = c(“USUBJID”, “OARM_”, “CFBLCHG”, “CFBLPCHG”, “CFSTRESN”))
> names(CDAI_Score_692) [names(CDAI_Score_692)==“CFSTRESN”] <- “score”
> names(CDAI_Score_692) [names(CDAI_Score_692)==“CFBLCHG”] <- “diff_score”
> names(CDAI_Score_692) [names(CDAI_Score_692)==“CFBLPCHG”] <- “diff_score_perc”

> #Combine both datasets

> CDAI_Score <- rbind(CDAI_Score_171, CDAI_Score_692)

> #Check for empty values

> test <- subset(CDAI_Score, is.na(score))

> #Define primary endpoint: clinical remission as CDAI below 150 points

> CDAI_Score$end1 <- 0
> CDAI_Score$end1 [CDAI_Score$diff_score<150] <- 1
> table(CDAI_Score$end1)

> #Load pharmacokinetic dataset and filter for data at week 6 in patients treated with vedolizumab
```

```
> pc_171 <- read_sas("E:/Source Data/NCT01224171/pc.sas7bdat", NULL)
> VedoSerum_171 <- subset(pc_171, VISITNUM==6 & PCTPT=="PREDOSE" & OARM_!="Placebo")
> VedoSerum_171 <- subset(VedoSerum_171, select=c("USUBJID", "PCSTRESN"))
> pc_692 <- read_sas("E:/Source Data/NCT01224171/pc.sas7bdat", NULL)
> VedoSerum_692 <- subset(pc_171, VISITNUM==6 & PCTPT=="PREDOSE" & OARM_!="Placebo")
> VedoSerum_692 <- subset(VedoSerum_692, select=c("USUBJID", "PCSTRESN"))

> #Combine both datasets
> VedoSerum <- rbind(VedoSerum_171, VedoSerum_692)

> #Combine CDAI and serum data and exclude empty values
> data1 <- merge(CDAI_Score, VedoSerum, by ="USUBJID"
> data1 <- subset(data1, !is.na(PCSTRESN))
```